# Verification of a Commercial Treatment Planning System based on Monte Carlo Radiation Dose Calculations in Intensity Modulated Radiation Therapy

by

Lourens Jochemus Strauss

UNIVERSITY OF THE FREE STATE
UNIVERSITEIT VAN DIE VRYSTAAT
YUNIVESITHI YA FREISTATA

January 2015

Submitted in fulfilment of the requirements in respect of the MMedSc degree qualification in the department of Medical Physics in the Faculty of Health Sciences, at the University of the Free State, South Africa

Supervisor: Dr FCP du Plessis

# TABLE OF CONTENTS

Abbreviations ..... a

**Chapter 1:** Introduction ..... 1-1

1.1. Cancer treatment ..... 1-1

1.2. The evolution of radiotherapy techniques ..... 1-1

1.2.1. 3D Conformal Radiation Therapy ..... 1-2

1.2.2. Intensity Modulated Radiation Therapy ..... 1-2

1.2.3. Intensity Modulated Arc Therapy ..... 1-3

1.3. Treatment planning ..... 1-3

1.4. Quality assurance ..... 1-4

1.4.1. IMRT QA ..... 1-4

1.5. Monte Carlo simulations ..... 1-5

1.6. Aim ..... 1-5

**Chapter 2:** Theory ..... 2-1

2.1. The Treatment Planning System: XiO ..... 2-1

2.1.1. Absorbed dose calculation ..... 2-1

a. FFT Convolution ..... 2-2

b. Multigrid Superposition ..... 2-4

c. Accuracy of dose calculation ..... 2-6

d. Monitor Unit calculation ..... 2-6

2.1.2. Beam modelling ..... 2-7

2.1.3. Clinical Treatment Planning ..... 2-7

a. Volume definition ..... 2-8

b. Dose prescription and reporting ..... 2-8

c. Plan optimization ..... 2-9

d. Segmentation ..... 2-10
2.2. The verification system: Monte Carlo ..... 2-10
2.2.1. Absorbed dose calculation ..... 2-11
2.2.1. The EGSnrc code ..... 2-12
a. Random numbers ..... 2-12
b. Particle transport: Photons ..... 2-12
c. Particle transport: Electrons ..... 2-13
d. BEAMnrc ..... 2-14
e. DOSXYZnrc ..... 2-15
f. Variance reduction ..... 2-16
2.3. Dose distribution comparison ..... 2-17
2.3.1. Isodose display ..... 2-17
2.3.2. 2D Gamma analysis ..... 2-17
2.3.3. Dose Volume Histograms ..... 2-18
**Chapter 3:** Method ..... 3-1
3.1. Creating the generic linac ..... 3-1
3.1.1. Structure in BEAMnrc ..... 3-2
3.2. Generating beam data for commissioning ..... 3-3
3.2.1. Water tank data ..... 3-4
3.2.2. In-air data ..... 3-6
3.2.3. Formatting data for transfer ..... 3-6
3.3. Commissioning linac on XiO ..... 3-7
3.3.1. Modelling ..... 3-8
3.4. MC software interface ..... 3-8
3.4.1. Program details ..... 3-10
3.4.2. Extracting CT data from DICOM files ..... 3-11
3.4.3. Extracting Plan data from DICOM files ..... 3-12

a. Calculating physical leaf/jaw positions ..... 3-13

b. Calculating required histories ..... 3-14

c. Creating input files ..... 3-15

3.4.4. Creating scripts for MC simulation execution ..... 3-15

3.5. System verification ..... 3-17

3.5.1. IMRT plans ..... 3-17

3.6. TPS dose verification ..... 3-19

**Chapter 4:** Results+Discussion ..... 4-1

4.1. The generic linac ..... 4-1

4.2. Beam data for commissioning ..... 4-2

4.2.1. RAW data de-noising ..... 4-3

4.2.2. Final dataset ..... 4-5

4.3. XiO modelling ..... 4-9

4.3.1. Spectra & PDDs ..... 4-9

4.3.2. Profiles ..... 4-11

4.4. System verification ..... 4-14

4.4.1. Process validation ..... 4-14

4.4.1. Watertank beams ..... 4-15

4.4.2. Extracted CT data ..... 4-16

4.4.3. 3D-CRT plan ..... 4-17

4.5. IMRT dose comparison ..... 4-19

4.5.1. Prostate ..... 4-19

4.5.2. Head-and-Neck ..... 4-25

4.5.3. Esophagus ..... 4-28

**Chapter 5:** Conclusion ..... 5-1

5.1.1. Verification system ..... 5-1

5.1.2. Dose comparison of XiO ..... 5-2

5.2. Similar studies ..... 5-3

5.3. Limitations / possible future work ..... 5-3

References ..... i

Summary ..... vi

Opsomming ..... viii

Acknowledgements ..... x

**Appendix A:** Additional Results ..... A-1

1. Beam data for commissioning ..... A-1

2. XiO modelling ..... A-3

3. Model verification ..... A-7

4. IMRT plan description ..... A-8

5. MC input files ..... A-13

**Appendix B:** Software codes ..... B-1

# ABBREVIATIONS

| | |
|---|---|
| 2D | 2 Dimensional |
| 3D | 3 Dimensional |
| AAPM | American Association of Physicists in Medicine |
| ADS | Adaptive Diffusion Smoothing |
| ASTRO | American Society For Radiation Oncology |
| BEV | Beam's-Eye-View |
| CAx | Central Axis |
| CDF | Cumulative Density Function |
| CSDA | Continuous Slowing Down Approximation |
| CF | Collimator Scatter Factor |
| CM | Component Module |
| CRT | Conformal Radiation Therapy |
| CT | Computed Tomography |
| CTV | Clinical Target Volume |
| DD | Dose Difference |
| DTA | Distance-to-Agreement |
| DVH | Dose Volume Histogram |
| EGS | Electron Gamma Shower |
| EPID | Electronic Portal Imaging Device |
| FFT | Fast Fourier Transform |
| FWHM | Full Width at Half Maximum |
| GTV | Gross Tumour Volume |
| GUI | Graphical User Interface |
| IMAT | Intensity Modulated Arc Therapy |
| IMRT | Intensity Modulated Radiation Therapy |
| ITV | Internal Target Volume |
| KERMA | Kinetic Energy Released per Mass of Absorber |
| LEE | Lateral Electron Equilibrium |
| Linac | Linear Accelerator |

| | |
|---|---|
| MU | Monitor Unit |
| MC | Monte Carlo |
| MLC | Multi Leaf Collimator |
| NRC | National Research Council (Canada) |
| PDD | Percentage Depth Dose |
| PDF | Probability Distribution Function |
| PSCF | Phantom Scatter Factor |
| PTV | Planning Target Volume |
| QA | Quality Assurance |
| QUANTEC | Quantitative Analysis of Normal Tissue Effects in the Clinic |
| RNG | Random Number Generator |
| ROI | Region of Interest |
| RTOG | Radiation Therapy Oncology Group |
| SS | Smart Sequencing |
| SSD | Source-to-Surface Distance |
| SnS | Step-and-Shoot |
| TERMA | Total Energy Released per Mass of Absorber |
| TPR | Tissue Phantom Ratio |
| TPS | Treatment Planning System |
| TSCF | Total Scatter Factor |

# Chapter 1: INTRODUCTION

## 1.1. Cancer treatment

Treatment modalities in the management of cancer patients share the same goal: the highest possible tumour control with the lowest normal tissue complications. Ultimately we want to cure the patient without any damage to other organs, but that is an ideal situation in a perfect world. In oncology this trade-off will always exist irrespective of the technique, and treatment techniques have to improve towards expanding the gap between these two.

External beam radiotherapy with ionizing radiation is one of several modalities used for cancer treatment, along with chemotherapy and surgery. It is estimated to be a vital part of cancer management, with around 50% of patients receiving radiotherapy as part of their treatment.[1] External beam radiation is mostly produced by a machine called a linear accelerator (Linac). Linacs produce either x-ray or electron beams of various energies which can be chosen by the user. The beam enters the patient from outside and deposits most of its energy within the patient. In turn the energy transferred leads to cell damage, and ideally in the case of cancer cells, cell death. Normal tissue receiving radiation dose also gets damaged, but can repair itself in time through various biological pathways.[2]

One of the benefits of linacs over other external radiation beam sources is that one has a lot of control over the radiation beam; shaping it, switching on or off, orientation, etc. The study and application of radiation, its effects on tissue, and optimal use of the machines that produce it to achieve better treatment outcomes, continually drives the world of radiotherapy forward.

## 1.2. The evolution of radiotherapy techniques

Since radiotherapy started in the 19'th century after Roentgen's discovery of x-rays, the radiation physics knowledge and treatment technology improved rapidly.[3] The concepts of using different energy beams and treatment angles, fractionating the therapy dose, and field shaping to focus dose in a specific area, all came about and were improved on as experience and knowledge were gained.[4] The early treatments were known as Conformal Radiotherapy (CRT).

In 2 Dimensional (2D)-CRT, typically a parallel opposing setup or four beam standard "box" field arrangement were used routinely. In this way the radiation dose could be "focused" where the beams overlap. Treatment planning was done from 2D x-ray images on what was known as simulators. However, in this type of treatment a large portion of the normal healthy tissue was irradiated in the process as well, and accuracy of treatment delivery still had its limitations.

### 1.2.1. 3D Conformal Radiation Therapy

When Computed Tomography (CT) scanners became available in the late 1980's a major advance was the possibility of planning the treatment in 3 dimensions (3D).[5] This meant that beam shaping to conform to the target in 3D was possible, immediately increasing the possible doses given to the tumour with less damage to normal tissue. This type of treatment was categorized as 3D-CRT.

Cerrobend woods alloy was initially used to manufacture blocks that were attached to the head of the treatment machine. These blocks could shape the radiation beam to conform to the desired treatment contours. However, these blocks had to be custom made for every patient, which was time-consuming and required extra quality checks to be performed. Later improvements saw the arrival of the Multi Leaf Collimator (MLC) as part of the linac head, which is now a standard feature in modern linacs. The MLC consists of multiple thin motorized tungsten 'leafs' (typically 80-160 leafs) which are moved in and out of the field separately to create a field shape closely resembling the tumour shape. A lot of research has gone into the design of MLCs, and each vendor has a slightly different product and therefore slightly different radiation characteristics.

The use of the MLC gives the possibility of shaping the radiation beam at every treatment angle around the patient, and increased the treatment dose conformity dramatically compared to 2D-CRT. This method is now known as Conventional 3D-CRT.

### 1.2.2. Intensity Modulated Radiation Therapy

With Conventional 3D-CRT it was now possible to give the radiation dose to the tumour shape and limit the dose to normal surrounding tissue, yet the actual dose was still a relatively uniform distribution over the whole (usually large) volume. This led to exploring a new method of 3D-CRT called Intensity Modulated Radiation Therapy (IMRT), where the radiation dose is modulated to have different intensities across the treatment volume. The modulation achieved by advanced treatment planning techniques (like inverse planning) and specialized control on the linac to position the MLC leafs accurately made IMRT possible.[1,6]

This meant that very high dose gradients could be produced, therefore increasing the potential dose to tumours in close proximity to sensitive structures. In several cases this leads to a much better clinical outcome.[7,8] Some of the drawbacks that comes with the improved dose distribution however is an increase in treatment time and workload on the linac. Planning these treatments is also a much different ball game than 3D-CRT, and the associated dose calculation significantly more complex.

### 1.2.3. Intensity Modulated Arc Therapy

The delivery of IMRT is usually a step-and-shoot (SnS) process at static gantry angles. Advances in the technology made arc treatment possible, where the field is shaped dynamically over an arc of gantry angles to conform to the Beam's-eye-view (BEV) of the target.[9] This is termed Intensity Modulated Arc Therapy (IMAT), also known commercially by their vendor names like VMAT™ (Elekta) and RapidArc™ (Varian). IMAT represents the current leading-edge in 3D-CRT. Nonetheless, full mastering of IMRT is vital to having a successful IMAT program, as it is built on the same fundamentals.

## 1.3. Treatment planning

The treatment of patients with radiotherapy is inseparable from planning and calculating the expected dose distributions. As the treatment techniques evolved, treatment planning - and more specifically Treatment Planning Systems (TPSs) - became more popular and more advanced.

Dose calculation in patients originates fundamentally from measured data in well-defined water tank setups. The initial patient dose calculations were performed by hand using isodose charts and beam data tables to get to an estimated dose distribution.[10] Several correction factors and planning experience were needed to get to the patient dose. In essence one has to consider the known water tank situation and alter the dose distribution to consider everything that is different in the patient setup: distances, field geometry, tissue density and inhomogeneities, etc. When computers became readily available, a lot of effort went into developing software to do these dose calculations. Soon work began on dose calculation algorithms: mathematical ways to compute the dose based on fundamental principles.

Today we have well established algorithms like convolution and superposition incorporated in modern TPSs, which can calculate dose very accurately and fast in most situations. Nevertheless, they still have shortcomings and limitations.

As the application of TPSs becomes more sophisticated with IMRT and furthermore IMAT, these also become more complicated. The ultimate form of dose calculation is using the Monte Carlo (MC) technique. With MC, each particle is transported in 3D through the patient volume and the dose deposition tracked. MC simulation has been proven to be the most accurate algorithm for radiation dose calculation.[11,12] The calculation takes quite some computation time, and only recently vendors have started to use MC in commercial TPSs.[13]

## 1.4. Quality assurance

As in all treatment modalities, these specialized machines used for IMRT must be properly maintained and checked to ensure quality treatment. Radiation is an invisible energy source and therefore errors are not simply detected during delivery. Regular quality assurance (QA) of the equipment through measurements and checks are a vital part of radiotherapy.

### 1.4.1. IMRT QA

One of the challenges especially encountered in IMRT is to ensure accurate delivery of dose to the tumour, and at the same time closely located healthy sensitive tissue must receive the least dose possible. Due to the complexity of IMRT plans, specific quality assurance procedures must be followed in order to verify the dose distribution delivered by the linac in comparison with the treatment plan dose distribution.[14–16] These plan verification procedures must be performed before the first treatment of every patient, using equipment ranging from ion chambers, diode arrays, phantoms, films, and Electronic Portal Imaging Devices (EPIDs).[17,18] Dose measurements using e.g. an ion chamber array attached directly to the treatment head greatly improves the efficiency of IMRT QA. However, most of these QA procedures are time-consuming and require additional access to the linac. For a therapy clinic this means that the linac cannot be used for treatment during QA time. A useful alternative is to simulate the dose distribution using computer calculations such as MC simulations. The EGSnrc-based MC codes are well-benchmarked methods developed by the Canadian National Research Council (NRC)[19] .

## 1.5. Monte Carlo simulations

Practical MC-based tools have been investigated for independent IMRT treatment plan monitor unit verification by various authors.[20–22] Dosimetric verification of IMRT prostate plans calculated on a commercial planning system using MC simulations has also been done by Yang *et al.*[23] Yamamoto *et al.* developed an integrated MC dose calculation system for clinical treatment plan verification, especially for IMRT QA.[24] All these authors achieved significant agreement between the MC derived dose distributions and the commercial TPS dose calculations in clinical conditions.

Several MC codes for simulating linacs and its dose distributions exist. The MC code BEAMnrc is a useful tool for modelling radiation source, e.g. linac treatment head components.[25] DOSXYZnrc can accurately calculate dose distributions in various media in a Cartesian coordinate system into which CT-based patient data can be incorporated.[26] These codes are based on the well benchmarked EGSnrc electron-photon MC transport code system.

## 1.6. Aim

The aim of this project is to be a first step towards full MC-based dose verification for IMRT dose distributions produced on a commercial TPS, by developing the system and demonstrating the accuracy thereof. The TPS used is XiO (CMS, Elekta, v4.62)[27,28], which utilizes a superposition dose calculation algorithm. To achieve this goal, a virtual generic linac will be created in BEAMnrc, data generated through DOSXYZnrc, and the linac modelled and commissioned on XiO. IMRT plans will be created on XiO, and software developed to automate the comparison process with the EGSnrc-based MC dose calculations, using this virtual linac. The objectives are outlined below in Figure 1-1:

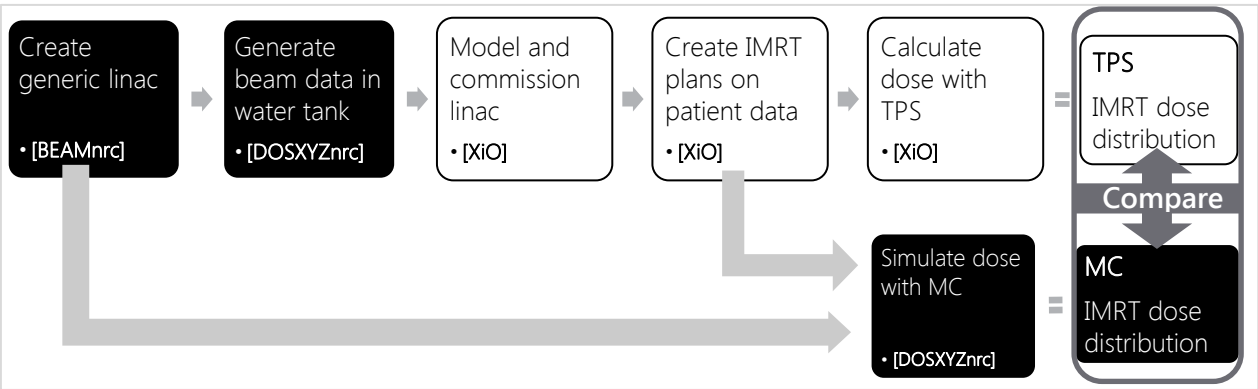


**Figure 1-1: Study process outline**
**Monte Carlo (MC) steps are indicated in black, while Treatment Planning System (TPS) steps are shown in white. The associated software programs are indicated as well.**

# Chapter 2: THEORY

## 2.1. The Treatment Planning System: XiO

The Treatment Planning System (TPS) provides the only tangible connection between treatment delivery considerations and the clinical effect on the patient.[29] In essence the TPS presents a virtual treatment before actually delivering dose to the patient. It is therefore very important to have an idea of the dosimetric trustworthiness of your TPS: where it might be less accurate and which parts are true reflections of reality. A full understanding of the inner workings of a TPS is essential to be able to use it optimally and generate the best plans for patients with confidence. Time efficiency is always an important factor in a busy radiotherapy clinic; therefore planning must occur as productively as possible.

### 2.1.1. Absorbed dose calculation

The various beams of radiation in a treatment plan are directed at a patient within a specific geometrical setup. Calculating the dose to tissue in a patient from these beams as closely to reality as possible is a TPSs main goal, while speed is also important. Several challenges have to be overcome to achieve this objective. There are 2 main aspects to consider: the radiation beams and the patient. The radiation beams are shaped and modified in various ways by the treatment device (Linac), while the patient geometry, tissue types and densities influence radiation transport and deposition.

Most current TPSs either utilize model-based dose calculation methods or Monte Carlo (MC). The earlier approach of treatment planning involved taking water phantom measured dose and adapting it with various factors applicable to the patient situation. Mathematical models goes one step further, using a limited set of measurements and applying a dose calculation model based on first principles. These models require a short computing time and are fairly accurate.[30,31]

In the TPS used in this study, XiO, only mathematical models are available. The mostly used options are Fast Fourier Transform (FFT) Convolution and Multigrid Superposition. The fundamentals of both are the same, but Superposition is more advanced and builds on the FFT Convolution method. The discussion given here is focused on specifics of the XiO TPS.[32]

### a. FFT Convolution

Dose is computed by convolution of the total energy released in the patient with predefined MC-generated energy deposition kernels. The kernels in XiO are taken from studies of Mackie et al.[33] The principle of this method is calculation of dose at a point (***P***) from 3D integration of the energy released from voxels centred on a point of interaction (***P'***). Figure 2-1 and Eq.2-1 illustrates this.[10] The calculation requires 2 main parts: a known TERMA (total energy released per mass of absorber) and an energy deposition kernel.

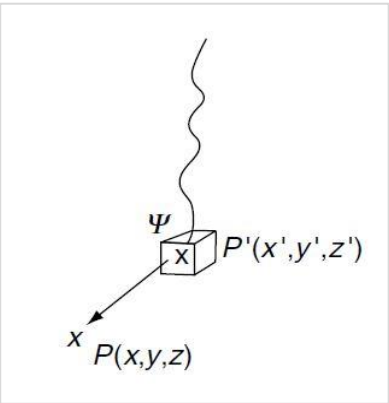


**Figure 2-1: Convolution calculation points**
**The photon interaction point (P′) and dose calculation point (P) are shown**
**[Taken from the *Handbook of Radiotherapy Physics*] [10]**

$$D(x,y,z) = \iiint \frac{\mu}{\rho}\Psi(x',y',z')K(x-x',y-y',z-z')dV' \qquad \textbf{Eq. 2-1}$$

| | |
|---|---|
| $\Psi$ | energy fluence at P′ |
| $dV'$ | elementary volume around P′ |
| $\frac{\mu}{\rho}\Psi$ | TERMA |
| $K$ | energy deposition kernel |

The TERMA is the energy imparted to secondary charged particles and the energy retained by scattered photons. It is therefore essentially the energy lost out of the primary beam. The linac spectrum cannot be measured directly and therefore the energy deposition kernel is computer-generated through accurate MC simulation, using detailed information on the properties of the treatment head.[32] The simulation forces a photon to interact at a specific point and records the subsequent energy deposition around it. In XiO, default spectra for various linacs are already included. The poly-energetic kernels for the open fields are formed from the mono-energetic surface spectra.

A kernel-hardening correction factor is also applied. By making use of the Kinetic Energy Released per Mass of Absorber (KERMA), the kernel-hardening correction is modelled using the collision KERMA-to-TERMA variation with depth. This correction can reduce errors in the depth doses due to hardening of the beam by a few percent.[34]

A fanned beam grid is used for dose calculation, and the energy deposition kernel is then convolved with the TERMA. This is done very efficiently in Fourier space by simply multiplying the two. The drawback of working in Fourier space is that the kernel must be spatially invariant, i.e. be constant independent of the position of the interaction point ($P'$). Thus it cannot account for tissue inhomogeneities. However, a significant speed-up is achieved by using the conversion to Fourier space, which produces dose distributions a lot faster.

The primary dose is calculated from the primary kernel and the scatter dose from the scatter kernel. The total dose is the sum of these two. The energy deposited can be calculated from spreading out the TERMA from the interaction point to the other points in the volume. This is referred to as the 'interaction point of view'. This however is not always efficient, since dose at all points are always calculated even if only certain points are required. Instead the inverted kernel probability distribution can be used to 'collect' the TERMA from all interaction points to the dose deposition point ('Dose point of view'), as illustrated in Figure 2-2.

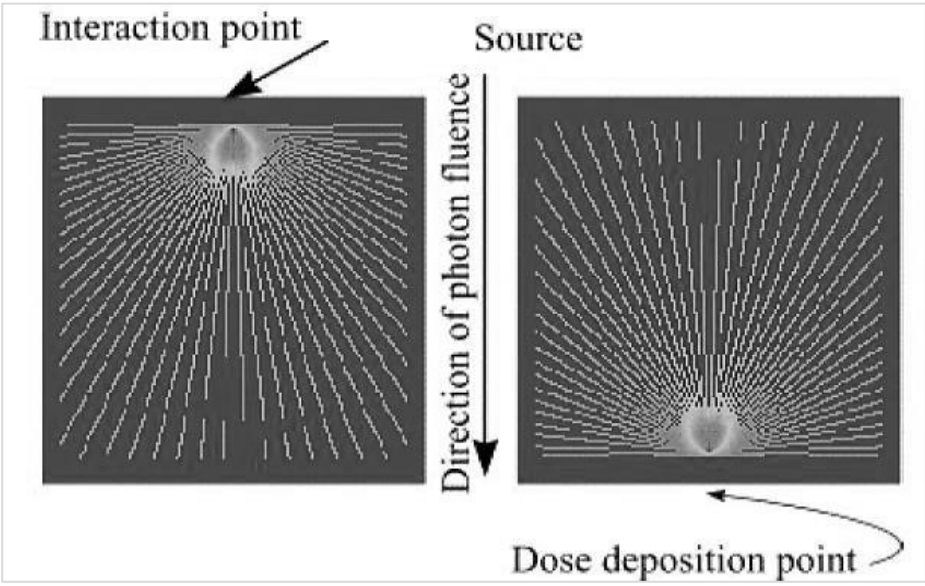


**Figure 2-2:** XiO **fanned beam grid with either interaction or dose point of views [Taken from the** XiO **manual]** [32]

A parallel-kernel approximation is used to account for the diverging beam, since invariant kernels are used. The approximation however does not fully account for the fanning out of the beam, which still leads to some errors. This produces an over-penetrative Central Axis (CAx) dose and underestimated dose from the penumbra outwards. An inverse-square based correction is applied to counter these effects, although some discrepancies will still exist.

### b. Multigrid Superposition

The Multigrid Superposition method is adapted from the 'collapsed cone' calculation method[35] and has the same principle as convolution. This means that most of the process described above also applies to superposition. However, it uses variant kernels to account for inhomogeneities and therefore is not a true convolution. The kernels are modulated by the TERMA by performing density scaling using the average density along the path between the interaction and dose deposition sites, and superposition done using varying kernels (i.e. dependent on $P'$). An example of a density scaled kernel is shown in Figure 2-3.

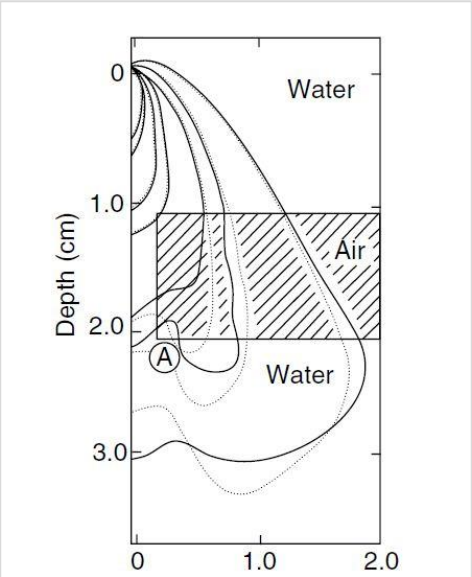


**Figure 2-3: Density scaled kernel**
**Density scaled kernel is shown (solid line) as compared to MC kernel (dotted line)**
**[Taken from Woo and Cunningham] [36]**

Superposition without some approximations can take a long time to calculate. Instead of calculating TERMA from each interaction point, a pre-set number of rays are chosen and a cone 'collapsed' onto the ray from around it. The XiO system uses 8 azimuth and 16 zenith rays to calculate the dose at each dose point (see Figure 2-4).

A fast superposition method is also offered, with only 8 azimuth and 6 zenith rays for each dose point. This increases the calculation speed, resulting in a small loss in accuracy. The fast mode gives doses with a 1-2% loss in accuracy compared to the standard method, and therefore is used in the initial planning but not for the final dose calculation. The dose at each point is finally super-imposed from all beams to obtain the full dose distribution.

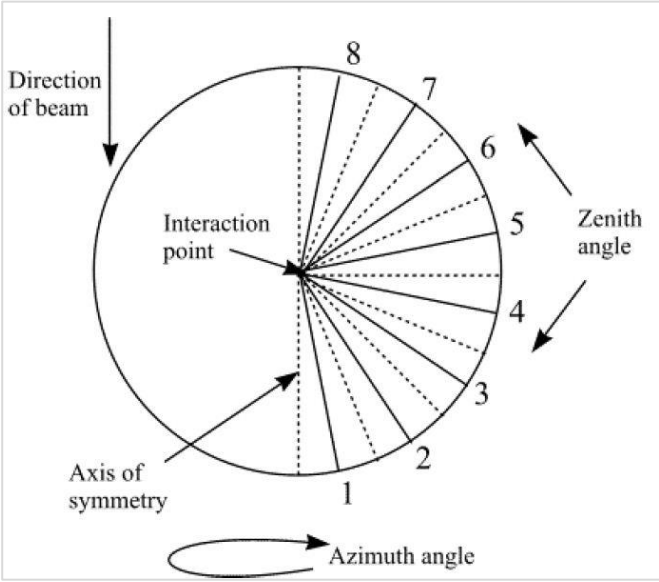


**Figure 2-4: Illustration of angles used in calculations**
**[Taken from the XiO manual]** [32]

Other techniques to reduce dose calculation time are also implemented in XiO. The major time-reduction is due to the Multigrid method (Figure 2-5). The principle is to increase the resolution of dose calculation points in areas of high importance and reduce the resolution in others. The number of points used in beam edges and high tissue density gradients are increased, while less points are calculated in other regions and interpolation applied in between. Another optimization method is to determine the points that will contribute to the user-defined dose volume, and not calculate dose from unnecessary points.

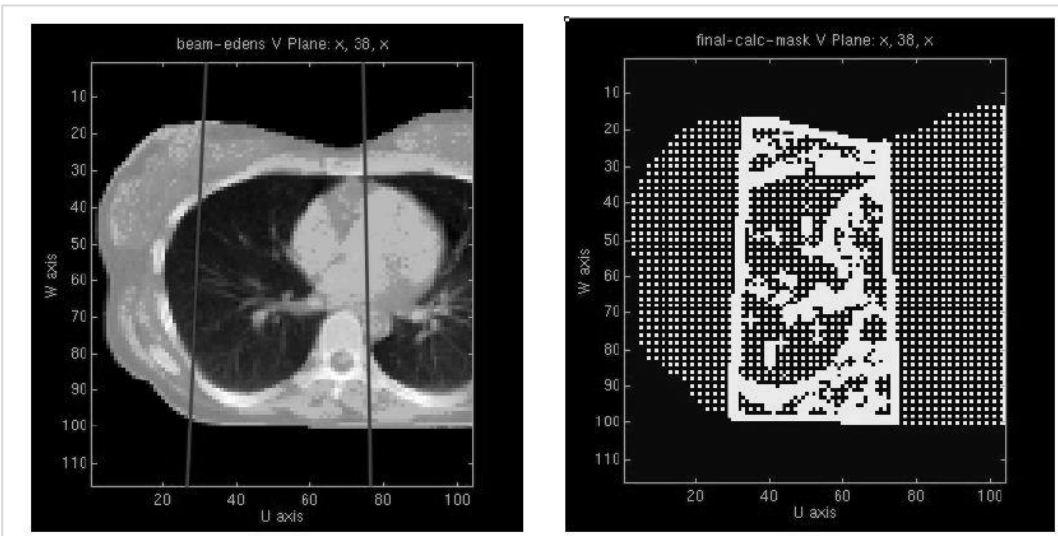


**Figure 2-5: The Multigrid method of XiO**
**The resolution of dose calculation points are marked in white on the right**
**[Taken from the XiO manual]** [32]

### c. Accuracy of dose calculation

The principles of the convolution and superposition algorithms clearly indicate that convolution will have inaccuracies in media other than water/soft tissue. Dose in tissues with relative electron densities differing considerably from water, like bone and lung, will not be calculated correctly unless some inhomogeneity correction is applied. In these cases superposition is the preferred option of the two. The kernel scaling used in superposition provides a much better dose calculation in these tissues.

A polyenergetic kernel approximation is applied in XiO to account for the lateral and depth spectrum changes. This is done through summing of TERMA-weighted monoenergetic kernels. Small errors can still be expected due to this approximation.[32,34] The error due to the parallel-beam approximation, which assumes the kernels not to be oriented along with the diverging beam, is greatly reduced through the correction applied in XiO. However, the correction mostly improves doses only on the CAx and also causes the modelled penumbra to be narrower than the true penumbra. Some deviations can be expected especially in large fields and deeper depths.

Other limitations in these algorithms are described in the vendor's manuals. These include, among others, (i) the absence of photon and electron contamination modelling under treatment aids, (ii) the assumption that the spectrum is independent of Field Size (FS), (iii) some assumptions on head scatter, and (iv) using the mass attenuation coefficient of water for all tissues.

### d. Monitor Unit calculation

Ultimately the Monitor Units (MUs) for the linac must be calculated to relate the absorbed dose calculated to something that the machine can deliver. For this the TPS requires some physical parameters of the linac (measured at commissioning), including Tissue-Phantom Ratios (TPRs), Phantom Scatter Factors (PSCF) and the dose output (DO). In XiO this is calculated as follow:

$$\mathrm{MU} = \frac{\mathrm{D}}{\mathrm{f}} \div \left[\frac{\mathrm{Iso}}{\mathrm{w}} \times \frac{\mathrm{TPR} \times \frac{\mathrm{PSCF(FS@wp)}}{\mathrm{PSCF(ref)}}}{\frac{\mathrm{PSCF(CesFS)}}{\mathrm{PSCF(ref)}}} \times \left(\frac{\mathrm{SCD}}{\mathrm{SWD}}\right)^2 \times \mathrm{DO}\right] \qquad \textbf{Eq. 2-2}$$

| | |
|---|---|
| D | Prescribed dose |
| f | Number of fractions |
| Iso | Isodose value (%) |
| w | Beam weight |
| wp | Weight point location |
| CesFS | Collimated Equivalent Square FS |
| SCD | Source-to-calibration distance |
| SWD | Source-to-weight point distance |
| ref | Reference conditions |

It is thus evident that the accuracy of the TPR, TSCF and DO directly influence the MU calculation, and care must be taken to determine these values correctly.

### 2.1.2. Beam modelling

Accurate dose calculation for the specific clinical setup is not only dependant on the algorithm, but also on accurate modelling of the linac to be used. This is a time-consuming process conducted by the clinic's Medical Physicist. The basic concepts involved in the modelling process are summarised here.

The TERMA is calculated from the energy spectra of the actual beam, and thus modelling of the spectra is essential. In XiO the mean energy is used as predictor of the effect of the spectrum change. The user models Central Axis (CAx) and off-axis spectra for each energy used, based on default spectra shipped with the TPS. The effect of spectra changes can be seen directly on the calculated Percentage Depth Dose (PDD) curve, and the adjustments required on the spectra can easily be deduced from this.

The lateral incident fluence of the linac is based on the measurement of diagonal profiles over the largest open FS. Different depths of these scans can be used to adjust the fluence profile. The Penumbrae modelling is done through the use of error functions, with a single error function applying to each collimator respectively over all FSs. In XiO this is governed by "sigma" values, where a lower value creates a steeper penumbra. A value for each collimator's transmission can also modified by the user to model the dose outside the open field area.

### 2.1.3. Clinical Treatment Planning

The Intensity Modulated Radiation Therapy (IMRT) planning approach differs from conventional 3D-Conformal Radiation Therapy (3D-CRT) in many ways. The main difference is in the planning strategy, using *inverse planning* instead of *forward planning*. With inverse planning the desired dose distribution is specified, and the beam setting to achieve this then calculated. Forward planning starts with specifying the beam settings and calculating the resulting dose, which are then manipulated until a satisfactory dose distribution is found. IMRT planning thus requires delineation of structures (target volumes and organs) and laying down objectives for these structures.

### a. Volume definition

A standardised way of defining structures has been presented by the International Commission of Radiation Units and Measurements (ICRU), together with recommendations on various aspects of treatment planning. Report number 83 is specifically focused on IMRT.[37] A summary of the volume definition is given here (Figure 2-6).

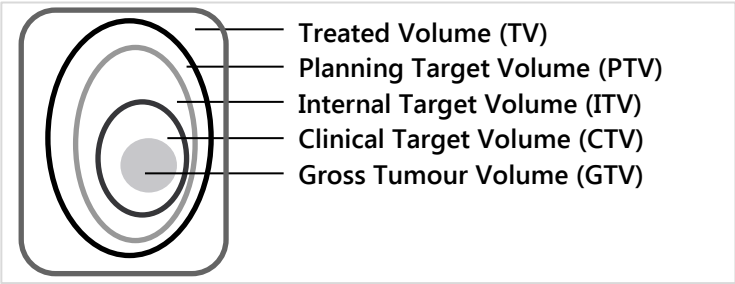


**Figure 2-6: Volume definition according to the ICRU**

The primary tumour defined by the Gross Tumour Volume (GTV) is surrounded by a Clinical Target Volume (CTV) which includes subclinical malignant disease. The Internal Target Volume (ITV) is an optional volume to accommodate uncertainties in size, shape, and position of the CTV. The Planning Target Volume (PTV) is the actual volume to be treated when all factors like motion and setup variations are considered. Critical normal tissue structures are contoured as Organ at Risk (OAR). These structures are in the vicinity of the CTV and are those that can possibly suffer significant morbidity if irradiated.

### b. Dose prescription and reporting

The ICRU recommends prescribing and reporting doses to volumes instead of a single point. A single point is insufficient especially in IMRT since, among other reasons, dose gradients are steep and if MC is used, statistical fluctuations may induce errors. Cumulative Dose Volume Histograms (DVHs) provide information on volumes of structures receiving a certain dose, and is a useful tool in reporting and plan evaluation. For target volumes, it is recommended to prescribe dose with the near-min ($D_{98\,\%}$) and near-max ($D_{2\,\%}$) values, i.e. the dose that at least 98% of the target receives and the dose that less than 2% of the target receives, respectively. The median absorbed dose ($D_{50\,\%}$) must be used in the reporting. For the OARs, dose is prescribed by setting several dose constraints on certain volumes, e.g. limit 50% of the volume to 30 Gy ($D_{50\,\%} \leq 30\ Gy$). In this way an ideal DVH can be set with only a few dose-volume points. The prescription parameters are usually also used for reporting. It is suggested that the volume $V$ receiving a significant dose $D$ (in terms of that organ) be reported using $V_D$. Several $V_D$ values can be used.

A very useful collection of clinical dose/volume/outcome data specific to radiotherapy is provided by the American Association of Physicists in Medicine (AAPM) and American Society for Radiation Oncology (ASTRO), known as the Quantitative Analysis of Normal Tissue Effects in the Clinic (QUANTEC) data.[38] In their published work, valuable information can be found on clinical endpoints pertaining to dose/volume parameters. Another source of clinical information is the reports of the Radiation Therapy Oncology Group (RTOG). The RTOG reports on clinical studies and compares the outcomes of studies using the same criteria for patient selection, treatment regime, etc. Using the relevant data from these sources, a suitable set of dose-volume objectives can be chosen for the patients to be treated.

### c. Plan optimization

The optimization process starts with defining dose objectives for each structure. Objective functions are either minimized or maximized to achieve certain constraints.[39] A 'cost' is associated to each objective: as the optimizer achieves a solution closer to the constraints the cost will decrease. XiO offers 3 types of objectives: minimum, maximum, and dose-volume objectives. The minimum and maximum objectives basically increase the cost quadratically as it approaches the set value. This applies for both targets and OARs. The dose-volume objective for OARs works in the same way, but only in the region from the set dose up to the current dose at the volume limit. An illustration is given in Figure 2-7 to aid in the explanation.

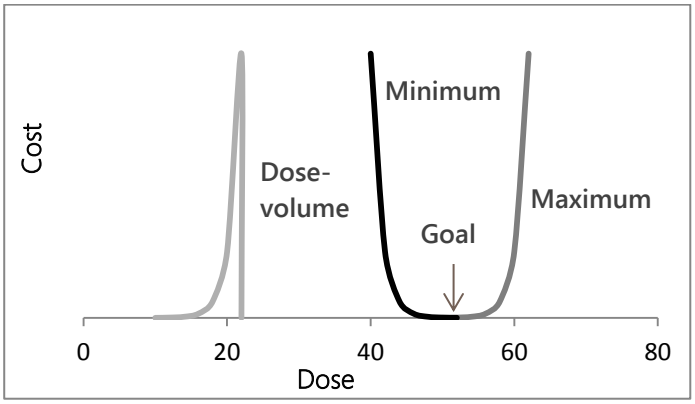


**Figure 2-7: Objective functions**
**Lines indicate increase in cost relative to the dose constraints**

The XiO IMRT optimizer uses a "conjugate gradient" optimization algorithm.[40] This means that it finds the minimum of the cost function from its negative gradient for each iteration. The cost function is the sum of dose objectives with beamlet weighting applied (i.e. fluence modulation). The gradient consists of a vector of partial derivatives of the objectives. The gradient is thus recalculated for each iteration until the cost function converges (this criteria can be chosen by the user).

### d. Segmentation

A major challenge in IMRT is to take the highly modulated continuous fluence map and change it into treatable segments, i.e. a series of shapes that can be formed by the linac MLC to produce the intensity modulation. One of the methods available in XiO for segmentation is Smart Sequencing (SS). This method makes use of adaptive diffusion smoothing (ADS), which smoothes the intensity map by using diffusion coefficients defined for each beamlet.[41] Positions of the MLC leafs are then calculated from these smoothed intensities.

The user can manipulate some parameters, like minimum segment size and monitor units (MUs) per segment, which will influence the number of segments created and subsequently the degree of modulation. A smaller allowed segment size and fewer MUs per segment will both increase the degree of modulation achievable and with it improve the dose distribution, but at the same time extend the treatment time. Careful selection of these parameters is important to balance clinically acceptable treatment times with a satisfactory dose distribution.

## 2.2. The verification system: Monte Carlo

The model-based approach can be quick and effective, but it will always be an approximation to reality and not "what actually happens". The best method would be to track each and every particle that is produced by the linac all the way to where it comes to rest. In essence, that is what MC does.

MC can be used to determine the kinetics of particles in various media. The principle of MC is to make use of known photon and electron interaction probability distributions, also known as probability distribution functions (PDFs), to simulate their transport through matter. The physical interactions can be computed from the knowledge gained through Quantum Electrodynamics. It is not limited to only absorbed dose calculations, since the complete path and interactions of each particle can be tracked. This means that it is also possible to obtain information on particle distributions for specific situations (e.g. photon fluence at a plane). In the radiotherapy environment we can thus 'simulate' the radiation transport from creation to dose deposition, and all steps in between.

The following explanation will focus on absorbed dose calculations, though the principle of particle transport is exactly the same in situations where other aspects of radiation are important, like particle fluence, energy spectra, orientation, etc.

### 2.2.1. Absorbed dose calculation

MC is a direct dose calculation method, transporting every particle from entering the calculation grid until it has lost all of its energy or left the volume. This is referred to as a particle 'history'. An example of a single photon history is given in Figure 2-8.

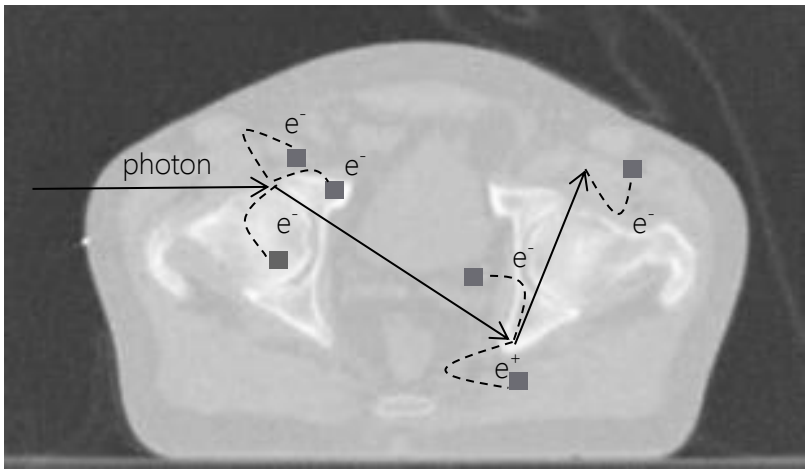


**Figure 2-8: Example of a photon particle history track**
**Interactions and subsequent dose deposition are scored in the volume**

When a photon enters the volume it will be forced to interact at a point after travelling a certain distance. Here it is scattered and electrons liberated (Compton interaction in this case). The electrons are transported until all energy is lost. The electron interactions can be elastic or inelastic scattering, and Bremsstrahlung events. The scattered photon is transported further in the volume and deposits energy in subsequent interactions. Photon interactions can be Rayleigh, Photo-electric, Compton or Pair-production. The particle is transported until it has lost all its energy or left the volume.

The interaction and energy deposition on this path is governed by the interaction cross sections. This is provided by random sampling from the PDFs. By simulating a large number of histories, the energy deposition can be mapped and the complex patient- and beam specific calculation solved. As more and more histories are added to the simulation, the statistical fluctuation in dose calculated in the volume becomes less until a complete picture of the actual dose emerges.

MC is probably the most accurate dose calculation method. However, following the dose tracks of millions of particles can be a very time-consuming process. It requires a lot of computing power, which has made it impractical for real-time clinical use in the past. As computers become faster and multi-processing more common, MC will become the future of TPS dose calculation. As dose verification tool however, MC can be used very effectively. Many software packages built for research purposes exist using the MC principle, including MCNP, Penelope, Geant4, and EGSnrc[42].

### 2.2.1. The EGSnrc code

The Electron Gamma Shower (EGS) system of codes developed by the National Research Council of Canada (NRC) is a package of MC codes for coupled photon and electron transport. It follows on the original EGS4 package, with many improvements added in the latest version: EGSnrc.

#### a. Random numbers

At the heart of each simulation lies a random number, from which the sampling of data occurs. Since computers cannot really create anything random, pseudorandom numbers are used instead. Algorithms are used to create a sequence of numbers that appear random, which are called pseudorandom numbers. The algorithm starts off from a "seed" number to generate the sequence, and after a certain amount of numbers the sequence will repeat. The length of this sequence (period) will therefore determine the effectiveness of the Random Number Generator (RNG).[43] Random numbers used are usually normalised to have a range between 0 and 1.

In EGSnrc the RANMAR and RANLUX[44] RNGs are available, which has a period of over $10^{165}$. The RANMAR RNG makes use of two input seeds, $i_{xx}$ and $j_{xx}$. One of the features of these RNGs is that it can produce random number sequences that are independent of other sequences, which makes it very useful for parallel runs.

#### b. Particle transport: Photons

*Path length*

First the interaction path length to the next interaction site is determined. The direct sampling method is used, which requires sampling from a Cumulative Density Function (CDF): the area of the PDF is normalised to 1 and integrated.[45] The mathematics is shown in Eq.2-3 and Eq.2-4.

$$\int_a^b p(x')dx' = 1 \qquad \textbf{Eq. 2-3}$$

| | |
|---|---|
| $p(x')$ | Probability Distribution Function (PDF) |
| $a, b$ | Range of PDF |

$$c(x) = \int_a^x p(x')dx' \qquad \textbf{Eq. 2-4}$$

| | |
|---|---|
| $c(x)$ | Cumulative Density Function (CDF) |

From this cumulative probability distribution based on the linear attenuation coefficients and the material type, a path length is determined for the specific conditions of the incident particle (energy, type, etc.). The particle is then transported this distance. Interaction distances can be described by

$$p(x) = \mu e^{\mu x} \qquad \textbf{Eq. 2-5}$$

| | |
|---|---|
| $\mu$ | Linear attenuation coefficient |

*Interaction type*

Next the interaction type must be selected. Random numbers are generated in the range from 0 to 1, and used to choose the interaction type from the PDF applicable to the interaction site. Branching ratios, which is simply the cross section for the specific interaction type divided by the total cross section, are illustrated graphically in Figure 2-9 for a simple case.

**Figure 2-9: Example of PDF sampling for interaction types**
**For a random number of 0.43, a Compton interaction is selected**

The photon particle transport in EGSnrc consists of simulations of Pair and triplet production, Compton scattering, Photo-electric absorption or Rayleigh scattering. In each process the particle cross section, energy and scattering angle is derived using further random numbers. For the primary interaction type selected, secondary particles are created and transported until they stop.

After this the transport of the primary particle continues and the process repeats (starting again from path length selection) until all energy is lost or the particle exits the volume. In order to determine when a photon has "lost all of its energy", a threshold value is chosen. In EGSnrc this is defined as PCUT; photons with energy less than this value will not be transported further and deposits all residual energy locally.

All information of the history is recorded, and the next particle transported. The addition of all histories leads to the total dose distribution.

*Material data*

The cross section, mean free paths, and electron stopping power data for different media types are contained in a file in the EGSnrc system generated by the pre-processor PEGS4. A specific set of data is given for lower electron energies of 521keV and 700keV respectively, based on the density effect corrections in ICRU Report 37.

### c. Particle transport: Electrons

The transport of electrons is handled differently from photons, mainly because of the free path length difference. Photons have interactions in the range of centimetres, while electrons undergo millions of interactions in the same space. To make the transport feasible, a class II Condensed History (CH) technique is used. Electrons can have elastic or discrete inelastic (Möller and Bhabha) collisions, or Bremsstrahlung.

If an interaction creates photons or secondary particles above a certain threshold energy value, the transport will continue explicitly. These are termed 'hard collisions'. The 'hard collisions' are transported in the same manner as photons, but with the corresponding interaction types. When electrons reach an energy value lower than the cut-off (ECUT), the history is terminated and energy deposited locally.

If this is not the case ('soft collisions'), grouping is performed. For the soft collisions, the multiple scattering properties and stopping power must be known. In EGSnrc, the Continuous Slowing Down Approximation (CSDA) is used to determine the multiple scattering energy loss. Important aspects when using the CSDA are the boundary crossing and electron step settings.

*Boundary crossing*

Adjacent voxels typically do not have the same material. Transporting electrons across such a boundary can lead to inaccuracies, and therefore a boundary crossing algorithm (BCA) is incorporated. The default in EGSnrc is EXACT. In any BCA, the perpendicular distance of the electron to the closest boundary is determined. For EXACT, if this distance is within a user specified value, electrons are transported in single elastic scattering mode instead of using the CSDA. The other option is PRESTA-I, which is faster but has some inaccuracies.[46]

*Electron step*

In EGSnrc the maximum fractional energy loss per electron step (termed ESTEPE) can be chosen. This is the step length in which multiple scattering deflections are ignored and condensed in a straight line in the original direction of the electron. If this is set too large, the approximation will be inaccurate, and if set too small computation time increase unnecessarily. Two options are available, PRESTA-I and PRESTA-II. The latter is the newer and more accurate of the two. PRESTA-II was developed for EGSnrc based on the original PRESTA algorithm.[47] It takes into account the curved and straight-line path lengths at each electron step through lateral and accurate interface transport.

### d. BEAMnrc

The general purpose code developed as part of the OMEGA-BEAM system of codes specifically focused on simulation of radiation beams from treatment units is called BEAMnrc. A broad set of geometric shapes resembling actual parts of a radiotherapy unit is available to the user, termed Component Modules (CMs). These include SLABS (used among others for targets), CONESTAK (used for primary collimator), FLATFILT (flattening filter), CHAMBER (monitor chamber) and MIRROR (reflecting mirror). The collimators can be created using any of the various JAW and/or MLC CMs.

The simplest forms of each are the CMs JAWS and MLC, both with diverging edges and no gaps in between (as illustrated in Figure 2-10, from the BEAMnrc manual).

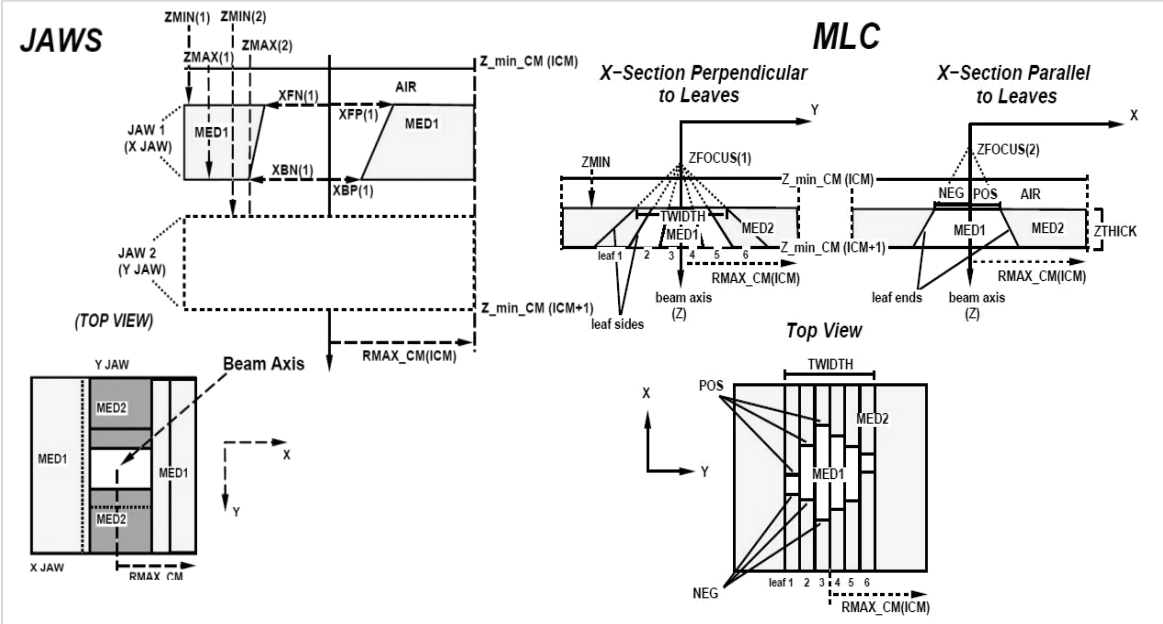


**Figure 2-10: CMs for collimators in BEAMnrc [Taken from the BEAMnrc manual]** [48]

The code can keep track of each particle history, and thus one can determine the dose contribution from separate components. The main area of interest though is the creation of a phase-space file (.phsp), where particles can each be 'frozen' in space, in a certain plane for example, by storing each particle's current energy, angle, type and positional information. In this way a fluence output of the linac can be created for use in dosimetric simulations.

### e. DOSXYZnrc

The code for calculating dose in a phantom with rectilinear voxel dimensions in the OMEGA-BEAM project is DOSXYZnrc. It utilizes input data in the form of phase-space files or beam characterization models, created from BEAMnrc. Included in the package is ctcreate, a tool for converting CT data to a new file that can be used in the simulations in DOSXYZnrc. The ctcreate output contains the density and material type data of the phantom.

Beams can be directed to fall in on the phantom from any direction and distance. The dose scoring in each voxel also includes the statistical variation of the complete simulation run. It is also possible to restart a simulation, i.e. adding more histories later on for the same conditions.

### f. Variance reduction

The MC process is a statistical in nature, and thus the number of histories simulated directly decreases the variance. However, it has an exhausting relation: a decrease in variance of a factor of 2 requires roughly 4 times the number of histories. This means that a dose calculation with acceptable statistical variation can take a long time to simulate. To reduce this, variance reduction techniques are employed which does not require longer simulation times.

*Range rejection*

The distance from the electron to the nearest voxel boundary is calculated, as well as the maximum range of the electron. This will depend on the electron energy and material type. If the maximum range of the electron is less than the distance to cross the voxel boundary, the transport can be terminated and its energy scored in that voxel. This method can translate to large gains in efficiency.

*Photon forcing*

An option available in BEAMnrc is to force a photon interaction in a specific CM. This is useful in situations of sparse interactions. When an interaction is forced, the photon is split into a scattered photon and an unscattered photon with appropriate weights.

*Bremsstrahlung splitting*

This technique creates a multiple of the amount of photons emitted during a bremsstrahlung interaction. The weight of these photons is reduced accordingly, and the electron's energy is lessened by the energy given off by one of these photons. On average, energy is conserved. The advantage lies in the reduced repetition of calculating various electron energy constants.

The splitting of photons creates more secondary particles to track, therefore actually increasing computing time. If the main importance is on the transporting of the bremsstrahlung photons and not on the secondary electrons and their effect, the gain can still be achieved if Russian roulette is used.

The basis of Russian roulette is that secondary charged particles resulting from split photons are given a survival chance. Using random numbers and a survival threshold, a secondary particle will either be eliminated or survive (and given a higher weight).

Other methods of reducing the statistical variation include smoothing of data after the simulation and the voxel size.

*Uncertainty reporting*

The EGSnrc MC codes employ a history by history method to estimate uncertainties.[49] The energy deposited is grouped, from which the statistics are determined. When using phase space sources, quantities are grouped by primary history.[50] The principle of history by history is well known, but has been adapted in BEAMnrc and DOSXYZnrc to reduce the increase in computation time of this method compared to the previous batch approach. Other advantages of this method include more accurate reporting for small samples, lower memory use, and taking into account the correlations between particles that occur due to variance reduction techniques.

## 2.3. Dose distribution comparison

Dose distributions in 2 or 3 dimensions can be compared using different methods.

### 2.3.1. Isodose display

The simplest dose display method is through isodose lines, which is a line connecting points of equal dose. Isodose lines can be presented as either absolute values or a percentage of the prescribed dose. The same information can also be displayed as a 'colourwash': a large number of isodose lines presented by means of a continuous colour change.

A normalised dose difference ($DD_{norm}$) map can also be created by voxel-by-voxel subtraction of the absolute dose values of each distribution, expressed as a % of the prescribed dose. The mathematics is given in Eq. 2-6. This map can be viewed in the same manner, with isodose lines or a colourwash display.

$$DD_{norm} = \frac{D_{MC} - D_{XiO}}{D_{presc}} \times 100 \qquad \textbf{Eq. 2-6}$$

| | |
|---|---|
| $D_{MC}$ | MC dose value |
| $D_{XiO}$ | TPS dose value |
| $D_{presc}$ | Prescribed dose for plan |

### 2.3.2. 2D Gamma analysis

The gamma ($\gamma$) tool compares 2 dose distributions by simultaneously evaluating two main elements: Dose Difference (DD) and Distance-to-Agreement (DTA). The DD is a simple difference of doses between points at the same location. The DTA is the closest (smallest) distance between points of the same dose value. Both of these metrics used independently have limitations/ over-response in certain areas, especially in either high or low dose gradient regions.

A new tool considering both of these metrics in a continuous manner that characterizes the dose difference in a $\gamma$-distribution was developed by Low *et al.*[51,52] The $\gamma$ function (as described by Ju *et al.*[53]) is defined by

$$\gamma(r_r) = min_{r_e}\, \Gamma(r_r, r_e) \qquad \textbf{Eq. 2-7}$$

| | |
|---|---|
| $r_r$ | reference dose point |
| $r_e$ | evaluated dose point |
| $\Gamma$ | individual gamma |

Where the individual gammas ($\Gamma$) are calculated from

$$\Gamma(r_r, r_e) = \sqrt{\frac{|r_e - r_r|^2}{\Delta d^2} + \frac{[D_e(r_e) - D_r(r_r)]^2}{\Delta D^2}} \qquad \textbf{Eq. 2-8}$$

| | |
|---|---|
| $D_r$ | reference dose |
| $D_e$ | evaluated dose |
| $\Delta d$ | DTA criteria |
| $\Delta D$ | DD criteria |

A point will subsequently pass the test if $\gamma(r_r) \leq 1$. A 2D map of these $\gamma$ values can be created to show areas of disagreement, as well as the relative magnitude, visually. The number of points within a contoured structure that pass can also be expressed as a fraction of the total area belonging to that structure. Note that this analysis is done per slice (2D) and not in all 3 dimensions.

### 2.3.3. Dose Volume Histograms

It can be difficult to interpret dose information in the complete 3D volume. A better picture can be formed by summarising the information relating to each structure on a single graph. This is called a Dose Volume Histogram (DVH).

Two types of DVHs can be used: Differential DVH (dDVH) or a Cumulative DVH (cDVH). The dDVH directly displays of the volumes receiving dose in equal dose intervals (bins), shown for all intervals covering the complete dose range. The cDVH is a plot of the volumes that receive a certain dose or more, i.e. the volume that gets at least that dose. It can be calculated as follow:[37]

$$DVH(D) = 1 - \frac{1}{V}\int_0^{Dmax} \frac{dV(D)}{dD}\, dD \qquad \textbf{Eq. 2-9}$$

| | |
|---|---|
| $D$ | Absorbed dose |
| $V$ | Volume of the structure |
| $D_{max}$ | Maximum dose in the structure |

The cDVH is a more useful tool in the clinical setup, and hence mostly the term DVH actually refers to a cDVH. An example of both types for a perfect target dose is shown in Figure 2-11.

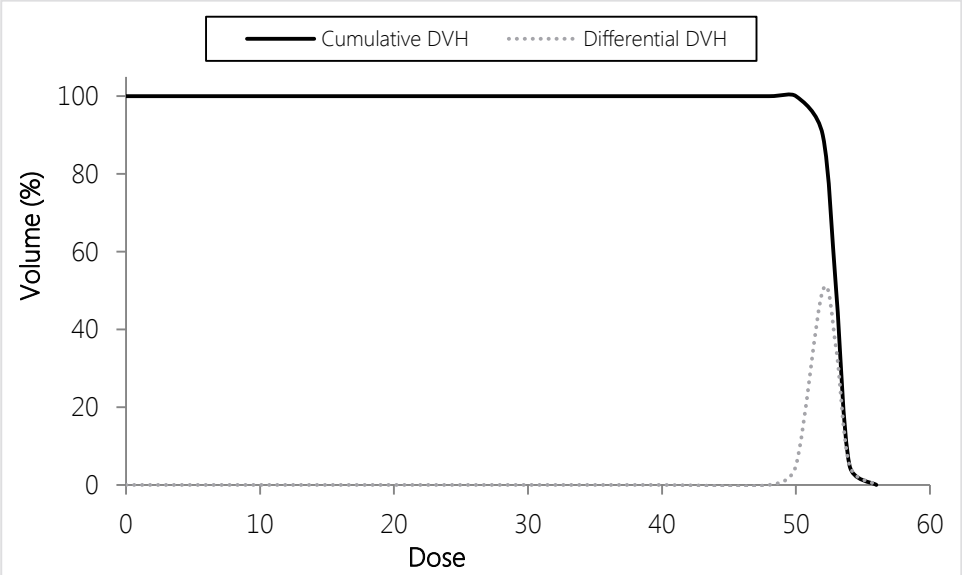


**Figure 2-11: dDVH and cDVH example**

Comparison of DVH data from different dose calculation methods on the same anatomy can thus give useful information on dose delivered to the entire organ/volume. From the DVH information quantitative dose-volume metrics can also be reported.

# Chapter 3: METHOD

## 3.1. Creating the generic linac

A generic virtual linac is constructed using the BEAMnrc Monte Carlo (MC) code.[48] A simplistic model of the basic treatment head structure is illustrated in Figure 3-1. The configuration and dimensions of the components are based on a typical Elekta linac.[54,55]

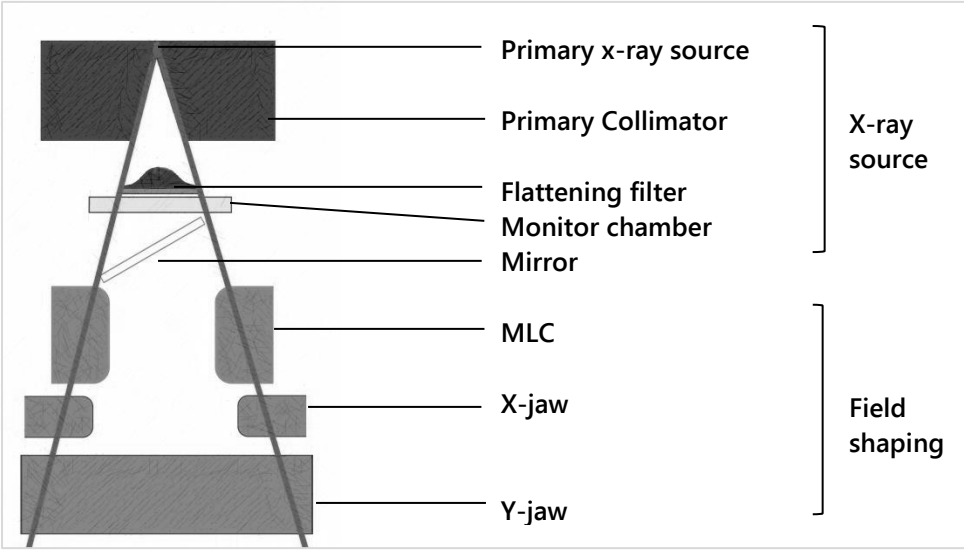


**Figure 3-1: Treatment head configuration**
**Basic structure of generic linac is shown, with x-ray source and field shaping sections indicated**

The components needed for the 'x-ray source' is created in BEAMnrc and comprise of the top section shown in Figure 3-1. In the BEAMnrc simulation, a narrow beam of electrons of the appropriate energy (6 or 10 MeV) is injected on the tungsten x-ray target to generate photons, serving as primary x-ray source. The steel conical primary collimator attenuates the x-rays to produce a useful forward beam, which passes through the flattening filter to modulate the beam profile to acceptable flatness. This should be less than 4% for a $20 \times 20$ cm$^2$ field at a depth of 10 cm.[56] The flattening filter shape will thus differ for the different energy beams. The exact dimensions and shape of the flattening filter had to be found by trial-and-error, simulating iteratively until a clinically equivalent and acceptable beam was produced. The monitor chamber is used clinically for dose monitoring and the Mylar mirror reflects light through the entrance window of the treatment head as a visual representation of the x-ray field geometry through the various jaws and the MLC.

This section (x-ray source) is fixed for the specific energy beam and is simulated once to produce a phase-space file that can be used as a starting point for all future simulations. The file is run for 100 million histories.

The final beam geometry per field setup is shaped by rows of the MLC in conjunction with the backup X jaws for the x-direction, and using the Y jaws in the y-direction. This section is shown in the bottom part of Figure 3-1. The beam shaping collimators are constructed from tungsten. In the IMRT plans the intensity of the beam will be modulated through using various segments/configurations of the MLC. The positions of these collimators differ per beam and thus this part of the simulation is run separately each time, using the phase-space file of the x-ray source as input.

### 3.1.1. Structure in BEAMnrc

To create the linac, standard Component Modules (CMs) found in BEAMnrc are used, as illustrated in Figure 3-2 and Figure 3-3.

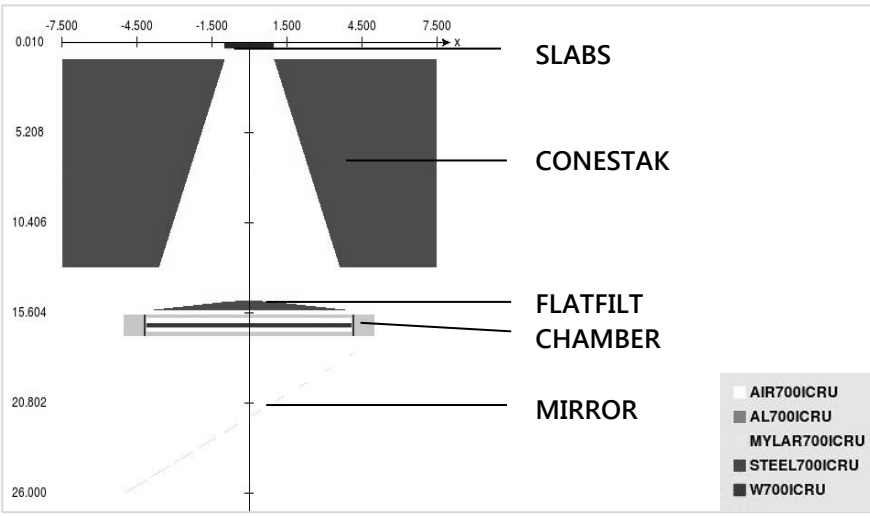


**Figure 3-2: Component Modules (CMs) for x-ray source**
**The CMs used with their materials and dimensions (cm) are shown for the 6 MV linac model**

The flattening filter consists of 2 layers, and the thickness is slightly different between the 6 and 10 MV linac models. All other CMs in the x-ray source section are identical for both energies.

The field shaping section has an 80-leaf divergent MLC and diverging jaws. The parameters in the JAWS and MLC CMs are chosen to create the required field sizes (FSs) at a Source-to-Surface distance (SSD) of 100 cm.

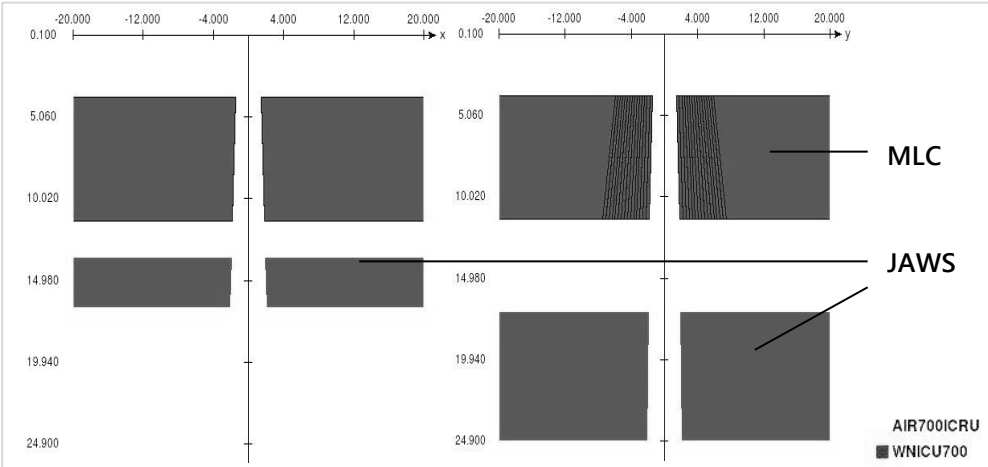


**Figure 3-3: Component Modules (CMs) for Field shaping section**
**Configuration shown is for a $10 \times 10$ cm$^2$ field. Dimensions are in cm**

## 3.2. Generating beam data for commissioning

The linac model described above is used to generate 6 and 10 MV photon energy beam data respectively, stored in phase-space files. The phase-space beam data from BEAMnrc is used as input for DOSXYZnrc. The DOSXYZnrc code is then used to generate the dose distribution in either a $50 \times 50 \times 50$ cm$^3$ water tank model or a 'chamber' in air, as required. The necessary beam data to be used in the TPS (as required in XiO[57]) are Profiles, Percentage depth doses (PDDs), Total scatter factors (TSCFs), Collimator scatter factors (CFs), absolute calibration data, and MLC & collimator transmission. The above are extracted from different simulations in DOSXYZnrc. A summary of the required square FSs and the data extracted from it is given in Table 3-1.

**Table 3-1: Summary of beam data required by XiO.**
**Profiles required are shown for Inplane (Inp), Crossplane (Crp) or Diagonal (Diag) directions. Percentage depth dose curves (PDDs), Total scatter factors (TSCF) and Collimator scatter factors (CF) are also indicated**

| FS (cm$^2$) | Profiles | PDDs | TSCF | CF |
|---|---|---|---|---|
| 1×1 | | | ☑ | |
| 2×2 | | ☑ | ☑ | |
| 3×3 | | ☑ | ☑ | ☑ |
| 4×4 | | ☑ | ☑ | ☑ |
| 5×5 | Inp, Crp | ☑ | ☑ | ☑ |
| 7×7 | | ☑ | ☑ | ☑ |
| 10×10 | Inp, Crp | ☑ | ☑ | ☑ |
| 12×12 | | ☑ | ☑ | ☑ |
| 15×15 | Inp, Crp | ☑ | ☑ | ☑ |
| 20×20 | Inp, Crp | ☑ | ☑ | ☑ |
| 25×25 | Inp, Crp | ☑ | ☑ | ☑ |
| 30×30 | Inp, Crp | ☑ | ☑ | ☑ |
| 35×35 | Inp, Crp, Diag | ☑ | ☑ | ☑ |
| 2×10 | Inp, Crp | | | |

In reality the various measurements require data from square FSs categorised as 'scanning' or 'non-scanning', depending on the type of measurement one would do with actual dosimetry equipment. The 'scanning' data are the profiles and PDDs on the Central Axis (CAx), and the 'non-scanning' data are the TSCFs, CFs, absolute calibration data and MLC & Collimator transmission factors. Apart from the CFs and transmission factors, all data are measured in water.

All DOSXYZnrc dose data is stored in 3D dose files (*.3ddose); one for each simulation run. These files contain the dose scored in each voxel. To extract the required data in the form of PDDs, profiles at specific depths, and scatter factors (as described in Table 3-1 and Table 3-2), a simple Fortran code was written. The code reads in the location of each voxel and its associated dose, and writes out only the required data to a text file. To ensure adequate profile/PDD data sampling, this code takes the average of the central voxel doses within 3 rows of voxels when extracting profile/PDD data. This is illustrated in Figure 3-4. The statdose code from the EGSnrc package can also be used, but cannot extract diagonal profiles. Therefore the Fortran code was written for this purpose.

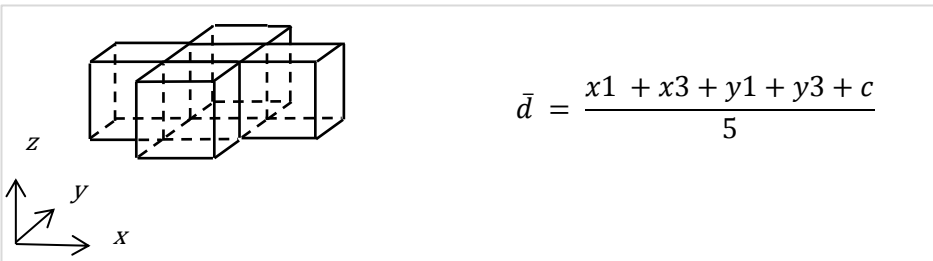


$$\bar{d} = \frac{x1 + x3 + y1 + y3 + c}{5}$$

**Figure 3-4: Dose averaging in 3D when extracting profiles/PDDs**

### 3.2.1. Water tank data

*'Scanning' data*

All of the 'scanning' data are collected at a SSD of 100 cm and various depths. A summary of the depths at which profiles are obtainable is given in Table 3-2. The depth '$d_{max}$' refers to the depth of maximum dose, which in this case is around 1.5 cm for 6 MV and 2 cm for 10 MV, depending on various scattering conditions.

For the 'scanning' data, the watertank phantom used in the simulations is created separately for each FS to ensure the best resolution where necessary (i.e. over field penumbrae and the peak of small fields, as well as the PDD maximum) while minimizing the amount of voxels used in areas where data is not required. This greatly reduces the number of histories to be run for adequate statistics, and therefore also the computer simulation time. As a rule of thumb, roughly 10 000 histories per voxel are needed for a variance of 1%. For all FSs the depth resolution is set to 2 mm covering the first 6 cm, and 5 mm thereafter. The lateral voxel size definition is set out in Table 3-3.

**Table 3-2: Summary of Profile depths**
**Depths in water for required profiles (Inplane and Crossplane) and Diagonals are shown**

| Profiles | Depths (cm) | | | | | | | | | | |
|---|---|---|---|---|---|---|---|---|---|---|---|
| Aligned | $d_{max}$ | - | - | - | - | - | - | 5 | 10 | 20 | 30 |
| Diagonal | $d_{max}$ | $d_{max}$-0.5 | $d_{max}$+0.5 | 0.5 | 1 | 2 | 3 | 5 | 10 | 20 | 30 |

**Table 3-3: Water tank lateral voxel size definition for 'scanning' data**
**The number of voxels with its associated size is shown for various FSs**

| FS ($cm^2$) | Number of voxels per size | | | | | | |
|---|---|---|---|---|---|---|---|
| | | | 5 mm | 0.5 mm | 5 mm | | |
| 1x1 | | | 46 | 80 | 46 | | |
| 2x2 | | | 45 | 100 | 45 | | |
| | | | 5 mm | 1 mm | 5 mm | | |
| 3x3 | | | 44 | 60 | 44 | | |
| 4x4 | | | 43 | 70 | 43 | | |
| 5x5 | | | 42 | 80 | 42 | | |
| | 5 mm | 2 mm | 5 mm | 2 mm | 5 mm | 2 mm | 5 mm |
| 7x7 | | | 39 | 55 | 39 | | |
| 10x10 | | | 35 | 75 | 35 | | |
| 12x12 | | | 32 | 90 | 32 | | |
| 15x15 | 25 | 50 | 4 | 5 | 4 | 50 | 25 |
| 20x20 | 20 | 50 | 9 | 5 | 9 | 50 | 20 |
| 25x25 | 15 | 50 | 14 | 5 | 14 | 50 | 15 |
| 30x30 | 10 | 50 | 19 | 5 | 19 | 50 | 10 |
| 35x35 | 5 | 50 | 24 | 5 | 24 | 50 | 5 |

*'Non-scanning' data*

The 'non-scanning' data, i.e. the TSCFs, is scored in a single central voxel within the watertank at a depth of 10 cm and a SSD of 90 cm. The chosen voxel width is 0.1 cm for FSs $1 \times 1$ to $4 \times 4$ $cm^2$, 0.5 cm for $5 \times 5$ and $7 \times 7$ $cm^2$, and 1 cm for $10 \times 10$ $cm^2$ and larger. The factors are calculated from the absolute dose ratios with reference to the $10 \times 10$ $cm^2$ field.

*Absolute dose*

The absolute calibration data in a real situation would be a measurement of the dose rate (cGy/MU) for setup conditions. However, in the simulated case the dose is a relative concept. The MC simulation will always produce an absolute dose output, irrespective of the number of histories run. For simplicity, the absolute MC calibration dose was subsequently related to be 1 cGy/MU for a $10 \times 10$ $cm^2$ field at the isocenter at a depth of 10 cm (i.e. SSD = 90cm). A simulation is run with these exact conditions and the MC dose scored in the isocenter voxel (average of 3 adjacent voxels to reduce variance) is related to 1 MU and used as dose conversion factor for all MC simulations.

### 3.2.2. In-air data

For the in-air simulations a chamber is created. The chamber consists of a couple of voxels of water surrounded by a copper 'cap'. The input file for DOSXYZnrc consists of a phantom containing the chamber, copper cap, and surrounding air, and is created from a code written in IDL.[58] A voxel resolution of 0.9 mm was used to produce an adequate number of voxels to model the 'rounded' edge. A copper cap is required in the measurement of CFs to ensure Lateral Electron Equilibrium (LEE). Li *et al.* have done a study showing the water thicknesses required to achieve LEE for linacs of various x-ray energies.[59] The required thickness of copper can subsequently be determined by its relative density to water. A factor of roughly 0.25 cm/MV is used as a conservative guide for the 2 energies used in this study, and the copper thickness calculated from Eq.3-1.

$$d \geq \frac{E}{\rho_{cap}} \times 0.25 \qquad \textbf{Eq. 3-1}$$

| | |
|---|---|
| $\mathrm{E}$ | Energy |
| $\mathrm{d}$ | thickness |
| $\rho_{\mathrm{cap}}$ | density of copper relative to water |

The CFs are then simulated with the chamber position at the isocenter (SSD = 100 cm) in a similar manner to the TSCFs. The MLC & Collimator transmission factors are also obtained from this setup, with the relevant collimator fully closed in each case. The factors are determined relative to the open field reading at the same position. Since the generic linac is fully manipulable, the transmission factors could be simulated without using special apertures.

### 3.2.3. Formatting data for transfer

The transfer of data to XiO requires data to be in a known file format. A list of vendor formats are supported.[60] Since the data in this study is generated with MC, transfer of the data is not a simple process. The OmniPro Accept[61] software is well known to the authors and works well with XiO. The ASCII file format used in OmniPro Accept was therefore chosen as template. An IDL code was developed to create ASCII files readable in OmniPro Accept containing the data required.

After reading the newly created ASCII files into OmniPro Accept, some de-noising is applied from within this software. The same filter is used as would be the case for measured data. PDDs are de-noised with an Envelope smoothing (4 mm) filter using Spline interpolation (0.5 mm) available in the software. For the profiles however, the smoothing in OmniPro Accept alone applied to the MC data was found to be inadequate. This is due to small variations in the 'flat' region of the fields.

To reduce this, the boxcar filter available under the function smooth in IDL (Eq.3-2) is applied on the profiles before converting to ASCII. The filter is used on the open-field part of the profiles only by using the weighted sum of five ($w$) adjacent voxels to calculate a floating average.

$$R_i = \frac{1}{w}\sum_{j=0}^{w-1} A_{i+j-\frac{w}{2}}, \qquad i = \frac{w-1}{2}, \dots, N - \frac{w+1}{2} \qquad \textbf{Eq. 3-2}$$

| | |
|---|---|
| N | number of elements in A |

This step provides adequate de-noising of the data to use the filter in OmniPro Accept. All profiles are first symmetrized and then de-noised using a median filter to remove noise while preserving the penumbrae. The final dataset is then saved as a single file (*.rfb) for transfer to XiO.

Multiple successive steps of de-noising/smoothing can cause artefacts on the data. Care was taken to avoid this by choosing a single filter on the PDDs and profiles respectively with negligible effect on the curves' shape, with the addition of only the boxcar filter in the open region of the fields to allow successful filtering of the profiles in OmniPro Accept. For more on data smoothing, the reader is referred to the book of Siminoff.[62]

## 3.3. Commissioning linac on XiO

This linac is fully commissioned on the TPS, following the procedure as recommended by the vendor.[60] Firstly, a new linac is created on the TPS and all physical parameters of the machine set. This consists of settings relating to the general machine parameters, gantry movements, jaw nomenclature, collimator and MLC values, and couch movements.

The measured data is then transferred to XiO by importing the dataset into the newly created linac via the connected computer with the OmniPro Accept software. The various factors (i.e. TSCFs, CFs, and absolute calibration data) are typed in manually. The modelling can be started after complete and accurate transfer of the data has been verified.

### 3.3.1. Modelling

The modelling process is clearly set out in the XiO beam modelling guide.[60] A short explanation will be given here for completeness.

A standard energy spectrum is selected from the template list as starting spectrum, as well as sigma and transmission values. In XiO, a single parameter per collimator can be changed to control the slope of the error function which models the penumbra. These are called sigmas($\sigma$): for the x-jaw ($\sigma_x$), y-jaw ($\sigma_y$), and the MLC ($\sigma_{mlc}$). Likewise there are transmission values per collimator: $T_x$, $T_y$ and $T_{mlc}$. These parameters are fixed over all FSs.

The relative contribution of particles in each energy bin is manually tweaked to converge to the actual data. This is evaluated through PDD comparison for various FSs. Next the sigmas and transmission values are optimized for small FSs ( $\leq 4 \times 4$ cm$^2$). The large fields are then calculated, and adjustments made to the lateral incident fluence setting and the off-axis spectrum. The final evaluation is done through comparison of PDDs and profiles over all FSs.

Due to the fact that only one sigma value can be chosen per collimator, a full convergence over all FSs is not readily achievable. This study is focused on IMRT planning with many small field segments. Emphasis is therefore placed on the smaller FSs ( $\leq 10 \times 10$ cm$^2$), using an acceptance criterion of 2mm/2% but allowing up to 3mm/3% for the bigger FSs.

The linac model is then accepted and validated for the Convolution/Superposition algorithm. The whole process is done separately for both commissioned energies. After validation, the models can be used for clinical treatment planning.

## 3.4. MC software interface

A Graphical User Interface (GUI) is created in Microsoft Visual Basic[63] to obtain all the necessary information from the DICOM files (exported from XiO) for running the simulations on the MC system. The software program is named XiO2MC. The GUI allows certain user inputs to be made and executes various commands, including code written in IDL, for certain tasks.

The user must place all relevant DICOM files (RTplan, RTstruct, RTdose, and CT data) from XiO in a single directory. In XiO2MC the user can then browse for these files, select all parameters to be used in the simulation, and start the process to create all the necessary files required by the MC system. The user interface of the XiO2MC program created in Visual Basic is shown in Figure 3-5.

The settings section includes options of the simulation parameters, including beam energy, MC variance/statistics, the number of CPUs to use, and the delivery type (to accommodate the difference in control point definition of IMRT vs. non-IMRT plans. A provision is made for future addition of dynamic MLC and VMAT plan verification.

The program output window displays the current execution commands and outputs for debugging. This includes Visual Basic and IDL feedback. This section which will be removed in the final GUI. The program status is displayed at the bottom by displaying the key steps, e.g. "Running ctcreate". A percentage bar also shows the overall progress visually.

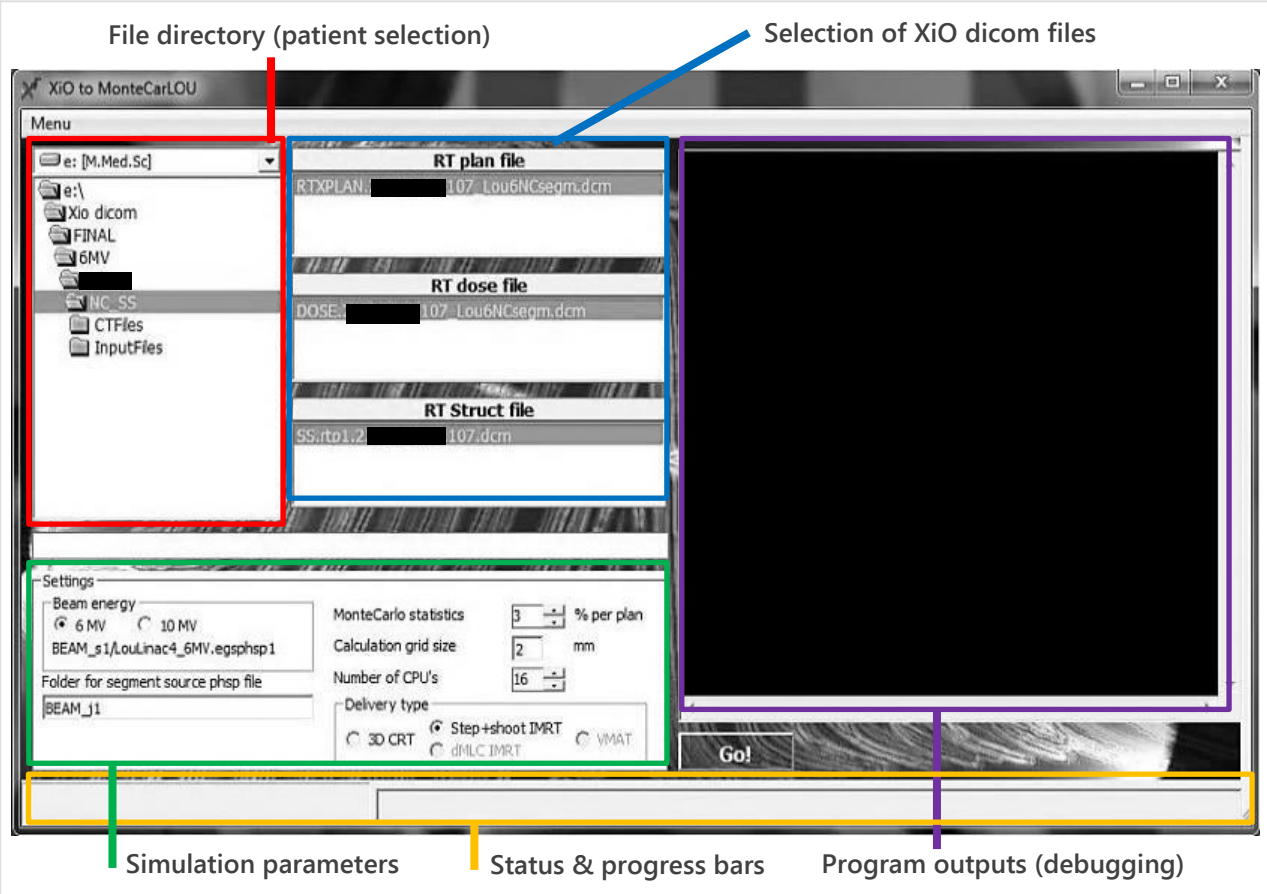


**Figure 3-5: Main GUI window of XiO2MC**

The advanced parameters as optional extra are shown in Figure 3-6. This sets various aspects of the MC simulation, saved in the input files.

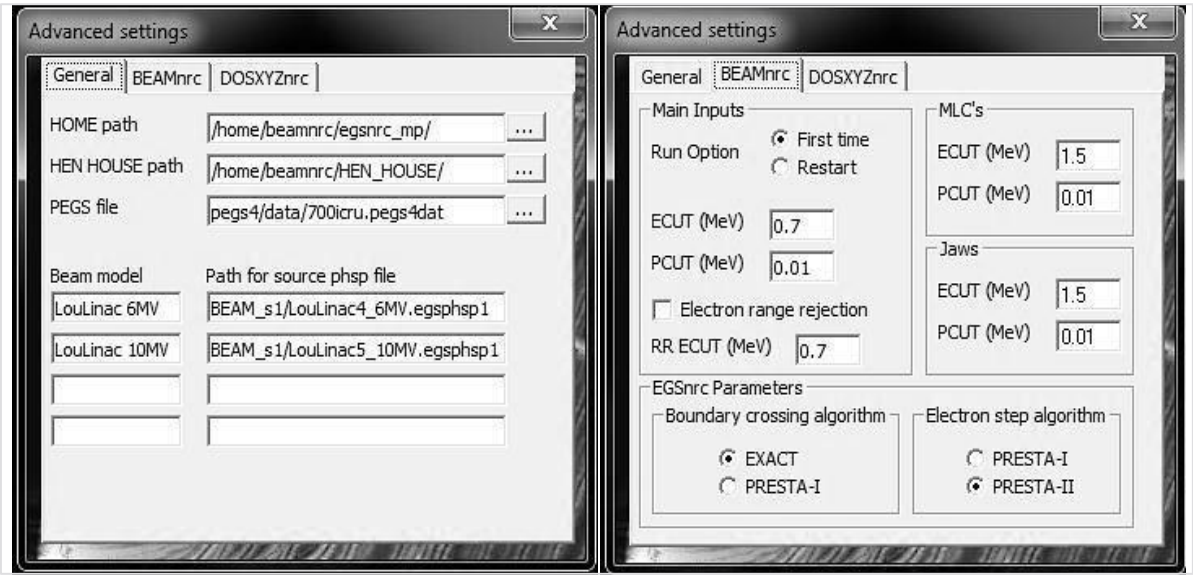


**Figure 3-6: Advanced settings windows**

### 3.4.1. Program details

The main steps of the program that executes when the user click on "Go!" are given in Figure 3-7 and will be described in more detail below.

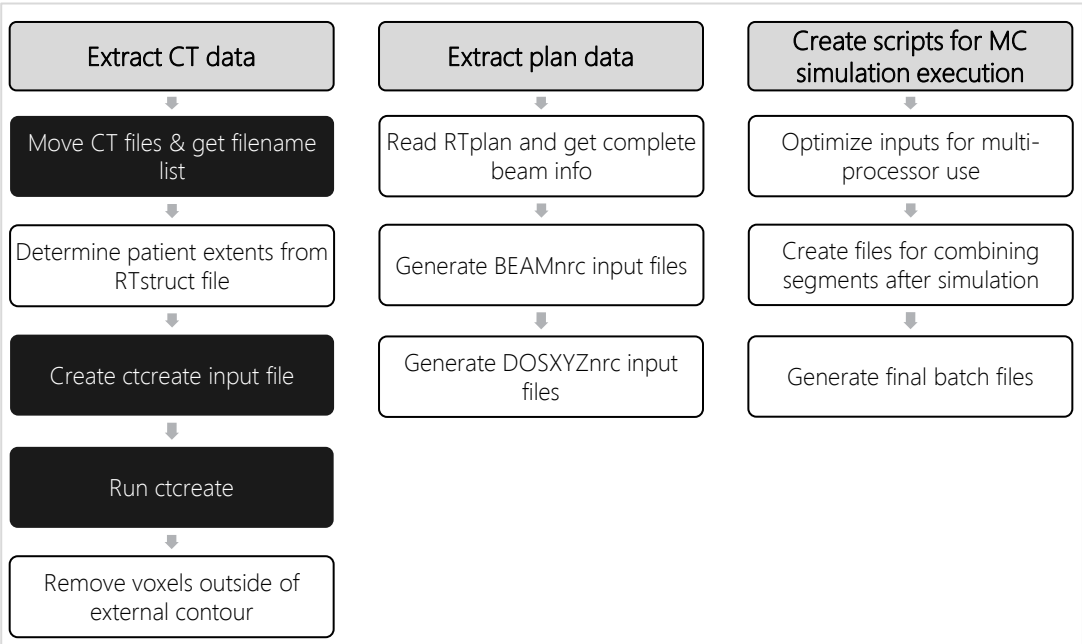


**Figure 3-7: Framework of** XiO2MC **software program**
**Sub-routines are shown in sequence; black blocks indicates** Visual Basic **and white blocks** IDL

DICOM files can be read by IDL using the built-in function IDLffDICOM. With this function, an object is created with the entire DICOM file's content linked to specific tags. Each attribute has a specific tag, which is standard in all DICOM files. For example, the attribute 'Patient's name' will always be found under the tag (0010,0010), and 'Leaf/Jaw positions' under (300a,011c). For attributes with multiple instances, like the leaf/jaw positions for each segment, a new matrix must be created in IDL and all instances of that specific tag read into a new row per occurrence.

### 3.4.2. Extracting CT data from DICOM files

The CT*.dcm series of files exported from XiO can be converted to the required format for DOSXYZnrc (*.egsphant) using the program ctcreate. This program is part of the OMEGA-BEAM package and its use is described in the DOSXYZnrc manual.[50] An input file containing the specific settings relating to the CT data to be used in ctcreate is created for this study and used throughout. The parameters chosen are: file type (based on TPS), sub volume selection, voxel size, and the conversion to electron density settings.

The sub volume limits are calculated in XiO2MC by finding the extents of the structure labelled as "external" in the RTstruct file. This is required to remove unnecessary patient data and reduce calculation time. The voxel size can be chosen by the user in the XiO2MC GUI. The conversion ramp relates a range of CT numbers with relative electron densities in a linear manner, while associating a tissue type with this range at the same time.

The Electron Density CT phantom from Qados[64] is used clinically to relate CT numbers to relative electron density values for use in TPSs. The values used in XiO are derived from measurements using this phantom, and thus these values were used for ctcreate as well. The tissue densities published in ICRU Report 44[65] are used to associate tissue types to the respective densities. The conversion ramp is shown in Figure 3-8 and the details given in Table 3-4. The tissue specific data used in the simulation is obtained from the 700ICRU pegs4data file in EGSnrc.

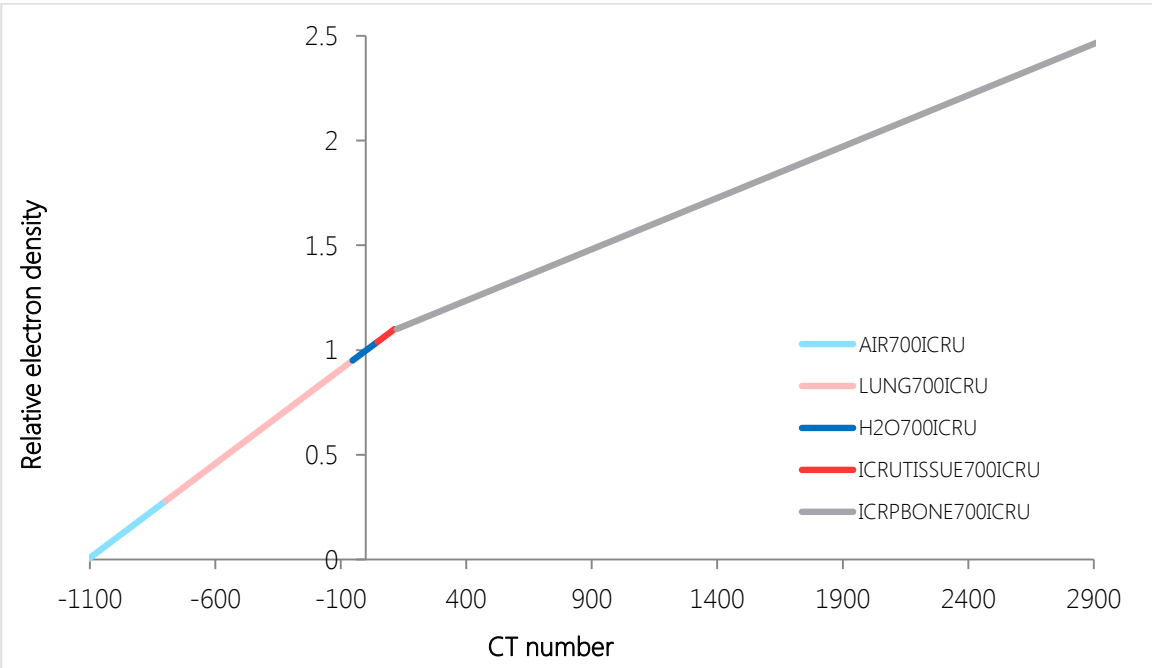


**Figure 3-8: CT number to relative Electron density ramp**
**The bi-linear ramp is exactly as in XiO, with tissue types added as shown**

**Table 3-4: CT number to relative Electron density ramp**

| Tissue type | Relative electron density | CT number |
|---|---|---|
| VACUUM | 0 | -1108.4 |
| AIR700ICRU | 0.28 | -797.3 |
| LUNG700ICRU | 0.95 | -52.8 |
| H2O700ICRU | 1.04 | 47.2 |
| ICRUTISSUE700ICRU | 1.10 | 122.7 |
| ICRPBONE700ICRU | 3.75 | 5530.9 |

In XiO2MC, the CT files are first identified and moved to a separate folder. Next, a file listing the CT*.dcm files is created, the ctcreate input file containing all set parameters is generated (as described above) and ctcreate initialized. After the .egsphant file is created through ctcreate, an IDL code is used to "remove" all voxels outside of the external contour, by setting the material type to VACUUM and the density to zero. This step ensures that no dose is scored outside of the contoured volume, as is also the case in XiO. A text file with the actual voxel dimensions and -locations in the simulation is also created to be used to match the XiO dose grid to the final simulated dose grid.

### 3.4.3. Extracting Plan data from DICOM files

The complete RTplan file is read and all attributes needed in the simulation stored in matrices in IDL. This is done by accessing the relevant DICOM tag. A list of the attributes and their DICOM tags required is given in Table 3-5.

**Table 3-5: Plan data from DICOM file**
**General and plan information are read once; Beam specifics are read for each control point**

| General info | Tag | Plan information | Tag | Beam specifics | Tag |
|---|---|---|---|---|---|
| Patient | 0010,0010 | Plan name | 300A,0003 | Gantry angles | 300A,011E |
| Patient ID | 0010,0020 | Plan description | 300A,0004 | Collimator angles | 300A,0120 |
| | | Number of fractions | 300A,0078 | Couch angles | 300A,0122 |
| | | # of beams | 300A,0080 | Monitor units | 300A,0086 |
| | | # of control points | 300A,0110 | MUs/segment | 300A,0134 |
| | | Accelerator name | 300A,00B2 | Beam energy | 300A,0114 |
| | | | | Isocenter location | 300A,012C |
| | | | | Leaf/jaw positions | 300A,011C |

The beams and segments are divided up in the RTplan file by using control points. Each segment has two control points with all settings associated to it: leaf/jaw positions and dose given. The other beam specific values are fixed for all segments in that beam. A control point gives the start conditions of the segment and the next control point its end conditions.

In step-and-shoot (SnS) mode IMRT these 2 control points have identical leaf/jaw positions and different dose/MU specification; for dynamic MLC movement they will both differ. In this way the linac is instructed all settings for the start and stop of each segment. All of the info is read and sorted in the IDL code.

The beam coordinate system of XiO is not the same as in DOSXYZnrc. A study by Zhan *et al.*[66] investigated this difference and found a way of translating from DICOM coordinates set according to IEC-61217[67] standards to the DOSXYZnrc coordinates. Their transformation is used in this study. The angles $\theta_G$ (gantry angle), $\theta_C$ (collimator angle) and $\theta_T$ (couch angle) are read from the plan, converted to radians, and mathematically translated to new values for DOSXYZnrc: $\theta$, $\varphi$ and $\emptyset_{col}$.

### a. Calculating physical leaf/jaw positions

The leaf/jaw positions in the DICOM file are in terms of the projected position at the isocenter (i.e SSD = 100 cm). However, for the simulation the exact position of the leaf within the linac $(MLC_{i,h})$ is required. To get this, a simple calculation stemming from the inverse square law and basic geometry is done, using Eq.3-3. The principle is described in Figure 3-9.

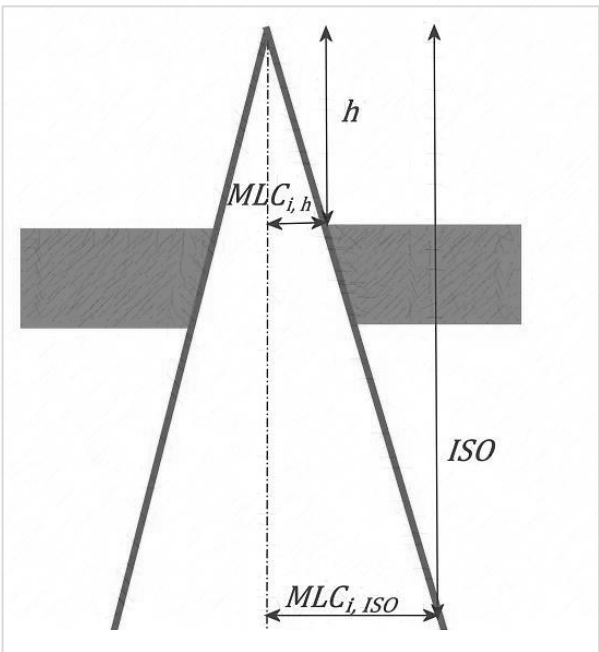


**Figure 3-9: Calculating actual MLC/jaw positions**

$$MLC_{i,h} = \frac{h}{ISO} \times MLC_{i,ISO} \qquad \textbf{Eq. 3-3}$$

| | |
|---|---|
| h | distance from source to start of MLC |
| $MLC_{i,ISO}$ | position of MLCi at ISO |
| ISO | distance from source to isocenter (100 cm) |

The slope of each leaf is calculated automatically in BEAMnrc according to the specified focus point of the linac (source to MLC distance) and MLC thickness. Similarly, the positions of the jaws can be found by replacing the MLC specifics (thickness and height) with those of each jaw in Eq.3-3.

It must be noted here that the goal was not to model a perfect MLC equivalent to that of a typical Elekta linac, but rather one based on it. Therefore the MLC described and used is simpler in geometry than an actual MLC would be, but is suitable for the purpose of this study.

### b. Calculating required histories

The required statistics of the final dose distribution is chosen by the user in the XiO2MC GUI. To achieve this, the number of histories to be run in both the simulation steps must be determined. First the open area $A$ at the isocenter per segment $i$ taken over the 40 leaf pairs is calculated (Eq.3-4).

$$A_i = \sum_{n=1}^{40} \left(x_{n,left} - x_{n,right}\right)_i \qquad \textbf{Eq. 3-4}$$

| | |
|---|---|
| $x_n$ | projected distance from the centre of the n'th leaf pair |

Here we assume a projected leaf width of 1 cm at the isocenter.

The number of voxels $v$ in the volume $V$ in which dose can be deposited resulting from segment $i$ is given by

$$v_i = \frac{A_i \times z}{res} \qquad \textbf{Eq. 3-5}$$

| | |
|---|---|
| res | resolution/dose grid size |
| z | patient thickness |

The number of histories required per segment in DOSXYZnrc ($H_dos_i$) is then

$$H_dos_i = \frac{\left(100/\varepsilon\right)^2 \times v_i}{\sqrt{N}} \qquad \textbf{Eq. 3-6}$$

| | |
|---|---|
| ε | Monte Carlo variance/ Statistics |
| N | total number of beams |

In this study a variance/statistics ($\varepsilon$) of 1% or less is chosen for all IMRT plans.

The DOSXYZnrc simulation requires an adequate number of particles in the input file (which is the result of the BEAMnrc simulation output). Thus from the required histories in DOSXYZnrc (from Eq.3-3, 3-4 and 3-5) the number of histories needed from the BEAMnrc simulations must be calculated.

To determine this, 22 different typical segment sizes were simulated in BEAMnrc using an equal number of histories each. The resulting number of particles in each .phsp-file were counted, and the result used to correlate each segment's number of input histories run, the calculated open area of the segment and the output number of particles in the phase-space files (which effectively equals $H_dos_i$). A linear relation was found, as shown in the following equation

$$H_beam_i = 0.1 \times \left[\frac{H_dos_i + (3.3\times10^6)}{A_i \times (1.77\times10^{-4})}\right] \qquad \textbf{Eq. 3-7}$$

| | |
|---|---|
| $\mathrm{H_beam_i}$ | number of histories in BEAMnrc |
| $\mathrm{A_i}$ | open area of segment |
| $\mathrm{H_dos_i}$ | number of histories in DOSXYZnrc |

### c. Creating input files

The input files for BEAMnrc and DOSXYZnrc are basic text files containing specifics of the simulation. Default settings are mostly used. However, the XiO2MC GUI allows the user to modify some parameters. The data needed are thus extracted en formatted as described previously, and written out in separate input files for each segment: a BEAMnrc and DOSXYZnrc input file each. Examples of each are given at the end of Appendix A.

## 3.4.4. Creating scripts for MC simulation execution

MC dose calculation time can be quite high for IMRT plans with multiple segments. A complete patient plan can have from 40 up to 120 segments or more. With the optimal use of multiple processors the total time can be reduced dramatically. The XiO2MC GUI has an option to choose the number of CPUs to use. This number is then used to sort the input files into batch script files so that the simulation process can run automatically.

To illustrate the process, a simple case of 4 CPUs and 10 segments is used: this is shown in Figure 3-10. A full explanation is given below.

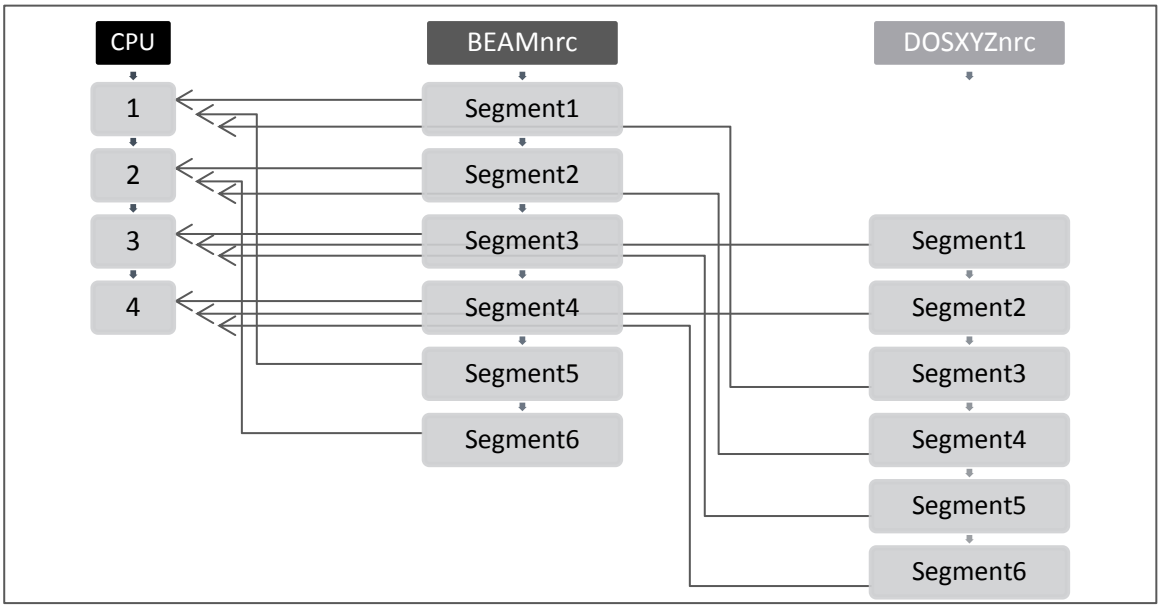


**Figure 3-10: Batch files creation process**
**Execution commands of selected input files are queued as shown**

Firstly, the segments are sorted according to the number of histories required in DOSXYZnrc ($H_dos$), in ascending order. The DOSXYZnrc simulations require the most time in the whole process, and therefore are used to govern the submission queue. From Eq.3-7 it can be seen that the number of histories required in BEAMnrc ($H_beam$) is proportional to $H_dos$. Therefore the same order applies to both simulation types.

Next, the least number of simulations per CPU is calculated to distribute the simulations over all available CPUs to ensure that all CPUs are used for the maximum time. What we have now is a list of segments in order of 'simulation time' and a number of available CPUs.

The segments are then each associated with a CPU by first adding the BEAMnrc inputs from quickest to slowest/longest to the queue, and subsequently the DOSXYZnrc inputs in the same order.

A master script is finally created to move all the files to their relevant subdirectories (as is required for the MC simulation, i.e. EGSnrc specific paths) and then execute the scripts of each CPU concurrently.

The only condition for this process to work is that there are more segments than CPUs. If this is not true, a DOSXYZnrc simulation will begin before its BEAMnrc simulation has run, resulting in a program halt. Since the number of CPUs can be selected in the XiO2MC GUI, this problem can be prevented.

After successful BEAMnrc and DOSXYZnrc simulation, the dose files have to be combined into one patient dose file. In this step, the dose of each segment is also MU scaled and converted to the absolute dose output of the linac (as defined in the TPS). A simple text file with all these details is created for this purpose: A Fortran program on the simulation computer is run by the user at the end of the simulations to combine the dose. Dose values are simply added, however the statistics (errors) are recalculated as follow (Eq.3-8):

$$\varepsilon = \frac{\sqrt{\Sigma(\varepsilon_i^2)}}{I} \qquad \textbf{Eq. 3-8}$$

| | |
|---|---|
| $\varepsilon$ | Statistics/error of complete plan |
| $\varepsilon_i$ | Statistics/error of segment $i$ |
| $I$ | Total number of segments in plan |

## 3.5. System verification

The accurate transfer of all data from the TPS to the MC system and correct implementation thereof is first tested and verified. For this purpose, several beams are set up on the TPS on various 'patients' using the newly commissioned linac models respectively. 'Patients' include a virtual water tank or scanned phantoms and actual patient data. Beams are chosen to cover a complete range of variables including gantry angle, collimator angle, and MLC and jaw positions, with their correct SSD and isocenter positions.

The absolute dose calculated for simple single-beam square fields on an actual scanned watertank are also used to validate the process.

As a final test, a conventional 3D-CRT plan is created on an anthropomorphic phantom as in an esophagus treatment case. This plan is used to ensure correct flow of the complete process from planning to dose comparison in the same way as all IMRT plans will be verified.

### 3.5.1. IMRT plans

Three different treatment sites are planned on XiO using the newly commissioned linac models; one plan per energy. The sites are ***a)*** *prostate*, ***b)*** *head and neck,* and ***(c)*** *esophagus* patients. Existing patient data is used for this purpose, and clinical dose constraints[37] are used in the dose optimization process.

The chosen protocols for each site are compiled from clinical trial data and current protocols at the clinic[68–70] for the specific patients used. The planning parameters and beam arrangements for each treatment site are summarised in Table 3-6 and Table 3-7.

**Table 3-6: Summary of Target and OAR doses**
**Fractionation schedule is shown in brackets**

| Target | Parameter | Dose (Gy) | OAR | Parameter | Dose (Gy) |
|---|---|---|---|---|---|
| Prostate (30#) | | | | | |
| Prostate + SV | $D_{100}$ | 79.2 | Rectum | $D_{50}$ | 60.0 |
| PTV1 | $D_{98}$ | 79.2 | | $D_{35}$ | 65.0 |
| PTV2 | $D_{98}$ | 50.4 | | $D_{25}$ | 70.0 |
| | | | | $D_{15}$ | 75.0 |
| | | | | $D_{max}$ | 84.7 |
| | | | Bladder | $D_{50}$ | 65.0 |
| | | | | $D_{35}$ | 70.0 |
| | | | | $D_{25}$ | 75.0 |
| | | | | $D_{15}$ | 80.0 |
| | | | | $D_{max}$ | 84.7 |
| | | | Small bowel | $D_{33}$ | 45.0 |
| | | | | $D_{max}$ | 80.0 |
| Head and Neck (30#) | | | | | |
| GTV | $D_{100}$ | 76.0 | Parotid gland | $D_{50}$ | 20.0 |
| PTV | $D_{98}$ | 72.5 | | $D_{max}$ | 81.3 |
| | | | Spine | $D_{max}$ | 50.0 |
| Esophagus (25#) | | | | | |
| GTV | $D_{100}$ | 45.0 | Lungs | $D_{55}$ | 5.0 |
| PTV | $D_{98}$ | 45.0 | | $D_{50}$ | 10.0 |
| | | | | $D_{30}$ | 20.0 |
| | | | | $D_{25}$ | 30.0 |
| | | | | $D_{max}$ | 49.5 |
| | | | Spine | $D_{max}$ | 50.0 |

**Table 3-7: Beam arrangement for IMRT plans**
**Increments between beams are shown over the range of gantry angles**

| | Prostate | Head & Neck | Esophagus |
|---|---|---|---|
| Number of beams | 7 | 8 | 5 |
| Increments | 51° | 33° | 52° |
| Range | 207° - 153° | 228°- 99° | 256° - 104° |

In all plans the immobilization device is contoured where applicable. The same external contour defined in XiO is used to define the dose calculation volume for MC as well. Dose calculation in XiO is done on a 2mm grid using the Superposition algorithm in all cases, and the segmentation method set to *SmartSequencing*. The option to apply heterogeneity corrections in XiO was also switched on to ensure dose calculation to the medium, as is the case in the MC dose calculations as well. The IMRT optimisation and segmentation settings include parameters like minimum segment size, minimum MUs per segment, smoothing, number of iterations, etc. These are set slightly different for each plan to obtain the best outcome. These settings can be viewed in the reports given in Appendix A.

## 3.6. TPS dose verification

The final output of the MC simulation process is a single .3ddose file containing the total dose scored in each voxel for the complete MU-scaled IMRT plan. Dose comparison is done by means of 4 methods: Single slice isodose/profile comparison, 2D-gamma ($\gamma$) analysis, Dose difference maps, and Dose Volume Histogram (DVH) comparison.

*Isodose/Profile and 2D Gamma comparison*

The first 2 tests are performed in the OmniPro I'mRT[71] software. Among other, this software can import and analyse dicom RTdose files, as well as general ASCII files. The .3ddose files are converted to ASCII using an IDL code. During this step the dose calculation statistics are also analysed and saved. Both dose volumes (MC dose in ASCII format and XiO RTdose) are imported side-by-side in OmniPro I'mRT and normalised to the prescribed dose. The reference slice is selected, and smoothing applied via a $3 \times 3$ median filter available in the software - this step provides adequate de-noising for comparing isodoses and produce sound DVHs without altering the dose distribution. Selected isodose levels are displayed in a separate overlay comparison window, or alternatively profiles can be shown for any line through the dose distributions.

The 2D-$\gamma$ is calculated automatically in the software for the user selected criteria. A fine grid is necessary for this step, thus both dose grids are converted to 1 mm resolution using the same linear interpolation method in the software. A $\gamma$-map is calculated and displayed in a separate window similar to the isodose comparison, using a Distance-to-Agreement (DTA) and Dose Difference (DD) criteria of 2mm/3%. A region of interest (ROI) is drawn and the Histogram of the $\gamma$-values $(0 < \gamma \leq 1)$ can be used to determine a % pass rate for the slice and selected ROI.

2D isodose comparison can also be done on mcshow,[72] a program included in the MCBEAM package developed by the Fox Chase Cancer Centre. This software reads the .egsphant and .3ddose files and displays it in a single window, as long as both dose files have the exact same voxel dimensions and amount as the .egsphant file. A quick conversion of the RTdose file to .3ddose format in IDL allows for displaying both dose distributions simultaneously with the patient densities in the background.

*Dose difference and DVH comparison*

The final 2 tests are done using an IDL code. The XiO RTdose and MC .3ddose files are read in, in conjunction with the RTstruct and egsphant files. The TPS and MC doses are subtracted from each other to generate a dose difference map at a chosen slice. The prescribed dose for the plan is asked from the user to normalise to. The actual dose distributions and difference map are overlaid semi-transparently on the egsphant data to visually illustrate dose discrepancies on the patient anatomy.

The built-in histogram function in IDL is used with the volume contour data from the RTstruct file to calculate the DVH for each structure in the plan. A bin size of 0.1 Gy is used. The output of the histogram function is a pure frequency distribution; a further summing of counts from highest to lowest dose is needed to get to the actual cumulative DVH. The DVH is calculated separately for the TPS and MC dose distributions, and plotted on a single graph. A few dose-volume parameters are also extracted from the data and saved in a simple text file to quantify differences seen in the DVH.

---

*The data collection, transfer and modelling work on the TPS was carried out personally, based on previous experience in the department*

*Programming work in this study was done on a standard computer running Windows 7*
*All simulations (BEAmnrc and DOSXYZnrc) were run on a dual Intel Xeon™ 2.4 GHz 8-core CPU computer using the Linux openSUSE 12.1 platform*

---

# Chapter 4: RESULTS+DISCUSSION

## 4.1. The generic linac

Virtual linacs were successfully created in BEAMnrc as described by Figure 3-2 and Figure 3-3 for both energies. The $20 \times 20$ cm$^2$ field BEAMnrc simulations were used to simulate dose in the watertank (in DOSXYZnrc) and analysed to determine adequate flattening of the flattening filter. Since the virtual linac is based on a typical Elekta linac, the filter dimensions (thickness and shape) were changed and simulations re-run until the flatness was within specifications. The final product is shown in Figure 4-1.

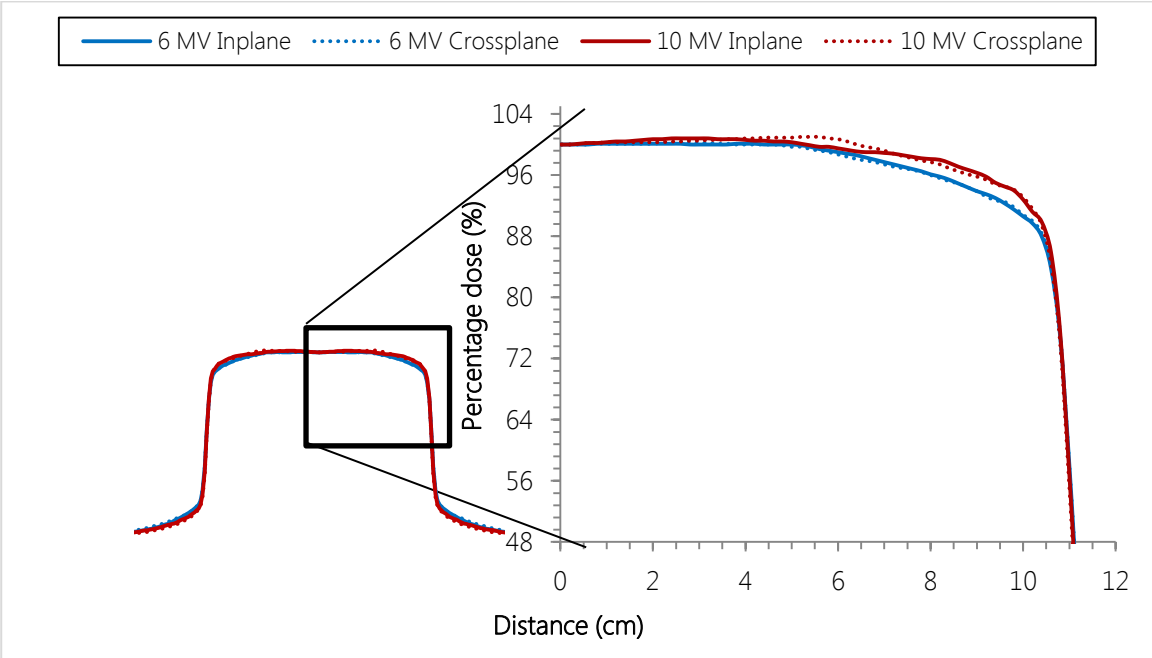


**Figure 4-1: 20x20 cm$^2$ Profiles for flatness analysis**
**Flatness is calculated over the central 80% of the field width**

The flatness is 3.0% Inplane and 3.1% Crossplane for the 6MV linac, and 2.1% Inplane and 2.6% Crossplane for the 10MV linac. This is well within the acceptable range of 4%.

A histogram plot of the energy spectra below the jaws for both energy linacs as obtained from the package BEAMdp (included as part of the BEAM software) are shown in Figure 4-2. Data are from the $10 \times 10$ cm$^2$ fields. Energy bins were set at 0.1 MeV over the complete energy range.

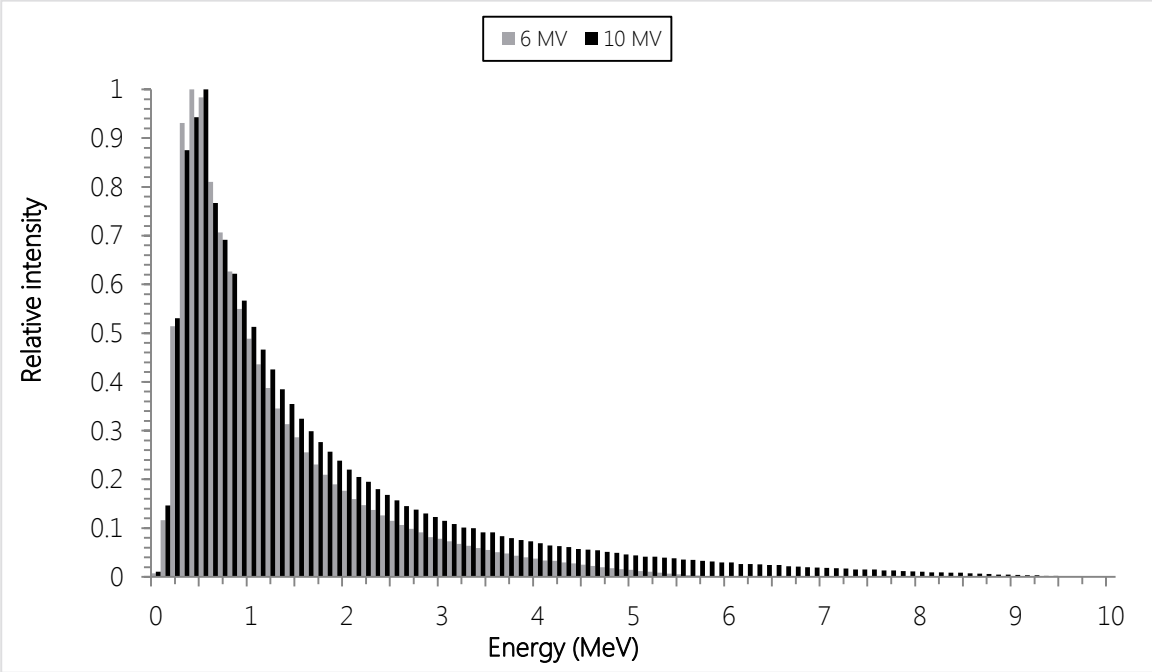


**Figure 4-2: Energy spectra of simulated linacs**
**Spectra were obtained below the last CM (JAWS) using** BEAMdp**.**

The energy spectra are typical of linear accelerators, with the highest contribution below $\frac{1}{3}$ of the maximum energy. The two linac models were accepted as reasonable representations of an actual linac, considering the intention of this study. With the acceptable flattening filter shape and realistic energy spectra known, full scale MC simulation could commence.

The upper portion of the linac (x-ray source), which includes all components from the primary x-ray source to just below the mirror, was simulated for both energies (see Figure 3-1). A phase-space plane was defined just above the secondary collimation system, to record the dynamic variables of exit particles from the simulation. Sufficient histories were simulated to create master phase-space files to use throughout the rest of the study. The latent uncertainty of the phase space files were less than 0.5%.

## 4.2. Beam data for commissioning

The 'scanning' part of the watertank data was simulated in DOSXYZnrc for each required FS as previously described. The simulations were split into smaller batches to utilize the available CPUs simultaneously and optimise their usage. The required profiles and PDDs were then extracted using the Fortran code as described in the 'methods' section. Simulation of any FS automatically produces a full 3D dose dataset. Profiles and PDDs were extracted for all required FSs from this watertank data.

### 4.2.1. RAW data de-noising

PDDs for a selection of FSs are shown in Figure 4-3. The effect of the de-noising filter in OmniPro Accept is indicated.

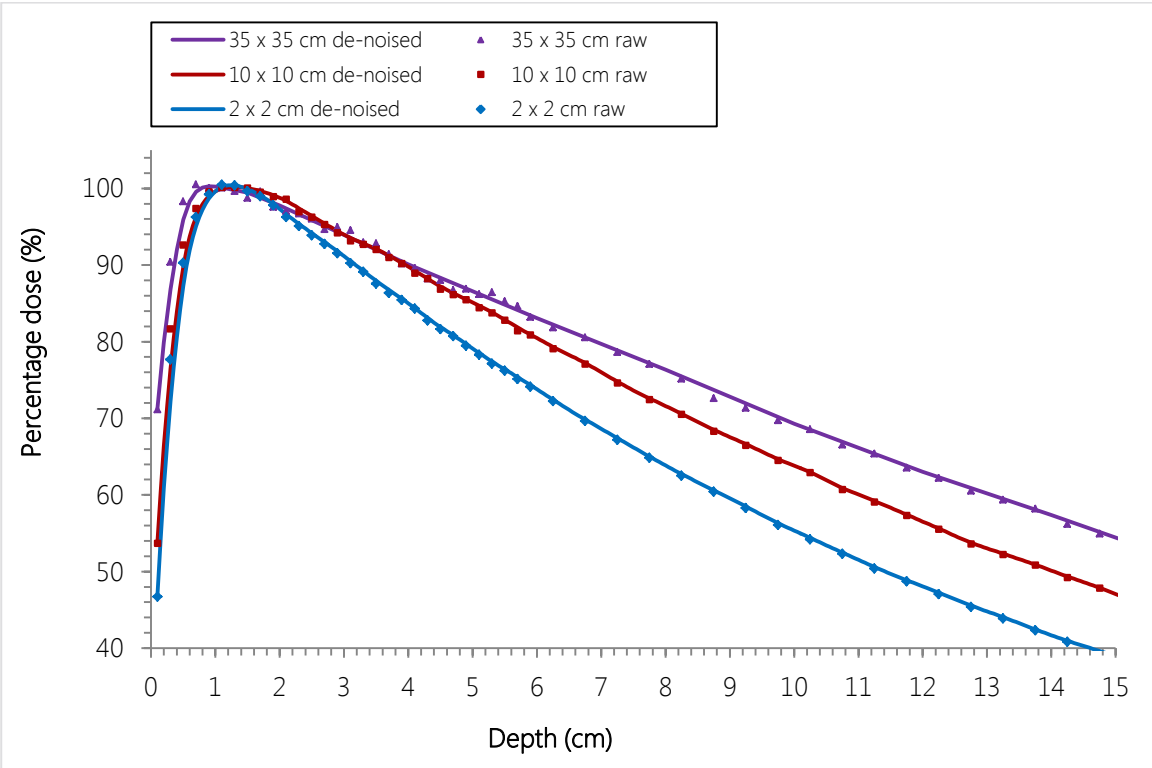


**Figure 4-3: De-noising effect on PDDs for 6MV linac over the first 15 cm depth**
**PDDs are normalized at $d_{max}$ (1.5 cm)**

As described already, the profiles were de-noised in 2 steps. First a boxcar filter was applied to the open field part of all profiles during the conversion to ASCII format (see Methods section 3.2.3 page 3-6). The effect of this de-noising is shown for the 6MV linac for selected FSs at various depths in Figure 4-4 and Figure 4-5. Only half-profiles are shown in this section, since profiles are made symmetrical.

The complete profiles were then further de-noised and symmetrized in OmniPro Accept separately for each FS. A Spline interpolation and Median filter (of width unique to each FS) was applied, followed by making the profiles symmetric (average of both sides). The effect was similar for the 10MV linac and therefore not shown here (see Appendix A for results of 10MV: Figure A-1).

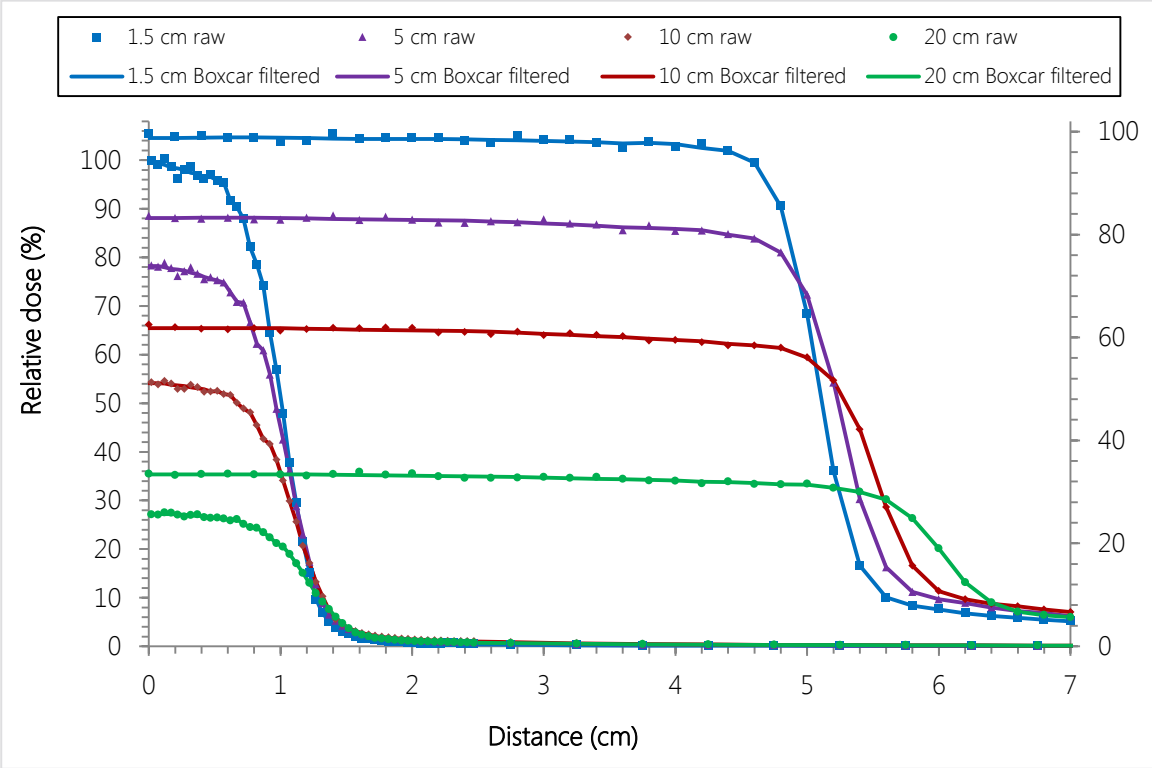


**Figure 4-4: Boxcar filtering for the $2 \times 2$ cm$^2$ (left axis) and $10 \times 10$ cm$^2$ (right axis) fields**
**Half-profiles are shown for the Crossplane direction at different depths**

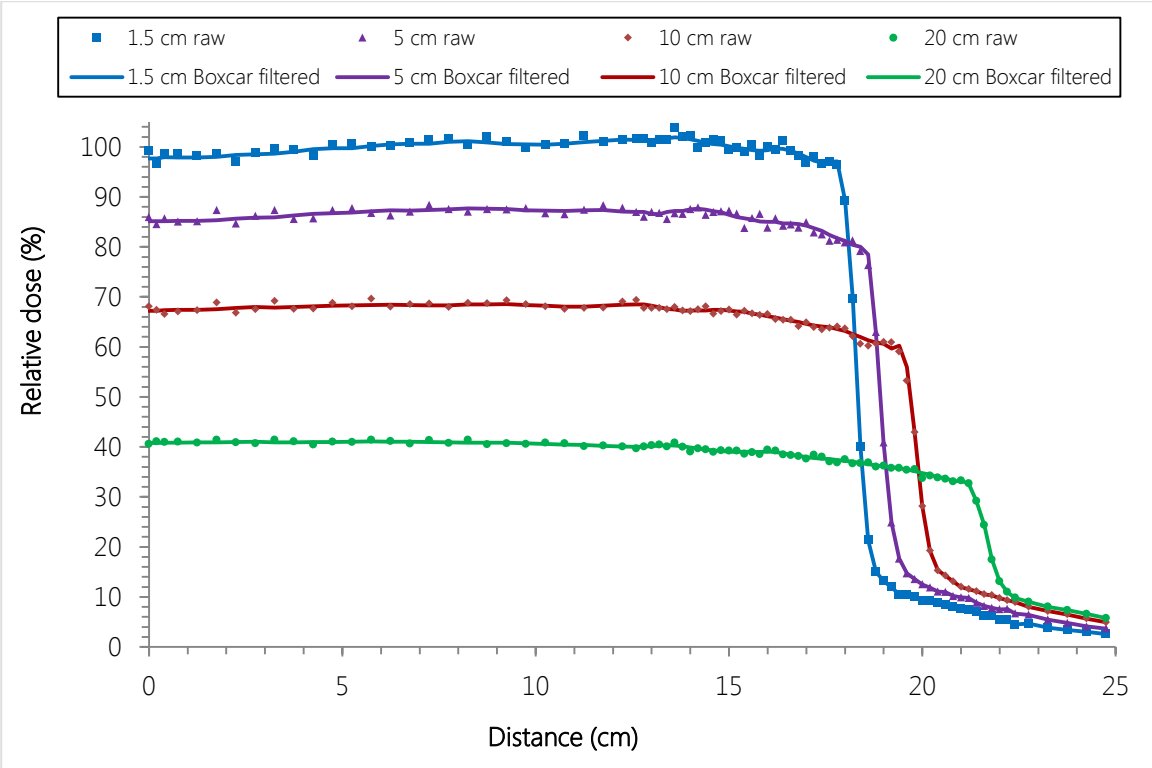


**Figure 4-5: Boxcar filtering for the $35 \times 35$ cm$^2$ field**
**Half-profiles are shown for the Crossplane direction at different depths**

The de-noising achieved with the boxcar filter was found to be a very effective tool, as long as the cut-off point was well away from the start of the penumbra. Although this retained a slightly noisy cross over from the open filed section to the field edge (especially on larger FSs and shallow depths), the effect was minimal and could be effectively removed in the final step in OmniPro I'mRT.

### 4.2.2. Final dataset

The final data were carefully analysed to confirm correct simulation of each field. In this step it was found that the odd FSs of the Inplane profiles measured at 10cm depth differed from the correct value, considering the SSD of 100 cm and beam divergence. E.g. the full width at half maximum (FWHM) of the $15 \times 15$ cm$^2$ field should measure 16.5 cm at this depth and SSD. The even Inplane profiles and all Crossplane profiles were spot-on. Careful investigation revealed a slight offset in the calculation of the Jaws' stopping positions. This happened due to automatic calculation of the jaw positions in BEAMnrc compared to manual calculations of the MLC.

As alternative to re-simulating data, the problem was circumvented by renaming the FSs affected to the actual dimensions, e.g the $15 \times 15$ cm$^2$ field becomes $16 \times 15$ cm$^2$. Only the odd Inplane profiles were affected due to the fact that the X-jaw has a small effect on the FS in comparison with the MLC due to the thickness difference. Also, the MLC leaves retract when the jaw above it covers less than 50 % of it, therefore the FS in the Y direction is largely determined by the Y-jaw position for odd FSs. The even FSs will be 'shadowed' by the MLC. This is explained in Figure 4-6.

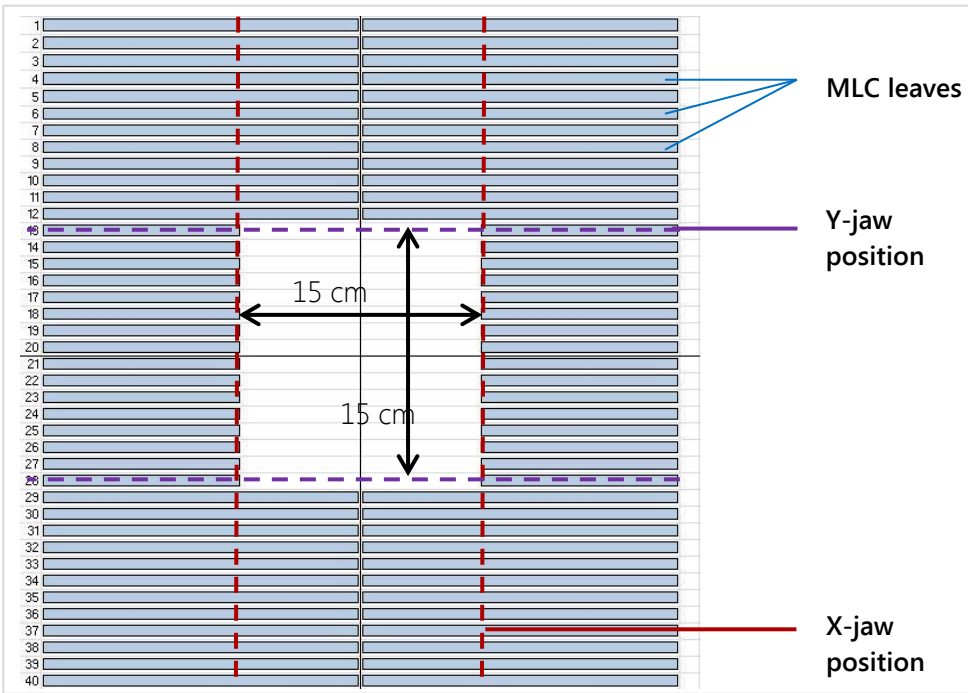


**Figure 4-6: Collimator and MLC settings to form a to $15 \times 15$ cm$^2$ field**

XiO accepted these FSs and also did calculations for the same geometries during the modelling step. The final dataset was saved in the required format (*.rfb). A selection of the profiles and PDDs is shown in Figure 4-7 -Figure 4-10.

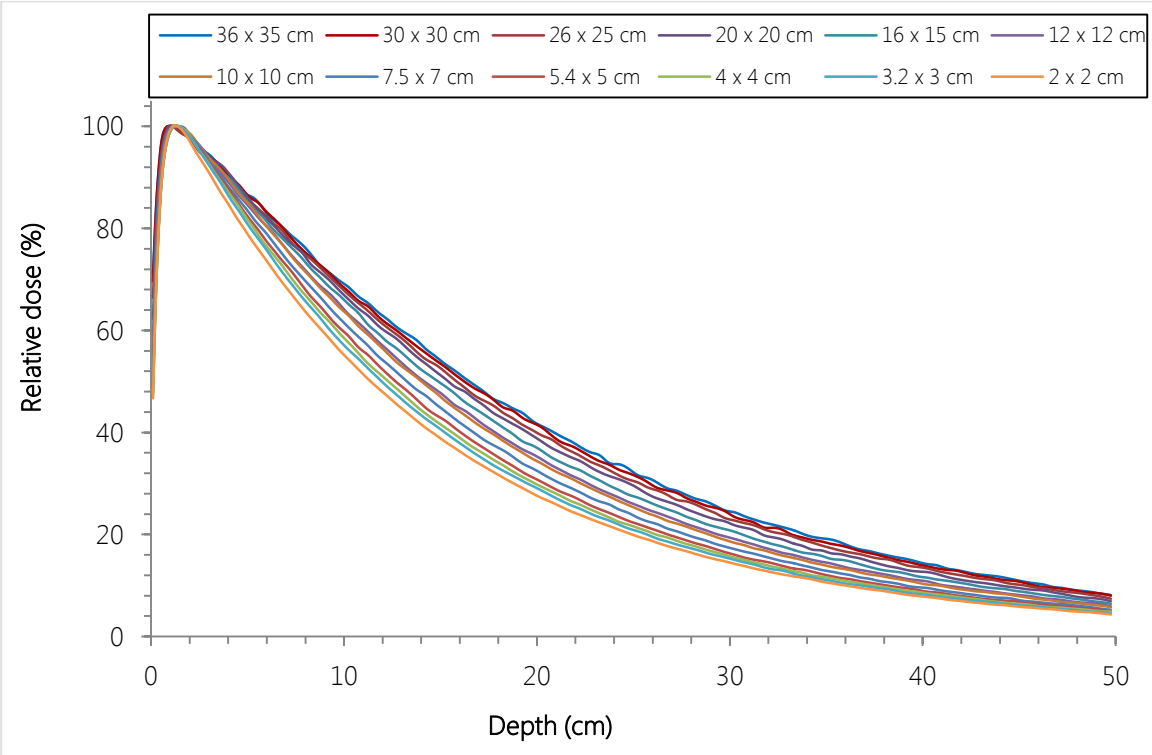


**Figure 4-7: Final PDDs for the 6MV linac over all FSs**

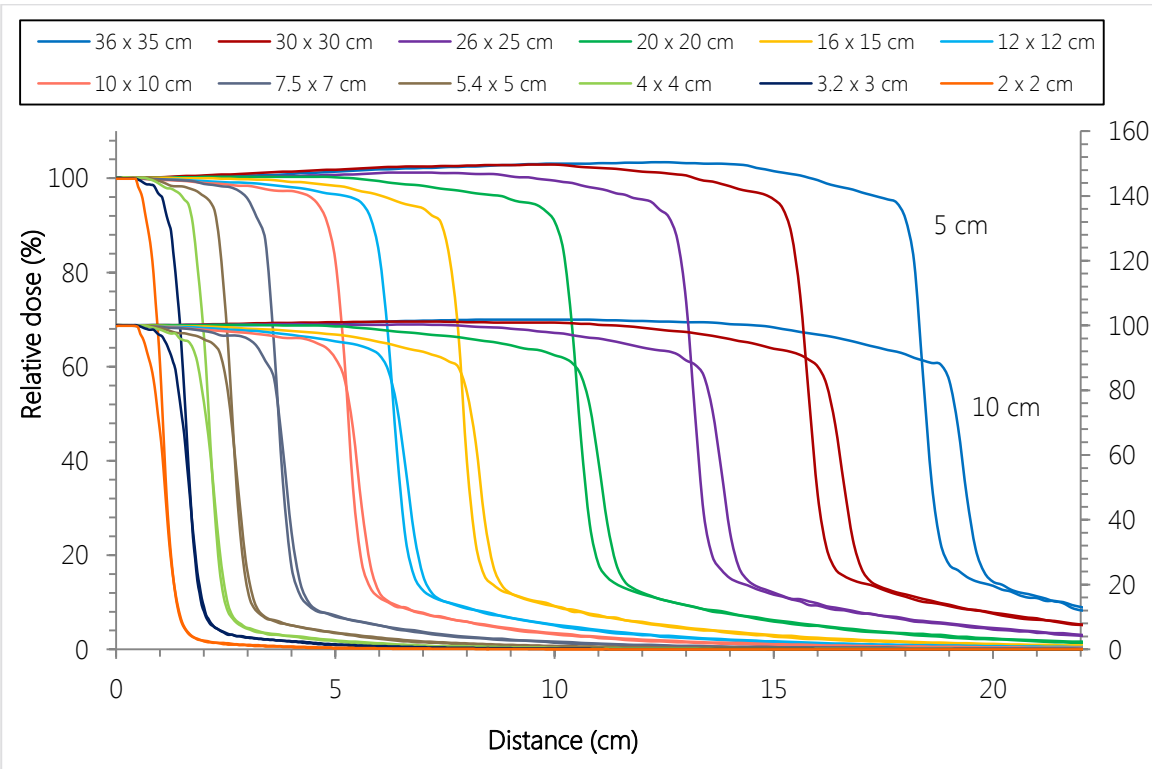


**Figure 4-8: Final Crossplane profiles for 6MV linac**
**Normalised profiles are shown at 5cm depth (top curves, left axis) and 10cm depth (lower curves, right axis)**

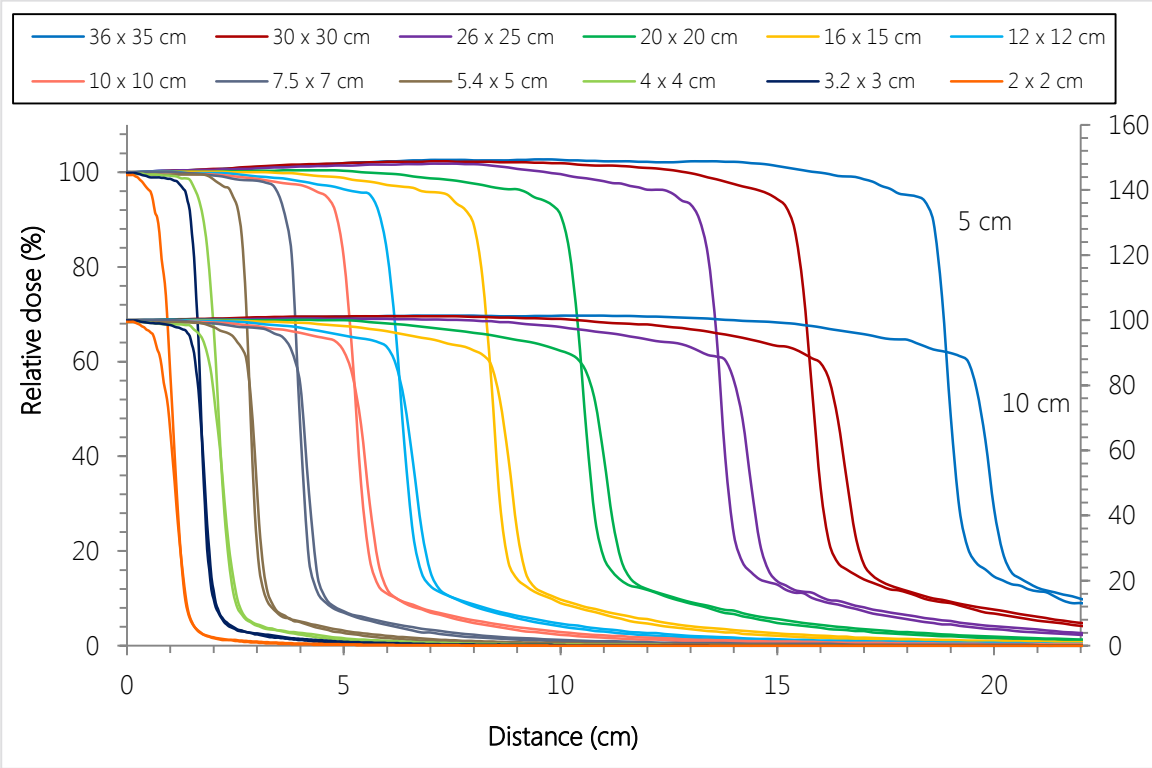


**Figure 4-9: Final Inplane profiles for 6MV linac**
**Normalised profiles are shown at 5cm depth (top curves, left axis) and 10cm depth (lower curves, right axis)**

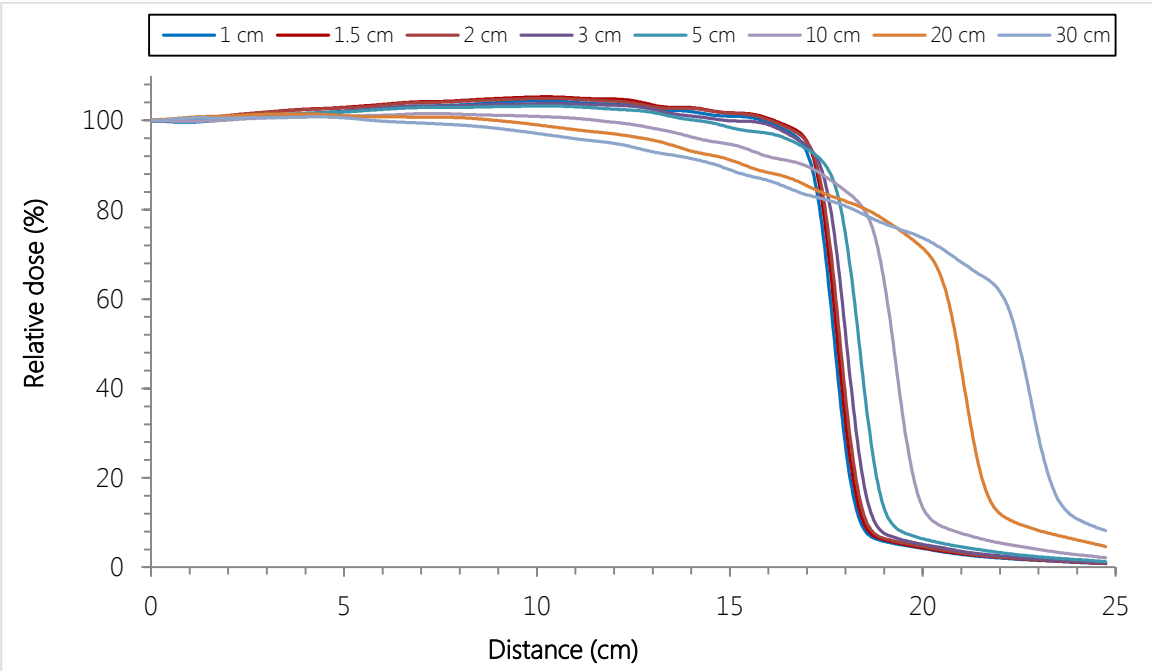


**Figure 4-10: Final diagonal profiles for the 6MV linac**
**Different depths are indicated**

The 10MV simulations were done after this was found, and thus the problem could be corrected before beam data simulations began. The data for the 10MV beam is added for completeness in the Appendix (Figure A-2- Figure A-5)

It can be seen here that some of the larger FSs are still not completely smooth. However, this is an acceptable fluctuation considering the application thereof. In the modelling process in XiO the fitting of profiles and PDDs will focus on the smaller fields and the complete shape of each curve, and not try to mimic each point.

The 'non-scanning' part of the watertank data were simulated separately. The chamber with its copper cap created in IDL (as described in section 3.2.2, page 3-6) is shown in Figure 4-11, and the calculated TSCFs and CFs in Figure 4-12.

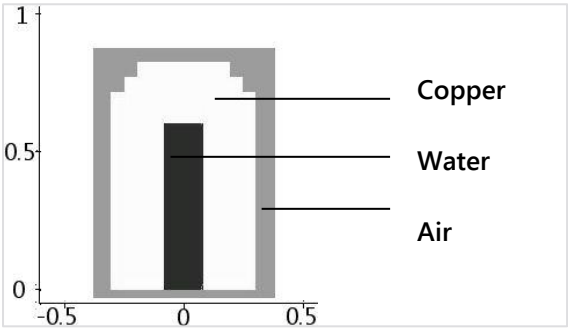


**Figure 4-11: Chamber for CF simulations**
**Dimensions are in cm**

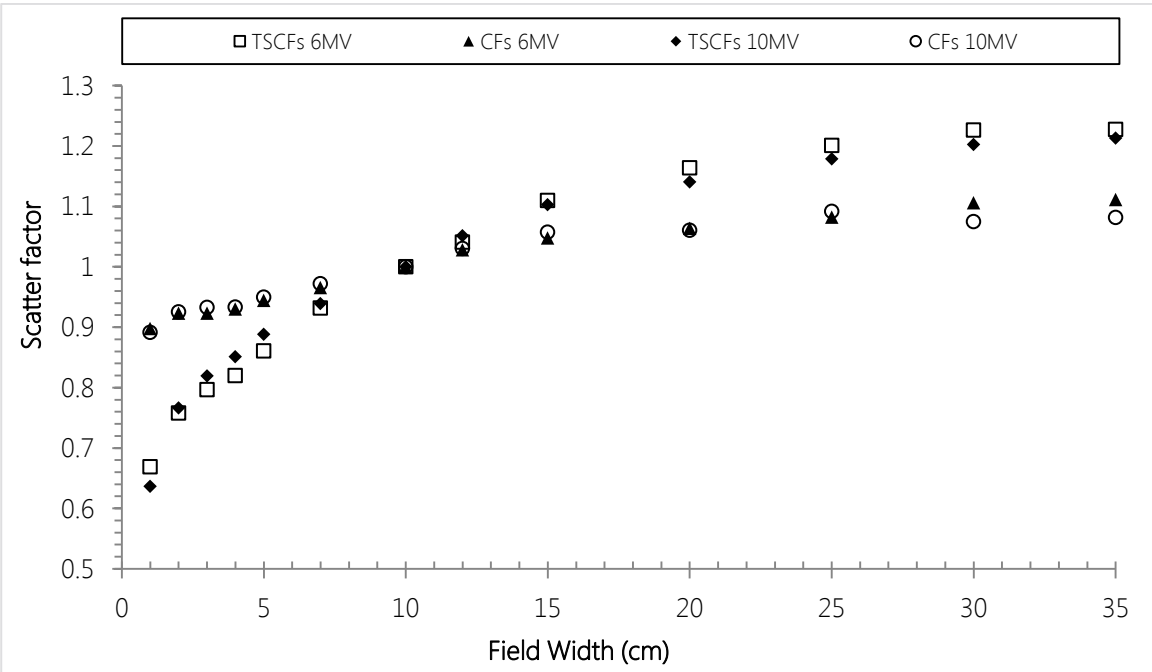


**Figure 4-12: Scatter factors for both energies for various square FSs**
**Factors are normalized to the $10 \times 10$ cm$^2$ field**

The scatter factors follow the expected trend and is comparable to factors measured on the actual linac. Factors are slightly higher above the reference FS, possibly due to the different Jaw and MLC geometries and scattering properties of the simulated linac.

The transmission factors are shown in Table 4-1 for both energies.

**Table 4-1: Transmission factors for both linac models**

| Collimator | 6 MV | 10 MV |
|---|---|---|
| Y jaw | 0.003 | 0.004 |
| X jaw | 0.084 | 0.104 |
| MLC | 0.004 | 0.005 |

The thickest collimator transmits the least radiation, as expected. The x-jaw is a backup for the MLC, hence the relatively high transmission. Values were found to be similar to actual linacs.

## 4.3. XiO modelling

The commissioning data could successfully be sent to the TPS through the OmniPro Accept program. The new linac models were created and all relevant parameters (physical dimensions and settings) entered.

### 4.3.1. Spectra & PDDs

The final CAx and off-axis spectra for the 6MV model are shown in Figure 4-13. (The 10MV spectra is shown in Appendix A: Figure A-6)

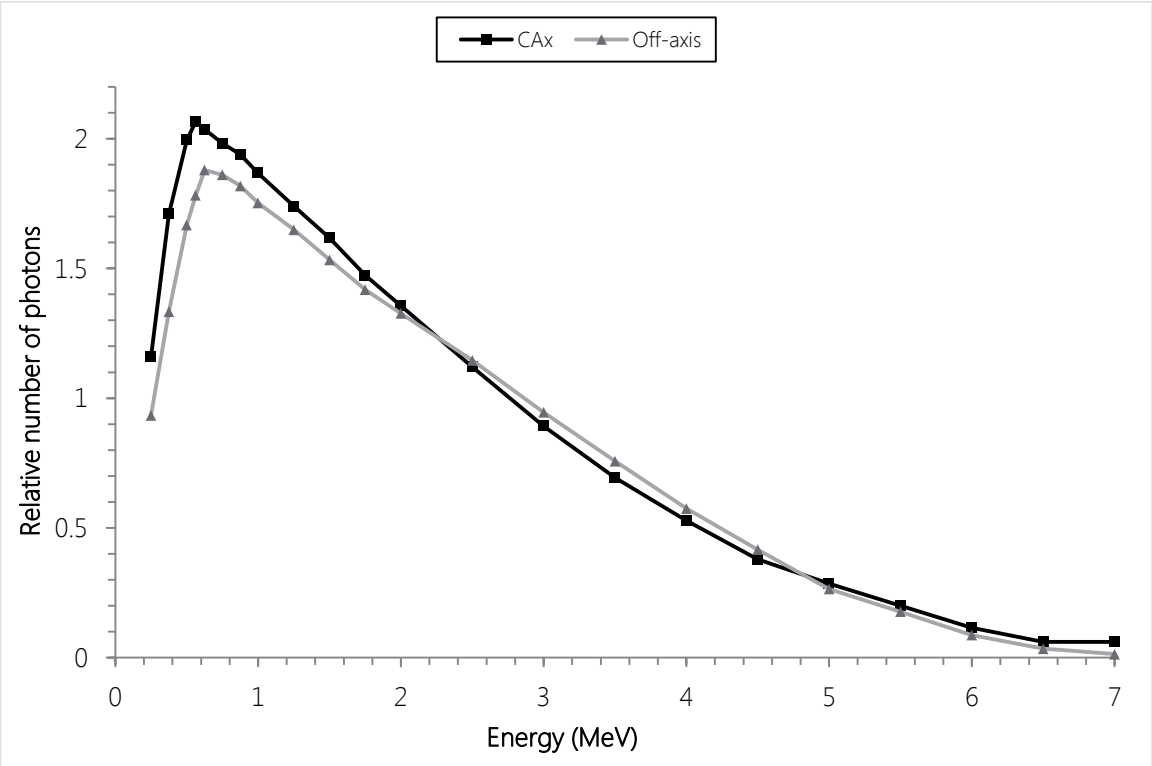


**Figure 4-13: Modelled spectra**
**The CAx and off-axis spectra are shown for the 6MV model**

The maximum energy typically exceeds the actual maximum of the linac in modelled spectra, as is the case here as well. The resulting PDDs using this CAx spectrum are shown for the smallest fields in Figure 4-14 and for larger fields in Figure 4-15. Other FSs are shown in Appendix A: Figure A-7.

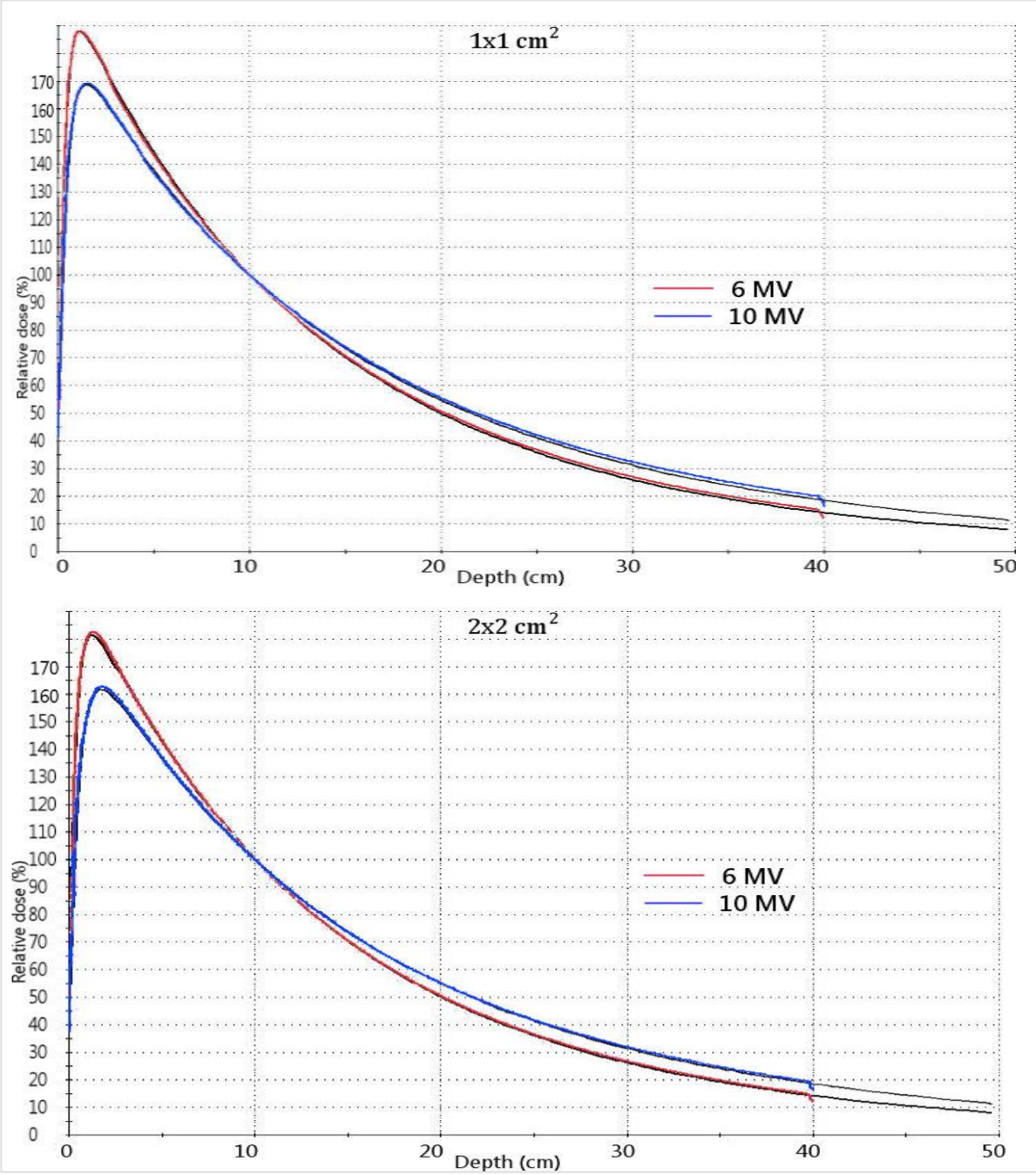


**Figure 4-14: Modelled PDDs for smaller fields**
**Calculated curves are shown in colour over the 'measured' data in black. PDDs are normalised at 10cm depth.**

Slight discrepancies in the tail region of the smallest and largest fields are evident, with XiO calculating a too high dose for the smallest field and too low dose for the largest fields. This deviation is very small and occurs at large depths, therefore having a negligible effect. The effect was similar for both energies.

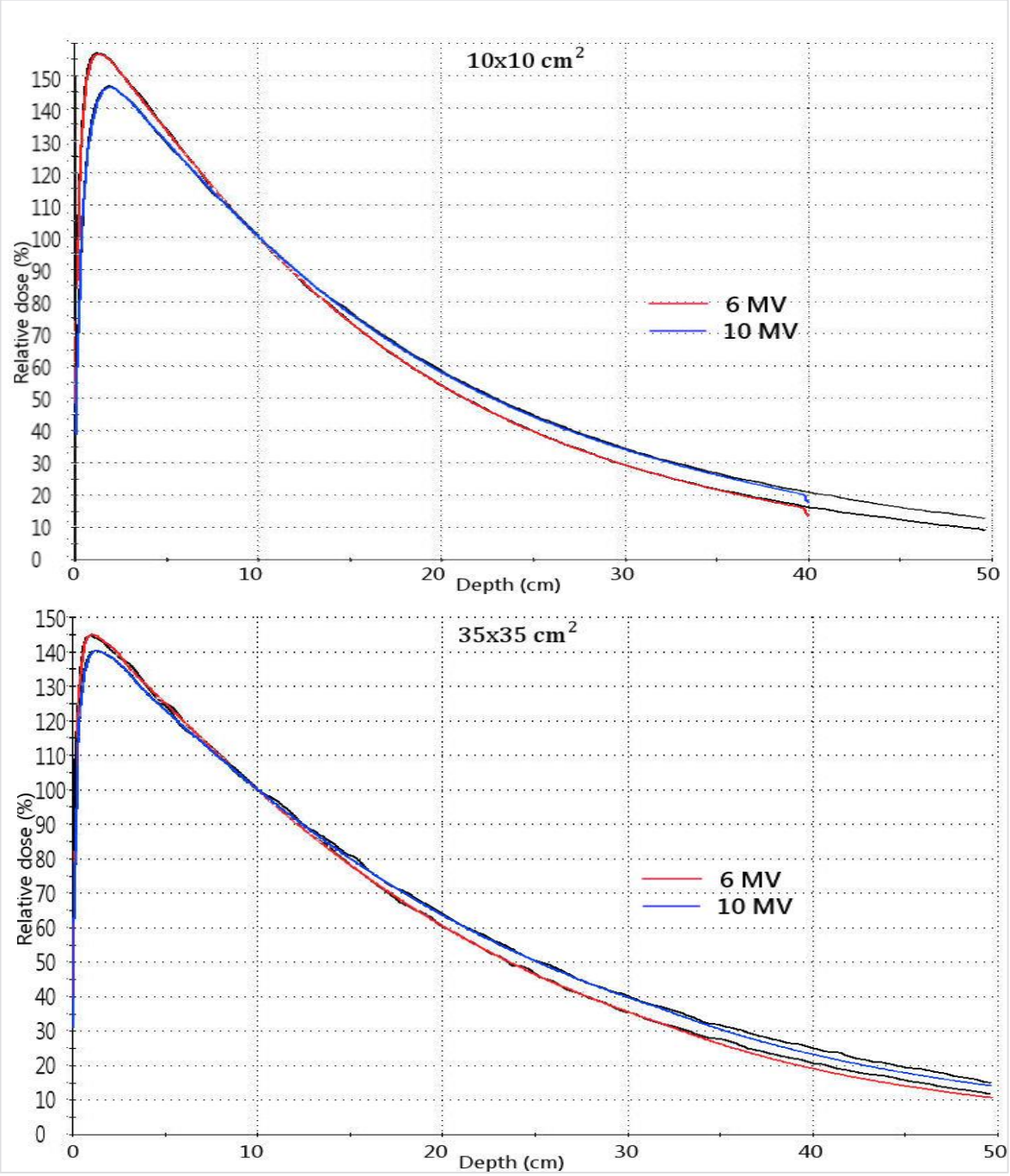


**Figure 4-15: Modelled PDDs for larger fields**

Very good agreement was found between the MC data and the XiO model over the complete set of FSs, with all calculated data points within 2mm or 2% of the 'measured' data.

### 4.3.2. Profiles

The profiles were modelled using the recommendations of the vendor, as set out in the XiO Beam modelling guide[60]. The profiles for both linacs over the range of FSs are shown in Figure 4-16 and Figure 4-17 (6MV) and in Appendix A, Figure A-8 and Figure A-9 (10MV).

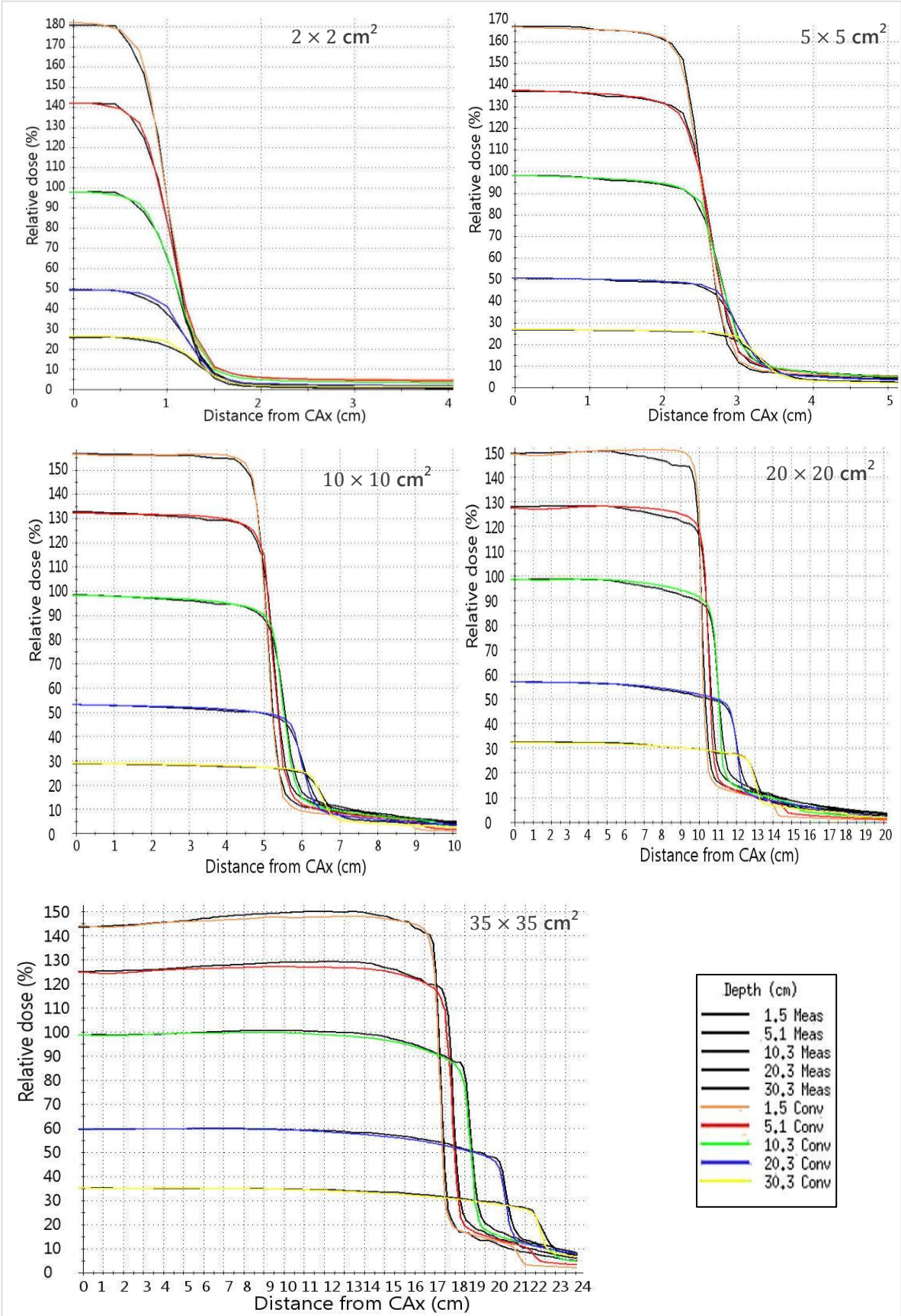


**Figure 4-16: Modelled Crossplane half-profiles for 6MV linac model**
**Calculated curves (convolution) are shown in colour over the 'measured' data in black**

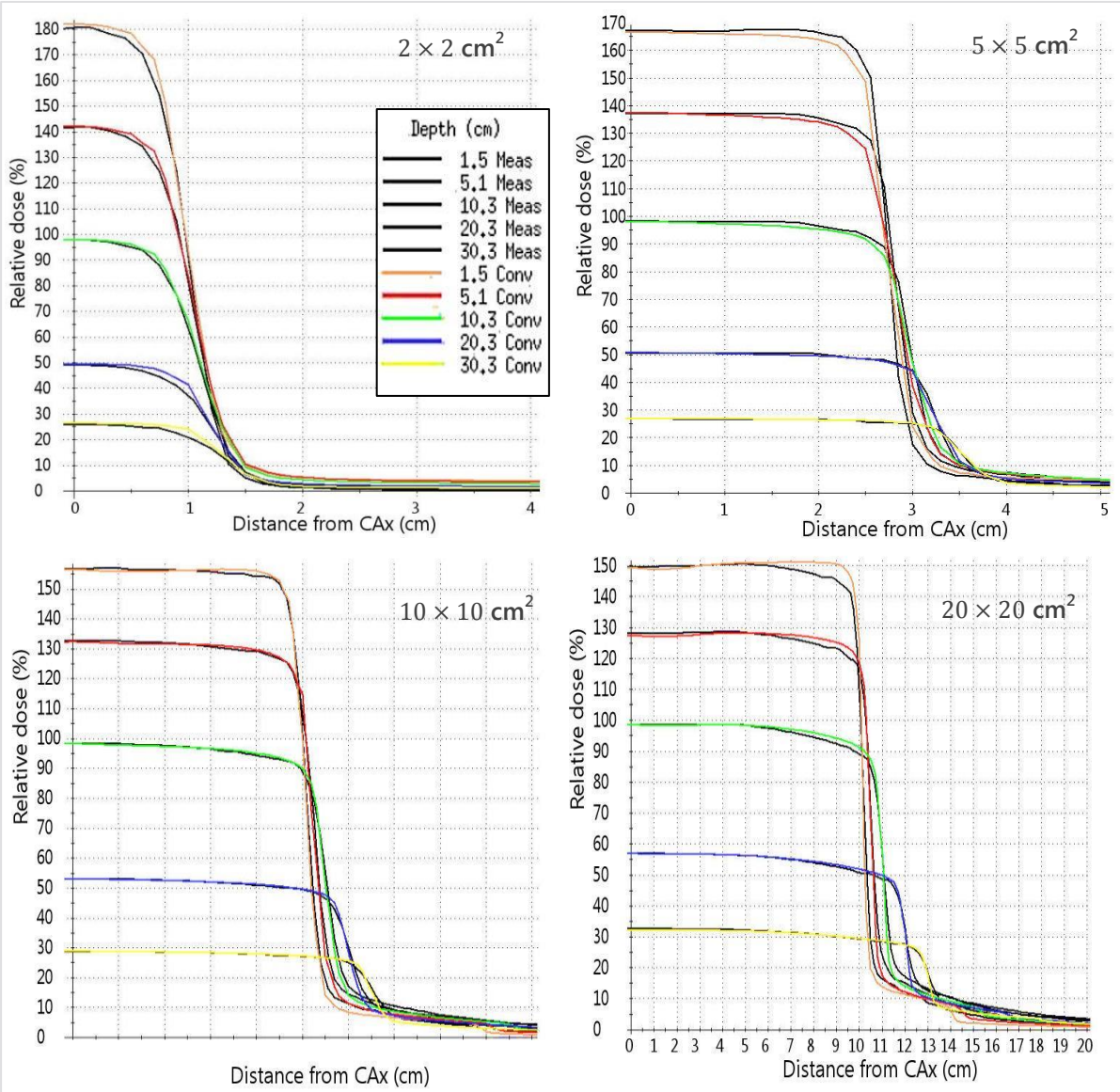


**Figure 4-17: Modelled Inplane half-profiles for 6MV**

The overall agreement was well within the accepted criteria for most FSs and depths. However, some discrepancies were found and will be discussed here.

Firstly, the main limitation of XiO modelling is evident: a single parameter per collimator for modelling the penumbrae is used over all FSs. Even considering the fact that the x-axis scaling in these graphs varies, it is clear that the slope of the penumbrae will change slightly with FS moving from very small to larger fields. Finding a suitable value is difficult; however the end result was adequate. For this study, the sigma value chosen for the MLC was the smallest possible value.

It must be noted here that the recommended scans do not explicitly require square field profiles smaller than a $5 \times 5$ cm$^2$ to be modelled, however a $2 \times 10$ cm$^2$ rectangular field must be modelled. The result of this rectangular field is virtually the same as for the Crossline profile of the $2 \times 2$ cm$^2$ field and the Inline profile of the $10 \times 10$ cm$^2$ field. FSs from $2 \times 2$ cm$^2$ to $4 \times 4$ cm$^2$ and $7 \times 7$ cm$^2$ field were modelled additionally for this study to improve the small field accuracy.

Evaluating the transmission tails of the profiles reveals the same problem: one factor per collimator describing each over all FSs. This leads to differences in this region for fields smaller than $5 \times 5$ cm$^2$ and larger than $20 \times 20$ cm$^2$.

The most obvious deviation is seen for the large fields at shallow depths, where the 'horns' of the profiles do not match. This shape is mainly influenced by the choice of depth for the fluence determination, based on the diagonal scans. The other factor that has an influence here is the off-axis spectrum. Again, a single choice influences the whole range of FSs. The largest FS seems to follow a slightly different curvature well off axis than the $20 \times 20$ cm$^2$ and $15 \times 15$ cm$^2$ fields. However, the choice of off-axis spectrum points and fluence from the diagonal scan seems to provide good results for the other FSs.

The focus of this study is on IMRT plans, which will normally create FSs well below $20 \times 20$ cm$^2$. Care was therefore taken to model the small fields as accurate as possible, in some aspects at the expense of the larger field correlation. This might have caused the deviations on the large fields. The vendor recommends modelling for IMRT treatment as aim to focus on the small to mid-sized fields (up to $20 \times 20$ cm$^2$). For these fields, the data modelling compared very well to the 'measured' data. Values were within the accepted criteria of 2mm/2%. The large fields agreed within 3mm/3%, with the exception at some specific areas as pointed out before.

## 4.4. System verification

### 4.4.1. Process validation

To ensure that the simulation geometries are read and converted correctly from XiO, test beams were created with different geometrical setups. This is described in Table 4-2, with the results in Figure 4-18.

**Table 4-2: Test beam configuration**

| | Jaw/MLC test | Gantry rotation test | Collimator rotation test |
|---|---|---|---|
| X1 position | 5 cm | 5 cm | 5 cm |
| X2 position | 15 cm | 5 cm | 5 cm |
| Y1 position | 5 cm | 5 cm | 5 cm |
| Y2 position | 15 cm | 5 cm | 5 cm |
| Gantry angle | 0° | 300° | 0° |
| Collimator angle | 0° | 0° | 70° |

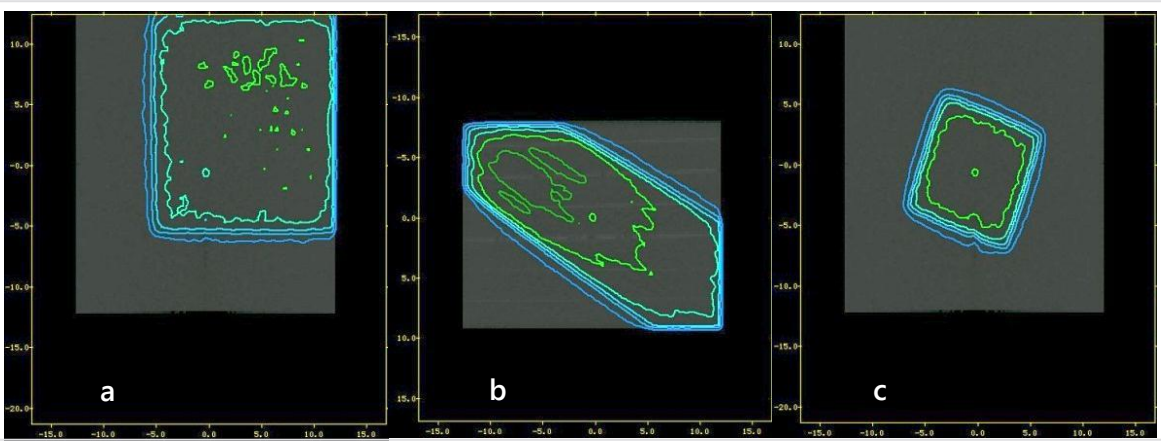


**Figure 4-18: Beams for geometry verification**
**a) Off-set field for Jaws/MLC (Beam's-eye-view), b) Gantry rotation (lateral view), and**
**c) Collimator rotation (Beam's-eye-view) tests**

The first beam is off-set in both X and Y directions, which verifies correct movement of the collimators in the planned directions. The second beam checks the gantry rotation relative to the patient/phantom and the last the collimator rotation. All movements were transferred correctly.

### 4.4.1. Watertank beams

The TPS versus simulated results for verification of the absolute dose setup is shown in Figure 4-19. The normalised dose difference is calculated according to Eq. 2-6, and the output created in IDL. The profiles and PDDs are of the actual dose distributions on the CAx and isocenter slice in OmniPro I'mRT.

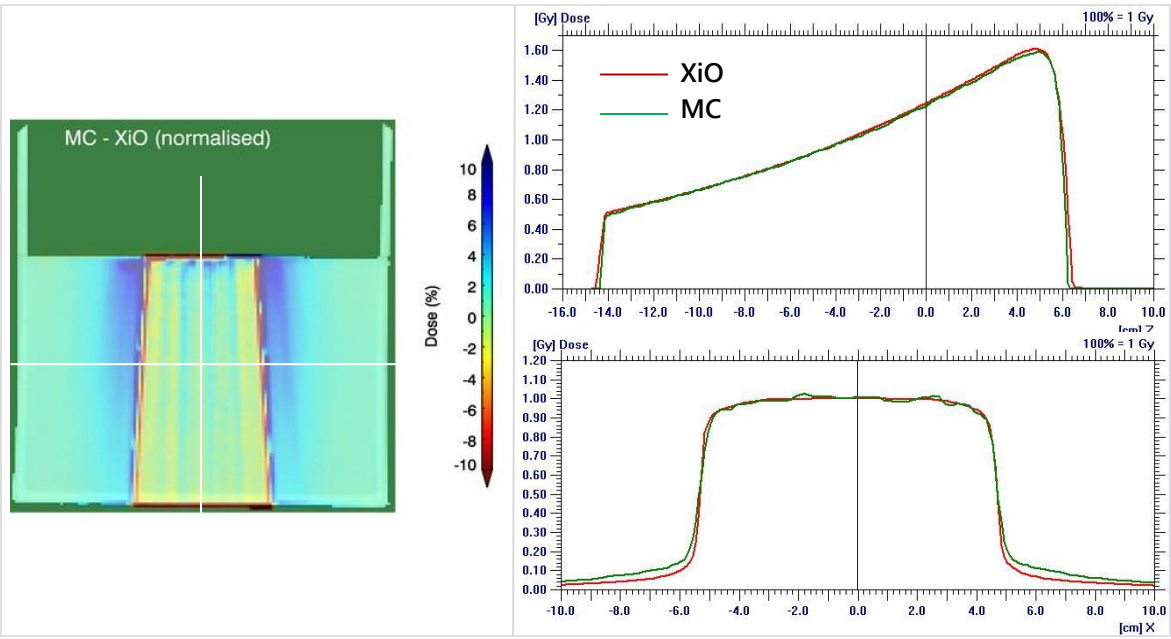


**Figure 4-19: $10 \times 10$ cm$^2$ field dose comparison for the 6MV simulation**
**Dose difference map (left) as well as CAx PDD and profile at the isocenter slice are shown (right)**

The comparison shows a perfect correlation on the PDD and absolute dose value at the isocenter. The entrance and exit doses differ slightly, due to the manner in which the IDL code removes data 'outside' of the patient. The difference will always be exactly one voxel or nothing. The difference seen on the profile tails (transmission) is in contrast with the expected outcome stemming from the modelling process. A possible explanation for this could be the actual handling of lateral scatter in the actual water density using Superposition as compared to the ideal water density and Convolution of the modelling stage, as well as the parallel-beam approximation of XiO (as described in the theory chapter).

A simple $\mathbf{2 \times 2}$ cm$^2$ square field with the same conditions is shown in Figure 4-20. The transmission in this case matches perfectly, with only slight differences across the open field. This agrees with the possibility of a calculation error with increased FS due to the parallel-beam approximation. The 10 MV results of these fields are almost identical to the 6MV. (See Appendix A: Figure A-10 and Figure A-11)

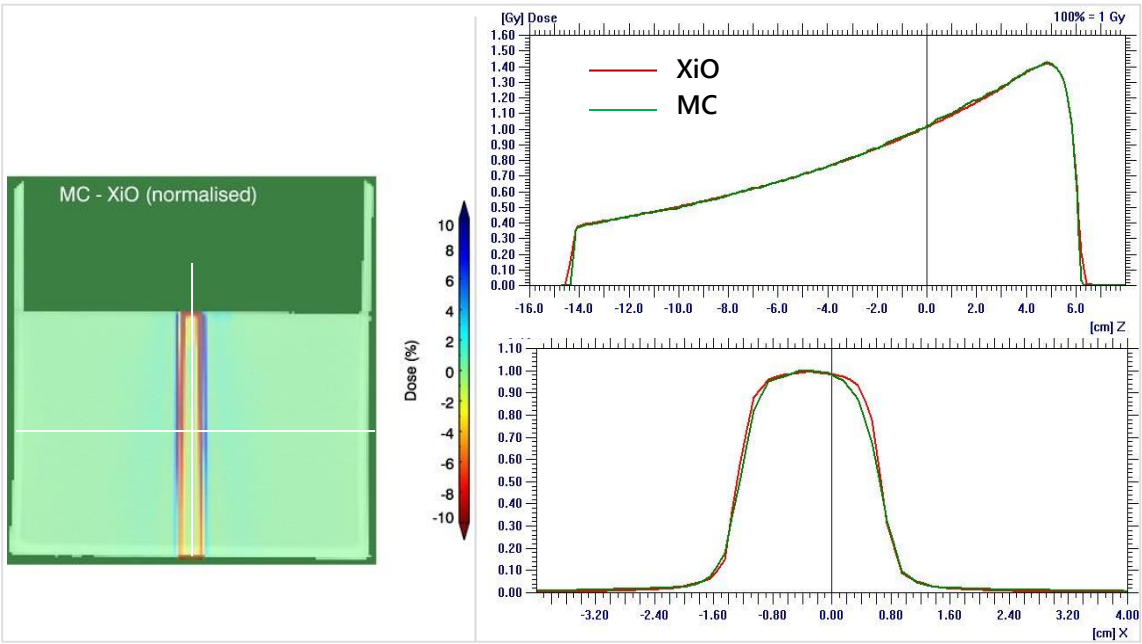


**Figure 4-20: $2 \times 2$ cm$^2$ field dose comparison for the 6MV simulation**
**Dose difference map (left) as well as CAx PDD and profile at the isocenter slice are shown (right)**

### 4.4.2. Extracted CT data

The CT data converted to *.egsphant format and subsequent removing of the data outside the patient contour is shown in Figure 4-21. Each material type has an associated number, e.g. "0" denotes Vacuum, "3" is Water, etc. The actual material densities follow the same format further down in the same file.

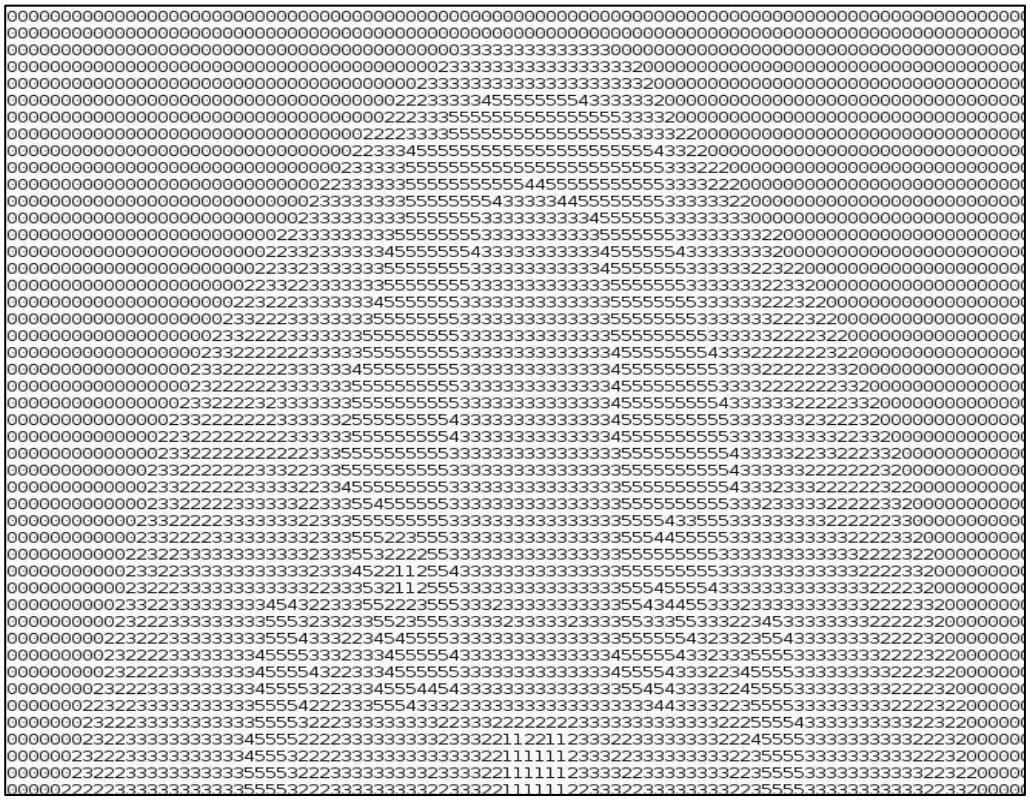

**Figure 4-21: *.egsphant file of Head-and-Neck patient**

### 4.4.3. 3D-CRT plan

A simple 3 field 3D-CRT plan was done on a scanned anthropomorphic phantom. Beams were conformed to a target without any beam weight manipulation, as the aim was not to get a good plan but rather test the flow of the verification process and dose display of results. The isocenter slice dose distributions for both XiO and MC are shown in Figure 4-22, and the dose difference map in Figure 4-23.

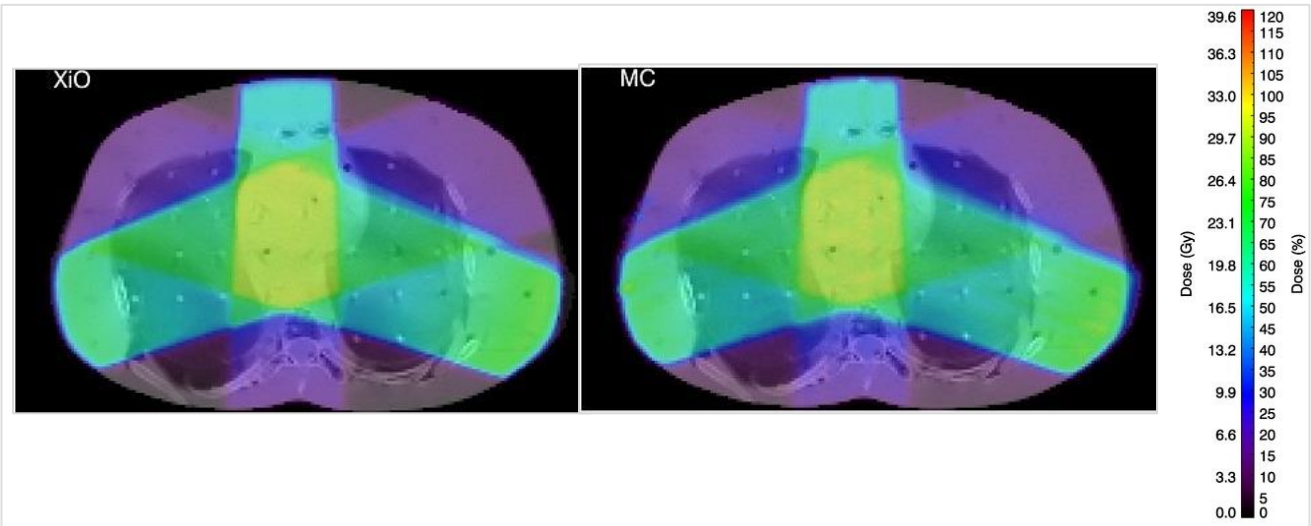


**Figure 4-22: Isocenter slice dose distributions of 3D-CRT plan**

The simulation process with multiple IMRT segments was handled effectively and the results could be displayed quickly. The dose difference map was calculated easily as well.

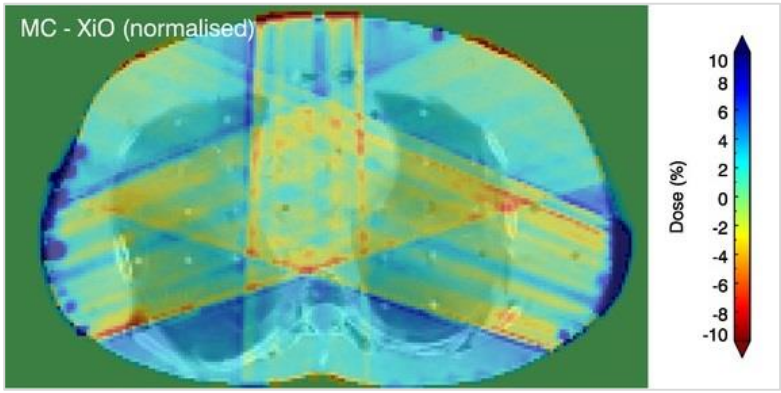


**Figure 4-23: Dose difference maps (MC-XiO) of 6MV 3D-CRT plan**
**Normalised differences are relative to the prescibed dose**

The normalised difference map gives a good indication of the magnitude of the differences in terms of the dose delivered to the patient. The XiO dose calculation differs by more than 3% from the MC dose in some of the patient volume. It can be seen here already that there are discrepancies especially in the low density lung volume, which directly affects the dose in the centre of the patient where all beams overlap. Entrance and exit dose differences are also evident.

The larger differences outside the beams' paths are in areas of larger statistical variation than the areas where the beams overlap, and can be expected. The area where all beams converge will always have the best statistics. Figure 4-24 illustrates the variance in the MC simulation for this slice graphically.

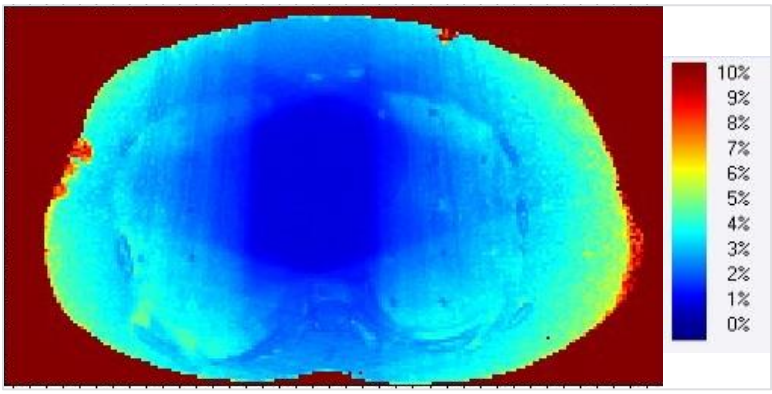


**Figure 4-24: Variance map at isocenter slice of MC simulated 3D-CRT plan**

The area outside the patient contour displays a seemingly large value due to the fact that the dose values are close to zero, therefore only data within the patient contour is considered. The 10MV model was tested in the same way with similar results, although the magnitude of the differences were slightly higher. (Appendix A: Figure A-12).

## 4.5. IMRT dose comparison

The full reports from XiO of all IMRT plans are included in Appendix A. The dose comparisons are given here.

### 4.5.1. Prostate

The isocenter dose distributions of the 6MV Prostate IMRT plan are shown in Figure 4-25. The 10MV plan was similar.

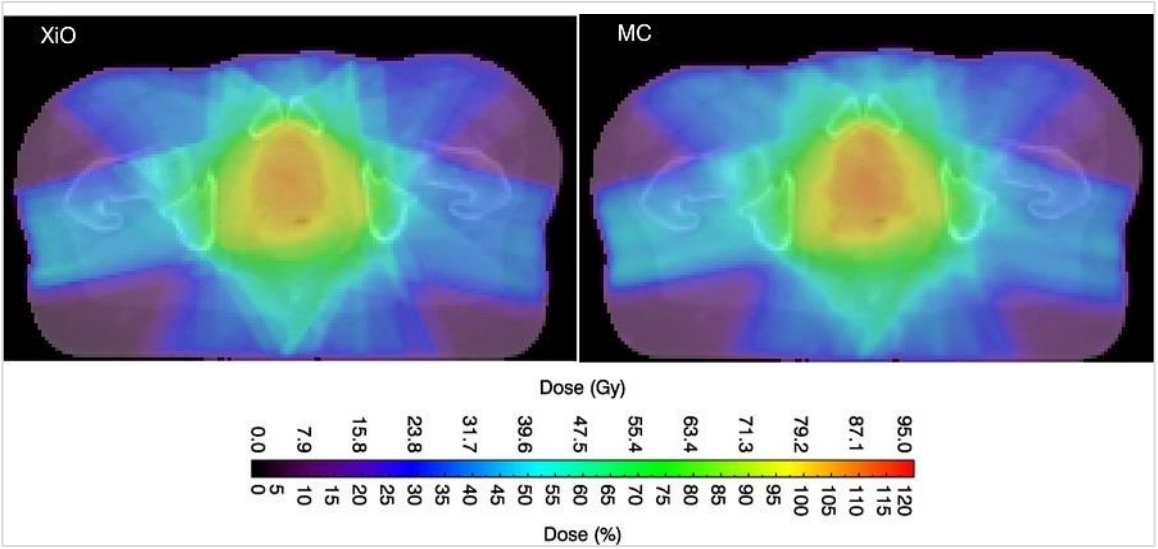


**Figure 4-25: Isocenter slice dose distributions for the 6MV Prostate IMRT plan**

The variance in the MC simulation of the 6MV Prostate IMRT plan for this slice is shown in Figure 4-26. The contour data of some targets and OARs are shown in the same figure. The variance was calculated from the combined segments as explained in Eq. 3-8 in section 3.4.4.

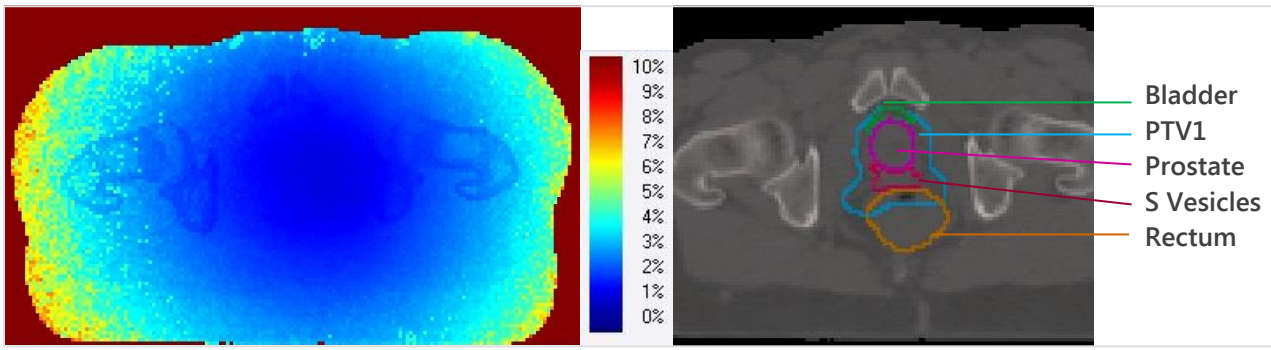


**Figure 4-26: Variance map of MC simulation of 6MV Prostate IMRT plan (left)**
**Some target and OAR contours are also indicated for the same slice (right)**

The variance map shows statistical variations of less than 1% in the target area, which slowly becomes larger moving outwards. Most of the volumes that contain the target or critical structures are still well within a 2% statistical variation level.

The corresponding dose difference maps and gamma analyses of both energy plans are shown in Figure 4-27. The gamma map is shown over the target area only, and the $\gamma$-values reported below are for this region as well.

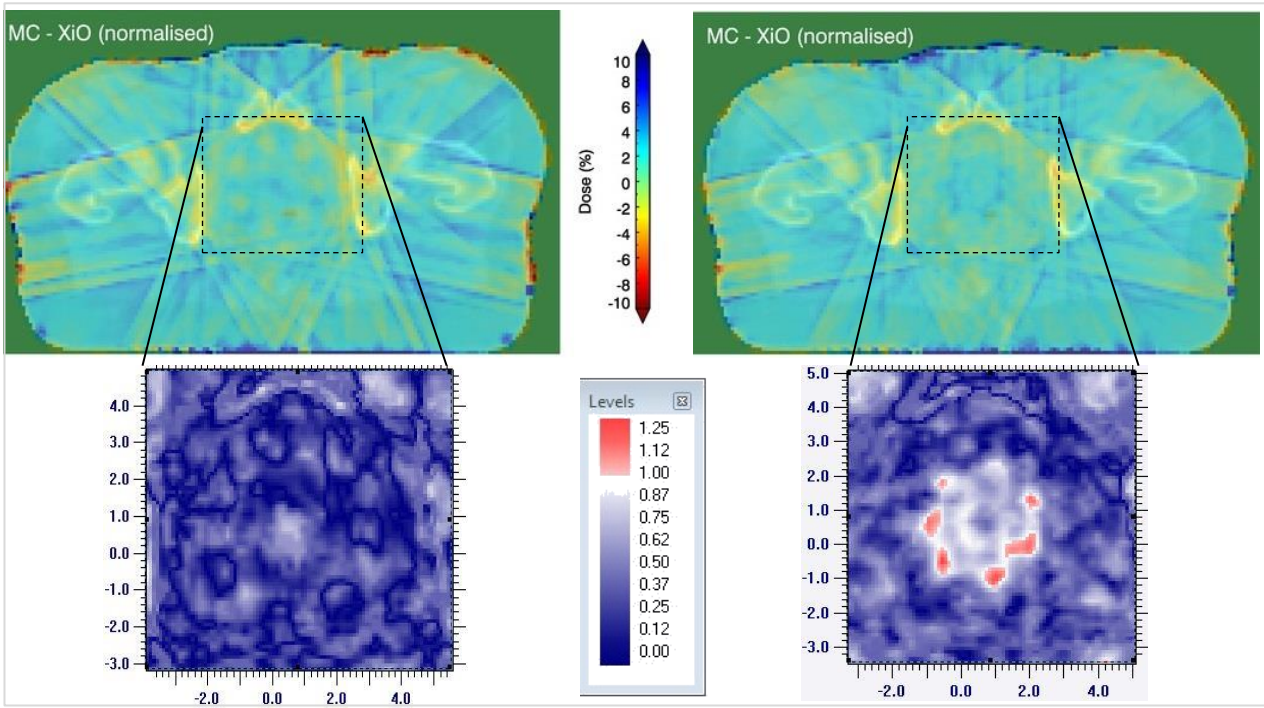


**Figure 4-27: Dose difference (MC-XiO) and gamma analysis for Prostate IMRT plans 6MV plan is shown on the left and 10MV on the right**

The $\gamma$ pass rate in the isocenter slice in the ROI was 99.5% for 6MV and 90.8% for 10MV. This selected area (ROI) has statistics of within 2%, and thus a gamma analysis of 3%/2mm will have significance. The area outside of this ROI has a statistical variation of more than 2%, which might fail the gamma test purely based on the variance. The ideal method would be to have a gamma test that accommodate the change in variance ($\varepsilon$), so that the criteria is always e.g. 2%+$\varepsilon$/2mm. However, for this study only the ROI is used with the gamma test.

An overall difference in dose is seen across the entire volume of around +2%, which means that the XiO calculated dose is lower than the MC dose. The beam entrance and exit doses differ as well, which is expected considering the superior handling of secondary electrons in the build-up and build-down regions of beams. The major differences can be seen in the regions containing pelvic bone. Here XiO calculates a higher dose compared to MC. The overall discrepancy over the patient volume might be a direct consequence of the difference seen in bone, as the MU calculation of XiO will be influenced by this. The 10MV plan shows the same characteristics, except that the differences are larger especially where all beams overlap. The gamma test shows good agreement in the target area.

The DVHs for these plans are shown in Figure 4-28 (6MV) and Figure 4-29 (10MV), and some of the DVH parameters for specific volumes are emphasised in Table 4-3.

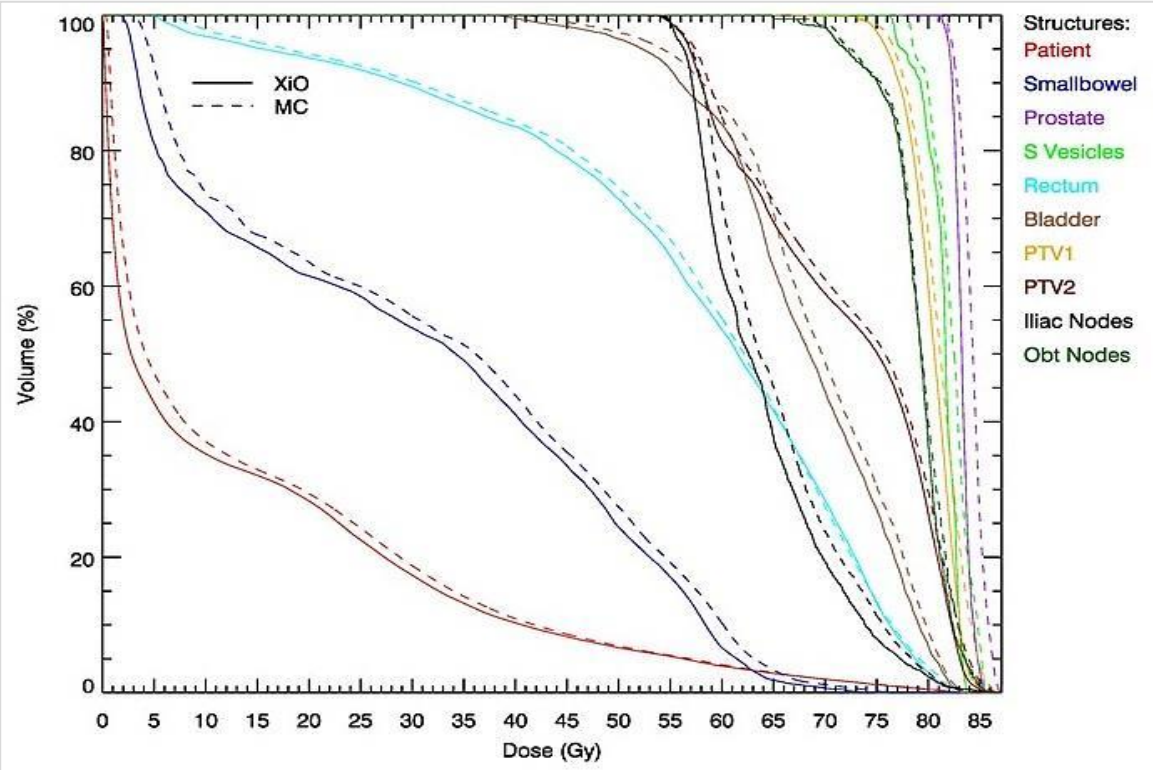


**Figure 4-28: DVH data for 6 MV Prostate IMRT plan**

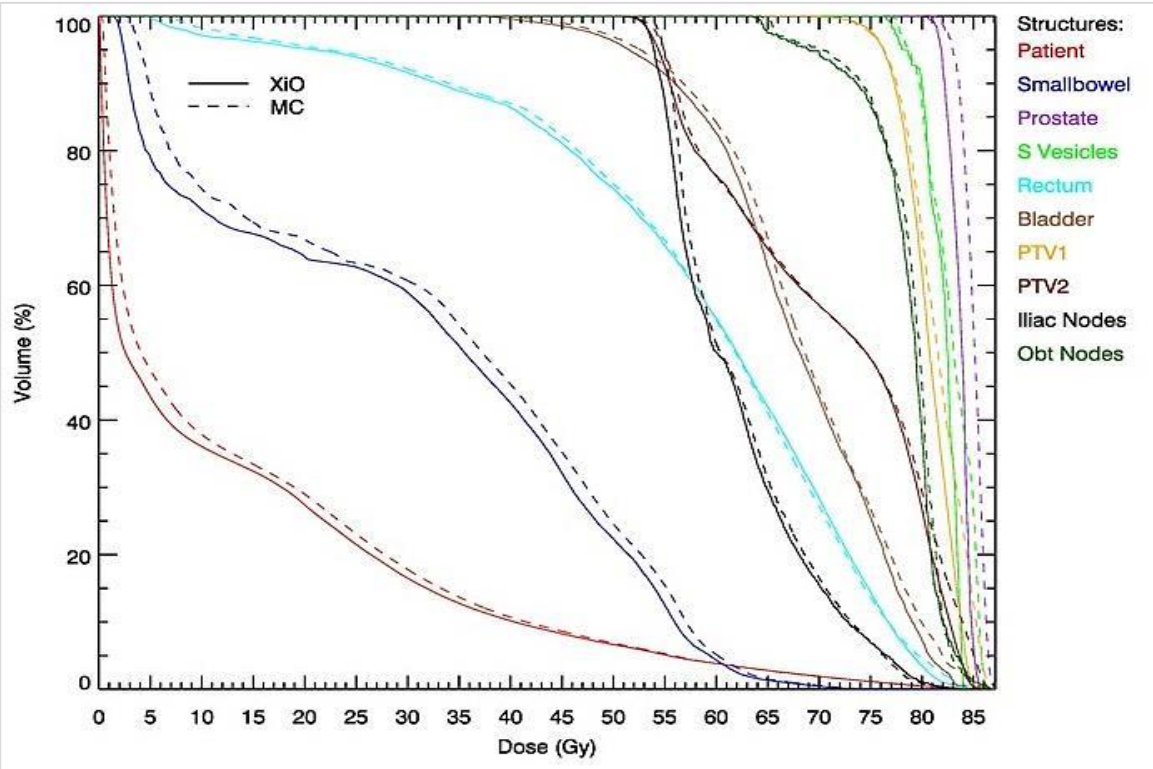


**Figure 4-29: DVH data for 10 MV Prostate IMRT plan**

**Table 4-3: Summary of DVH parameters for Prostate IMRT plans**

| | | 6 MV | | | 10 MV | | |
|---|---|---|---|---|---|---|---|
| Structure | | XiO | MC | MC-XiO | XiO | MC | MC-XiO |
| PTV1 | $D_{98}$ | 74.8 Gy | 75.6 Gy | 0.7 Gy | 74.8 Gy | 74.5 Gy | -0.3 Gy |
| | $D_{mean}$ | 80.3 Gy | 81.0 Gy | 0.7 Gy | 80.6 Gy | 81.4 Gy | 0.8 Gy |
| | $D_2$ | 84.2 Gy | 85.5 Gy | 1.3 Gy | 84.6 Gy | 86.1 Gy | 1.5 Gy |
| Rectum | $V_{50}$ | 72.9 % | 74.6 % | 1.8 % | 74.4 % | 75.1 % | 0.7 % |
| | $V_{75}$ | 13.2 % | 13.4 % | 0.2 % | 14.4 % | 13.7 % | -0.7 % |
| Bladder | $D_{max}$ | 81.8 Gy | 82.1 Gy | 0.2 Gy | 82.7 Gy | 84.1 Gy | 1.4 Gy |
| | $V_{65}$ | 62.8 % | 71.0 % | 8.2 % | 62.7 % | 67.0 % | 4.3 % |
| | $V_{80}$ | 6.9 % | 9.1 % | 2.3 % | 7.4 % | 9.9 % | 2.5 % |
| Small Bowel | $V_{45}$ | 33.5 % | 35.5 % | 2.0 % | 32.1 % | 35.2 % | 3.1 % |

The DVH comparison show good correlation between the dose calculations. Most of the volumes have slightly lower doses calculated by XiO than MC. The targets will therefore receive a slightly higher dose than planned, but this is acceptable. Considering that most of the voxels in structures are within a 2% variance level, differences of more than 1.5Gy become significant. The effect on the volume parameters are not so easy to determine, however the differences seen are small.

*Prostate IMRT with couch*

The patient used for the prostate IMRT plans was CT scanned on an actual Linac treatment couch (iBEAM evo couchtop[73]). To quantify the calculation accuracy of XiO if the couch were to be included, the same 6MV plan was recalculated with the treatment couch as part of the patient contour. The plan was not re-optimised; the dose was simply recalculated with the same segments. XiO automatically increases the MUs for the beams traversing the couch to achieve nearly the same target and OAR dose. The dose distributions and dose difference maps are given in Figure 4-30 and Figure 4-31.

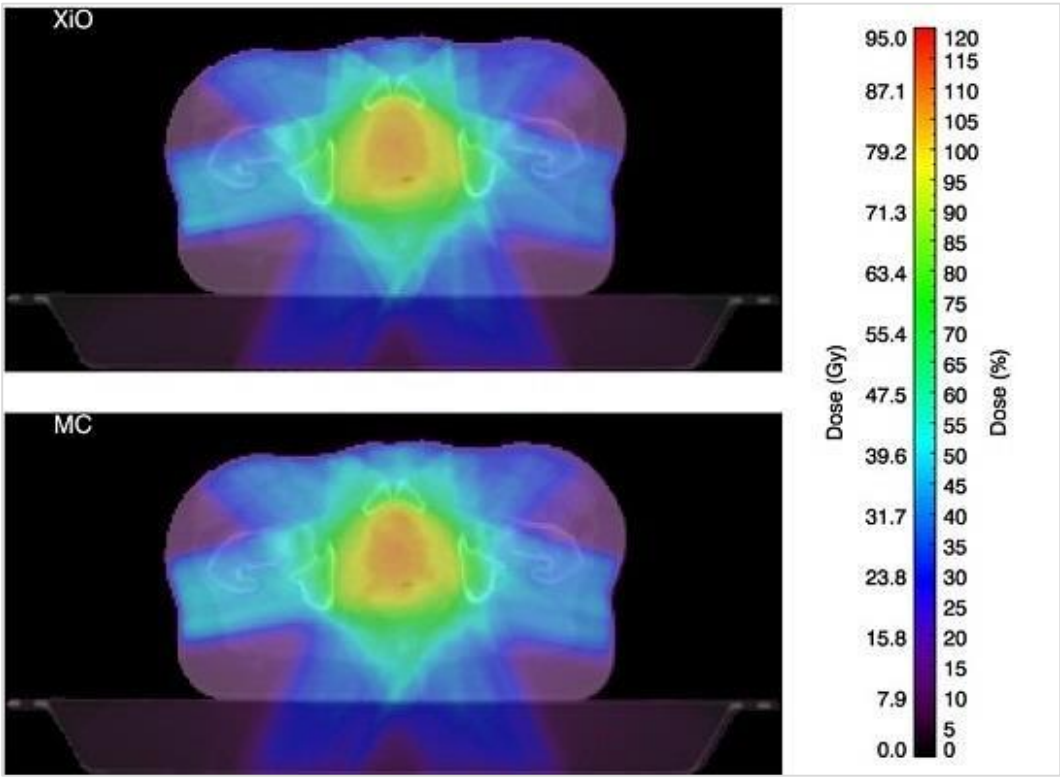


**Figure 4-30: Isocenter slice dose distributions for 6MV Prostate IMRT plan with couch**

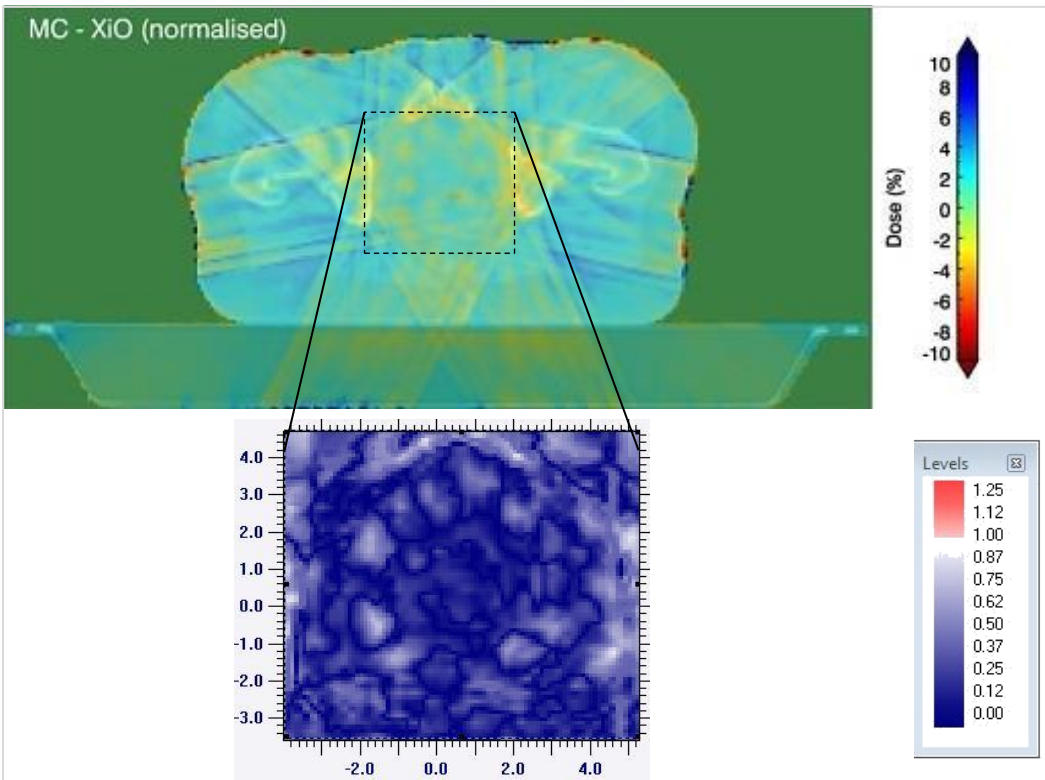


**Figure 4-31: Dose difference (MC-XiO) and gamma analysis for Prostate IMRT plan with couch**

The $\gamma$ pass rate for this slice in the ROI was 99.4%. The DVH for this plan is shown in Figure 4-32.

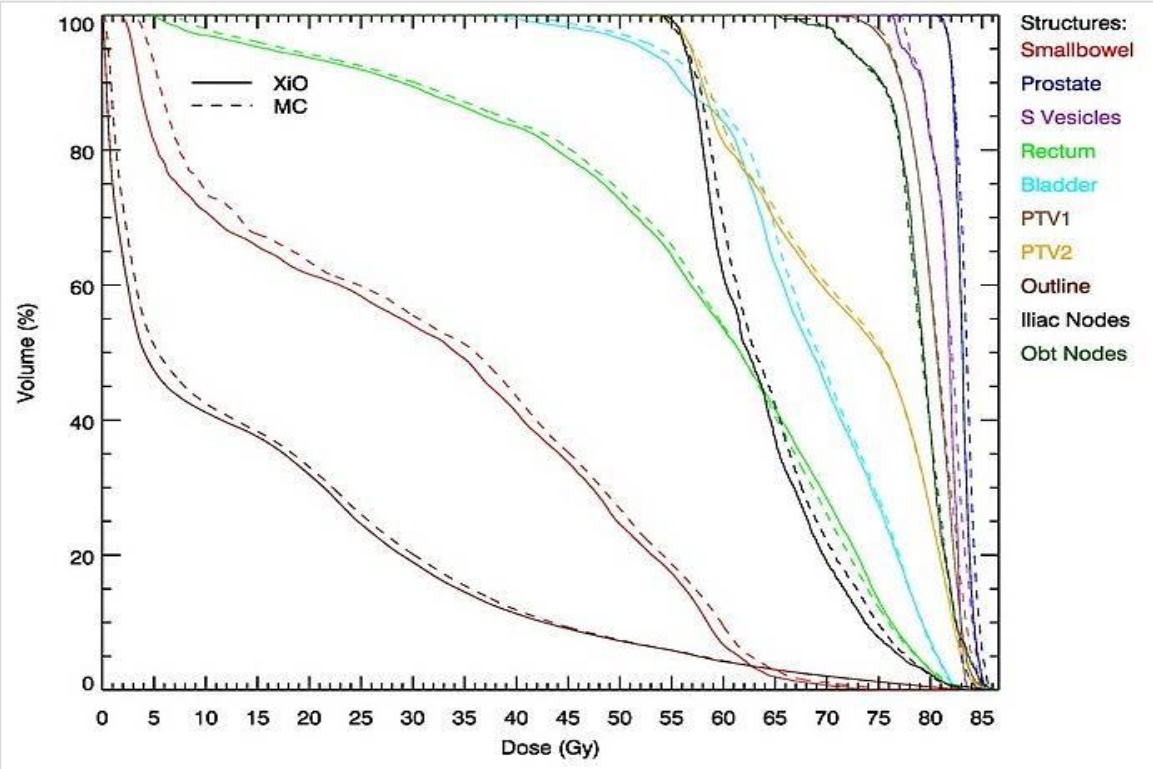


**Figure 4-32: DVH data for 6 MV Prostate IMRT plan with couch**

Some of the DVH parameters for specific volumes are highlighted in Table 4-4.

**Table 4-4: Summary of DVH parameters for 6MV Prostate IMRT plan with couch**

| Structure | | XiO | MC | MC-XiO |
|---|---|---|---|---|
| PTV1 | $D_{98}$ | 74.5 Gy | 75.0 Gy | 0.5 Gy |
| | $D_{mean}$ | 80.3 Gy | 80.5 Gy | 0.2 Gy |
| | $D_2$ | 84.1 Gy | 84.5 Gy | 0.4 Gy |
| Rectum | $V_{50}$ | 72.7 % | 74.0 % | 1.3 % |
| | $V_{75}$ | 13.2 % | 12.2 % | -1.0 % |
| Bladder | $D_{max}$ | 81.7 Gy | 81.6 Gy | -0.2 Gy |
| | $V_{65}$ | 63.1 % | 68.0 % | 5.0 % |
| | $V_{80}$ | 7.2 % | 6.8 % | -0.4 % |
| Small Bowel | $V_{45}$ | 33.7 % | 35.2 % | 1.5 % |

The differences are similar to the 6MV plan without the couch, and in some cases even slightly less. The dose difference seen in the couch itself indicates that XiO calculates slightly higher dose values than MC. The effect of this translates to less energy being available from these 2 beams interacting in the patient volume, and thus a lower dose deposition in the target area. In the plan without the couch included, the target dose was too high. The results therefore seem better with the couch, however considering the two scenarios together might suggest that the outcome is worse with the couch added. An in-depth investigation into this might resolve the issue, which is not the focus of this study.

### 4.5.2. Head-and-Neck

The isocenter dose distributions of the 6MV Head-and-Neck IMRT plan are shown in Figure 4-33. The variance in the MC simulation of the 6MV plan for this slice together with the contours of the PTV and Spine is shown in Figure 4-34.

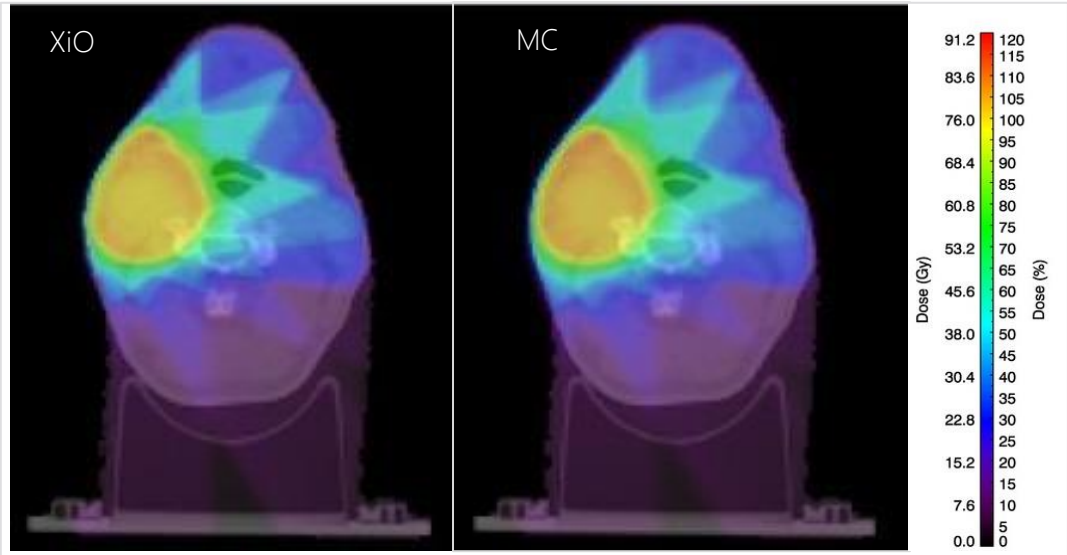


**Figure 4-33: Isocenter slice dose distributions for 6MV Head-and-Neck IMRT plan**

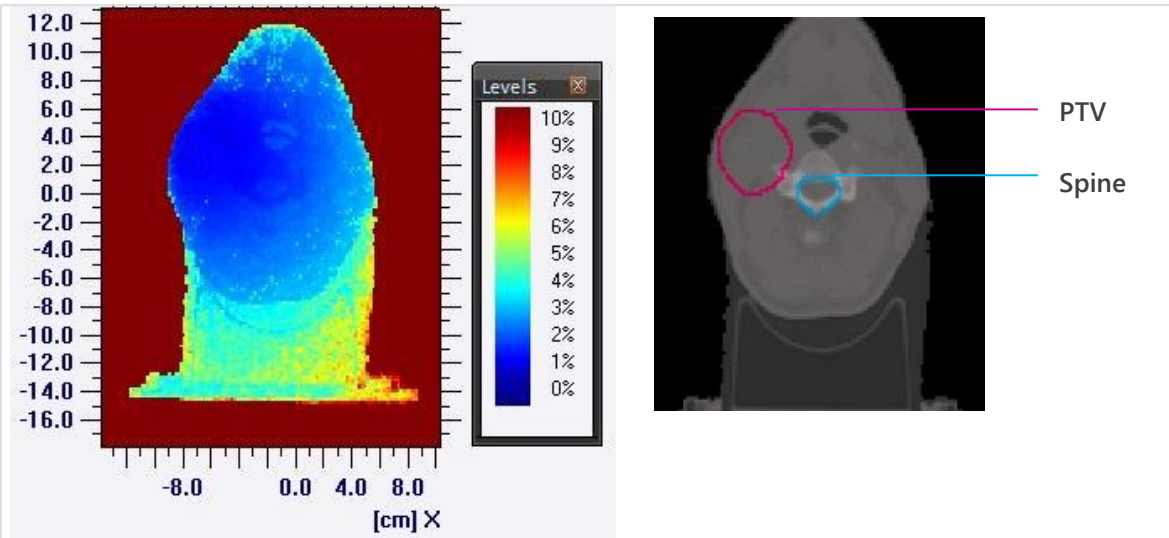


**Figure 4-34: Variance map of MC simulation of 6MV Head-and-Neck IMRT plan (left)**
**The target and OAR contours are also indicated for the same slice (right)**

Almost all of the patient's head seen in this slice is within a 2% statistics region, with the critical structures enclosed within 1% variance. The corresponding dose difference maps and gamma analyses of both energy plans are shown in Figure 4-35.

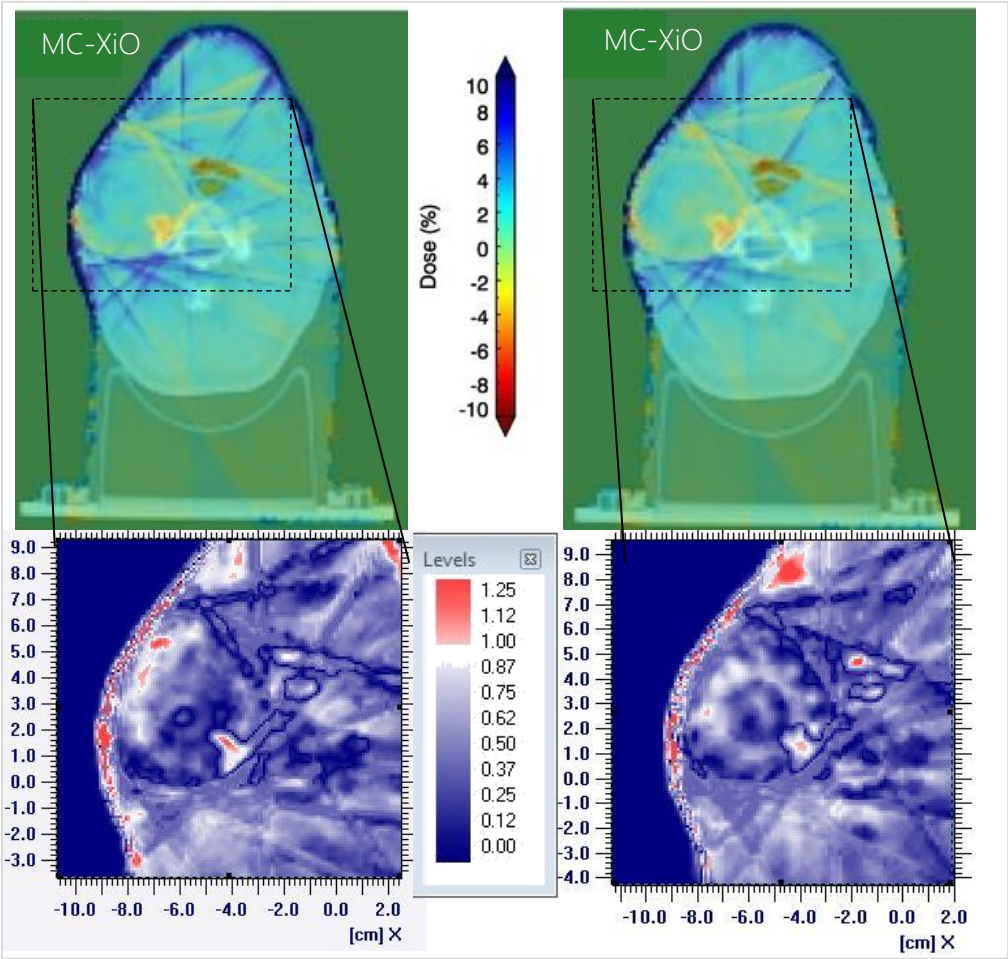


**Figure 4-35: Dose difference (MC-XiO) and gamma analysis for Head-and-Neck IMRT plans 6MV plan is shown on the left and 10MV on the right**

The $\gamma$ pass rate for the isocenter slice in the ROI was 91.3% for the 6MV plan and 93.6% for 10MV. As shown previously the ROI is within a region of statistics below 1%, and therefore the gamma test of 3%/2mm is a good representation of the differences. Most of the voxels pass the test, and the major differences are seen on the surface. In this case the patient has an immobilisation mask fitted around the head, which introduces a thin plastic and air layer before the actual interactions take place in the patient. This in combination with the slight error in entrance/build-up dose of XiO causes most of the dose differences seen.

Similar to the Prostate case, the overall dose level calculated by XiO is lower MC. The surface dose of XiO is much less than what MC suggests. Also, the dose calculated in bone is higher in XiO than MC. The same is seen in the air cavities of the esophagus and trachea, with the XiO dose higher than MC.

Another prominent difference is seen at the beam penumbrae, creating a streaky effect. Differences are also seen in the head rest. In this case the beams are not directed through the head rest, and thus the effect is minimal. The same rationale as for the couch influence might apply here.

The DVHs for these plans are shown in Figure 4-36 (6MV) and Figure 4-37 (10MV), and some of the DVH parameters for specific volumes are emphasised in Table 4-5.

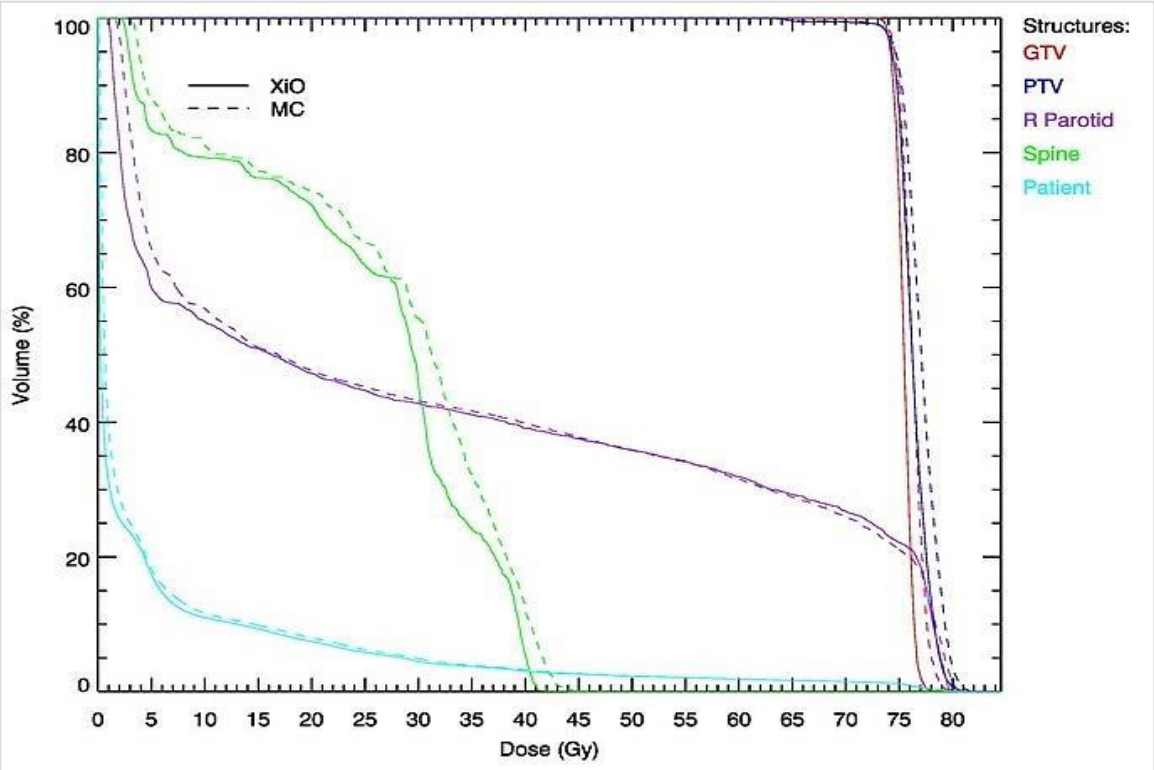


**Figure 4-36: DVH data for 6MV Head-and-Neck IMRT plan**

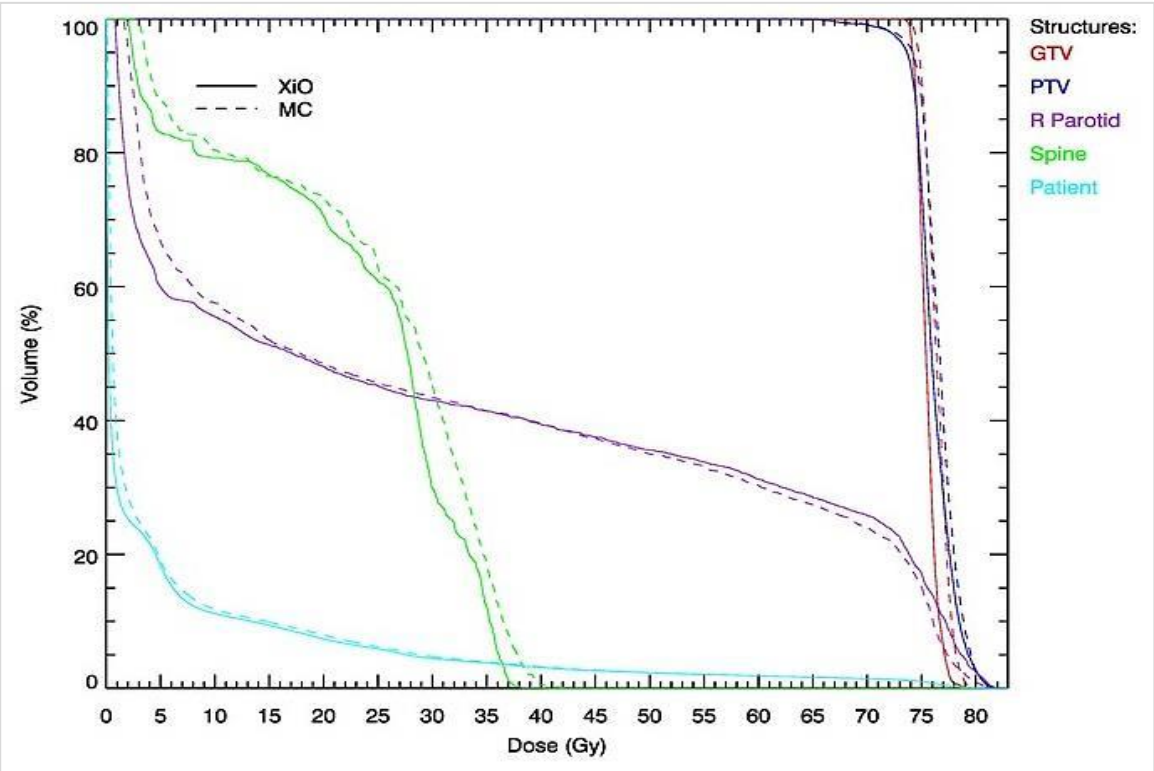


**Figure 4-37: DVH data for 10MV Head-and-Neck IMRT plan**

**Table 4-5: Summary of DVH parameters for Head-and-Neck IMRT plans**

| | | 6 MV | | | 10 MV | | |
|---|---|---|---|---|---|---|---|
| Structure | | XiO | MC | MC-XiO | XiO | MC | MC-XiO |
| PTV | $D_{98}$ | 73.8 Gy | 73.8 Gy | 0 Gy | 72.2 Gy | 72.5 Gy | 0.3 Gy |
| | $D_{mean}$ | 76.3 Gy | 77.1 Gy | 0.8 Gy | 76.1 Gy | 76.7 Gy | 0.5 Gy |
| | $D_2$ | 79.4 Gy | 80.4 Gy | 1.0 Gy | 80.2 Gy | 80.3 Gy | 0.1 Gy |
| Spine | $D_{max}$ | 40.6 Gy | 42.6 Gy | 2.0 Gy | 36.8 Gy | 39.2 Gy | 2.4 Gy |
| Parotid | $D_{mean}$ | 32.5 Gy | 33.2 Gy | 0.7 Gy | 32.1 Gy | 32.5 Gy | 0.4 Gy |

The dose agreement of the 10MV plan was slightly better than the 6MV plan, which correlates with the gamma analyses results. The PTV coverage is in good agreement for both energy plans, with a slightly higher $D_2$ value seen in the 6MV plan. The parotid gland dose is also within acceptable bounds. The biggest difference is seen in the entire spinal cord volume. XiO calculates a lower dose than MC, most probably as a direct consequence of the dose calculation difference seen in the bone. Note that the 'spine' contour is drawn on the inside of the bony anatomy of the actual vertebrae. The resulting dose difference in the spine is quite large and can be of concern.

### 4.5.3. Esophagus

The isocenter dose distributions of the 6MV Esophagus IMRT plan are shown in Figure 4-38.

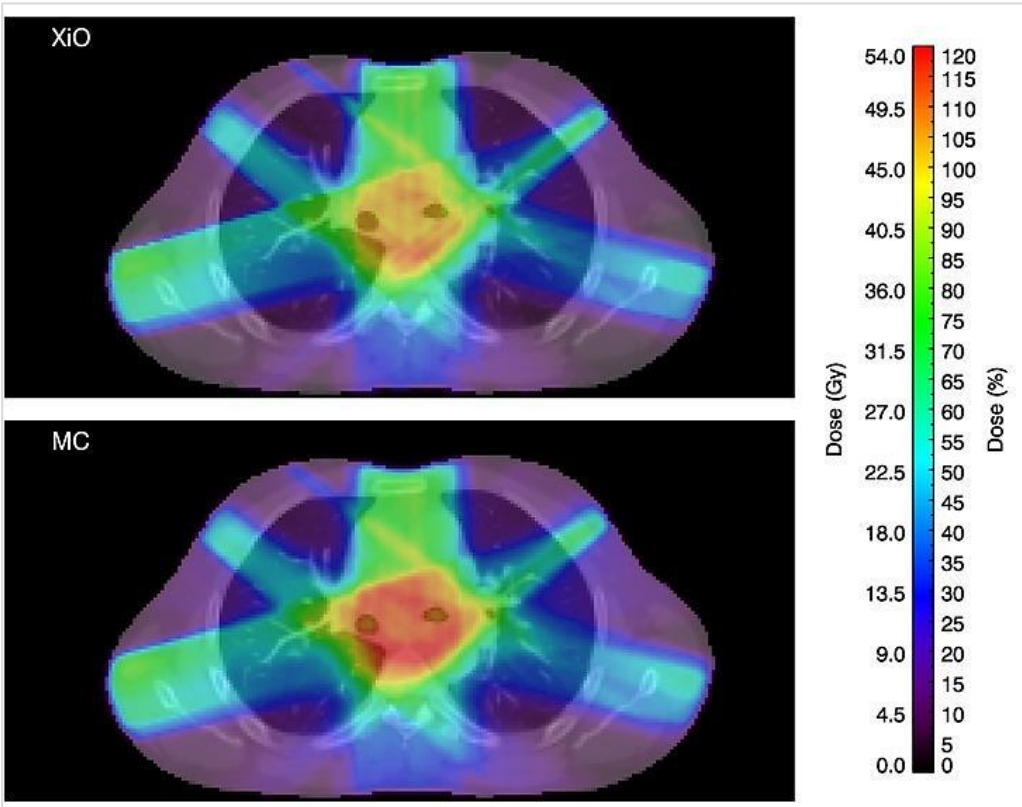


**Figure 4-38: Isocenter slice dose distributions for 6MV Esophagus IMRT plan**

The dose distributions already show a large difference in target region.

The variance in the MC simulation of the 6MV plan for this slice together with the contours of the PTV, lungs and spine are shown in Figure 4-39.

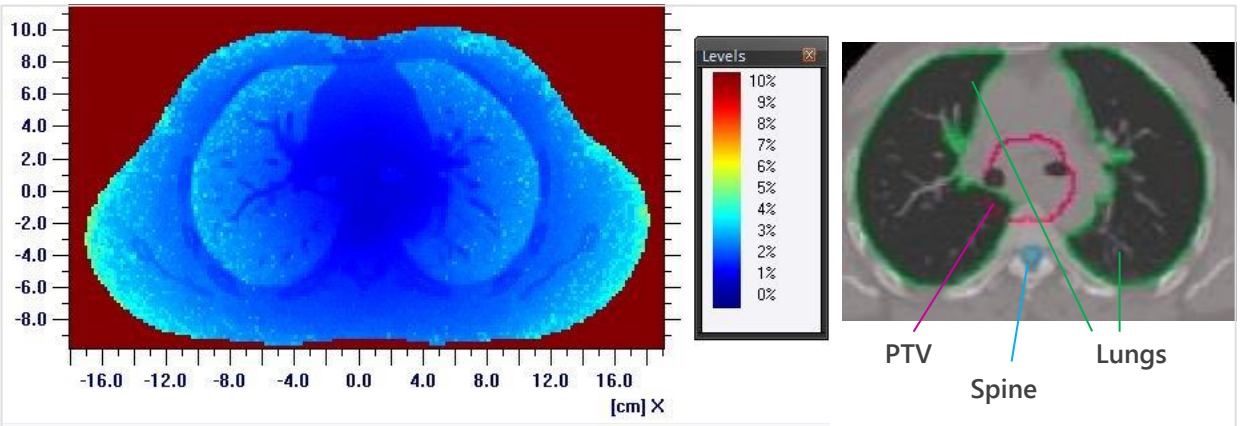


**Figure 4-39: Variance map of MC simulation of 6MV Head-and-Neck IMRT plan (left)**
**The target and OAR contours are also indicated for the same slice (right)**

The variance in the entire patient volume in this slice is below 3%, and the targets fall well within the 1% region. The statistical variations in the lungs of closer to 3% can be expected due to the lower density. The corresponding dose difference maps and gamma analyses of both energy plans are shown in Figure 4-40.

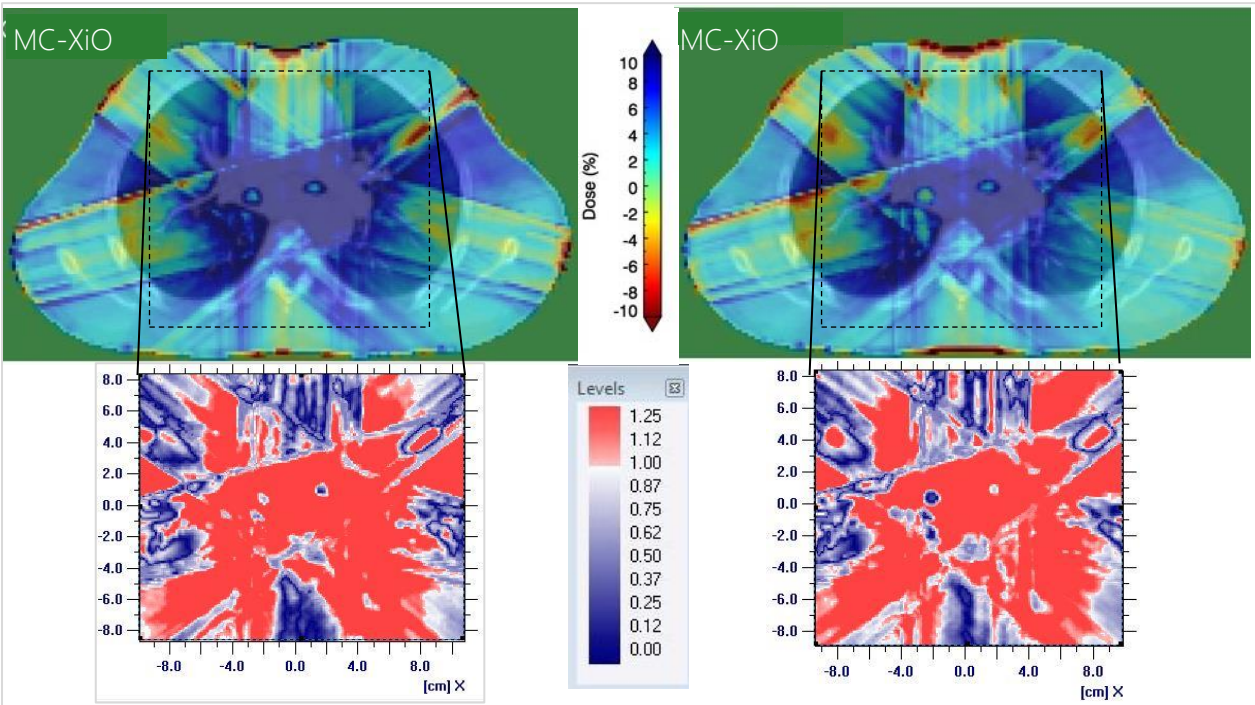


**Figure 4-40: Dose difference (MC-XiO) and gamma analysis for Esophagus IMRT plans**
**6MV plan is shown on the left and 10MV on the right**

The $\gamma$ pass rate for this slice in the ROI was **42.3%** for 6MV and **41.9%** for the 10MV plan.

From the variance map the criteria of 3%/2mm should be adequate in most of this ROI except small parts of the lungs. Large differences are seen in most of the target volume, as well as the lungs itself.

The differences seen in the patient volume outside the lungs are similar to the other treatment sites, with XiO calculating slightly lower dose than MC. The differences in bone dose are seen here again as well. The major deviation though is seen in the lung volume, where XiO overestimates the initial dose and then progress to an under-dose as the beam penetrates the low density volume. The discrepancies seen in the PTV area are most probably due to the dose deposition calculation differences in the lungs.

The DVHs for these plans are shown in Figure 4-36 (6MV) and Figure 4-37 (10MV), and some of the DVH parameters for specific volumes are emphasised in Table 4-6.

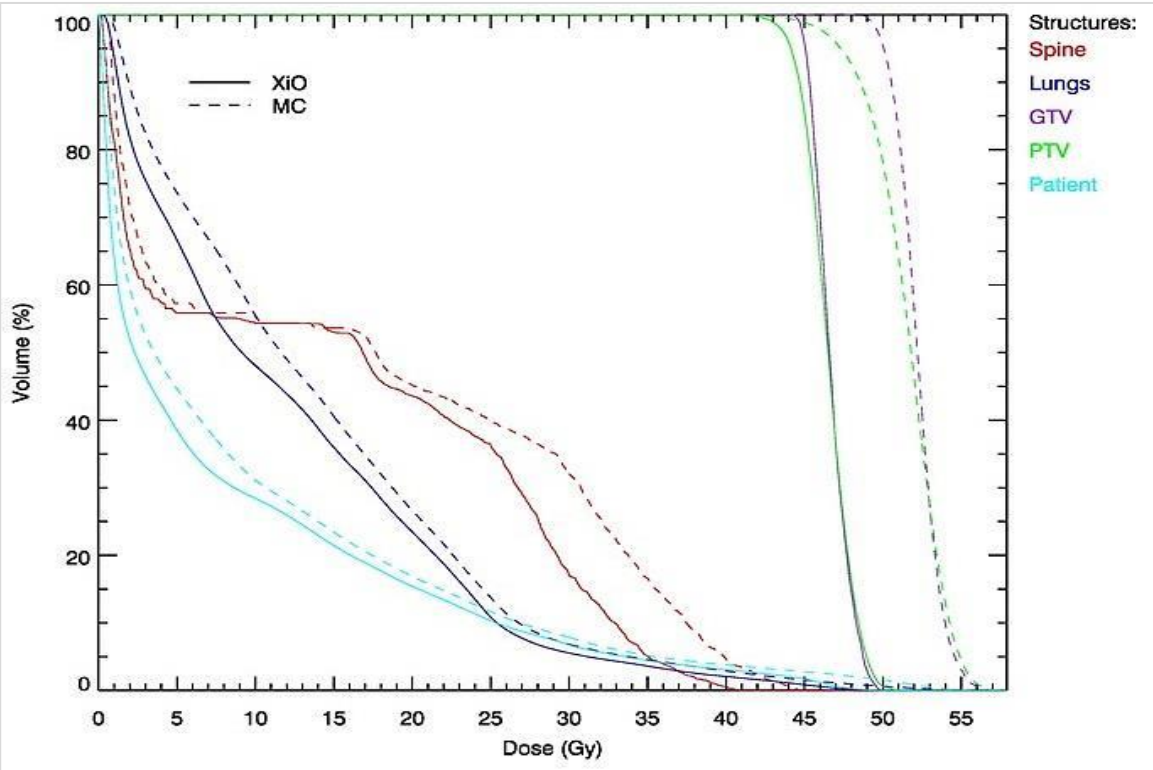


**Figure 4-41: DVH data for 6MV Esophagus IMRT plan**

**Table 4-6: Summary of DVH parameters for Esophagus IMRT plans**

| | | 6 MV | | | 10 MV | | |
|---|---|---|---|---|---|---|---|
| Structure | | XiO | MC | MC-XiO | XiO | MC | MC-XiO |
| PTV | $D_{98}$ | 43.5 Gy | 45.9 Gy | 2.4 Gy | 43.3 Gy | 44.4 Gy | 1.1 Gy |
| | $D_{mean}$ | 46.5 Gy | 51.6 Gy | 5.1 Gy | 46.6 Gy | 50.1 Gy | 3.6 Gy |
| | $D_2$ | 49.5 Gy | 55.6 Gy | 6.1 Gy | 49.4 Gy | 53.8 Gy | 4.4 Gy |
| Spine | $D_{max}$ | 38.0 Gy | 42.4 Gy | 4.4 Gy | 37.4 Gy | 41.3 Gy | 3.9 Gy |
| Lungs | $V_{20}$ | 23.5 % | 26.6 % | 3.1 % | 21.0 % | 22.9 % | 1.9 % |
| | $D_{mean}$ | 12.2 Gy | 13.8 Gy | 1.6 Gy | 11.6 Gy | 13.0 Gy | 1.4 Gy |

The dose differences are clearly clinically significant in almost all volumes. The lungs have a smaller deviation than some of the other organs, with a larger volume receiving doses below 20 Gy according to MC than what XiO calculates. The target volumes and spine receive much larger doses than XiO predicts.

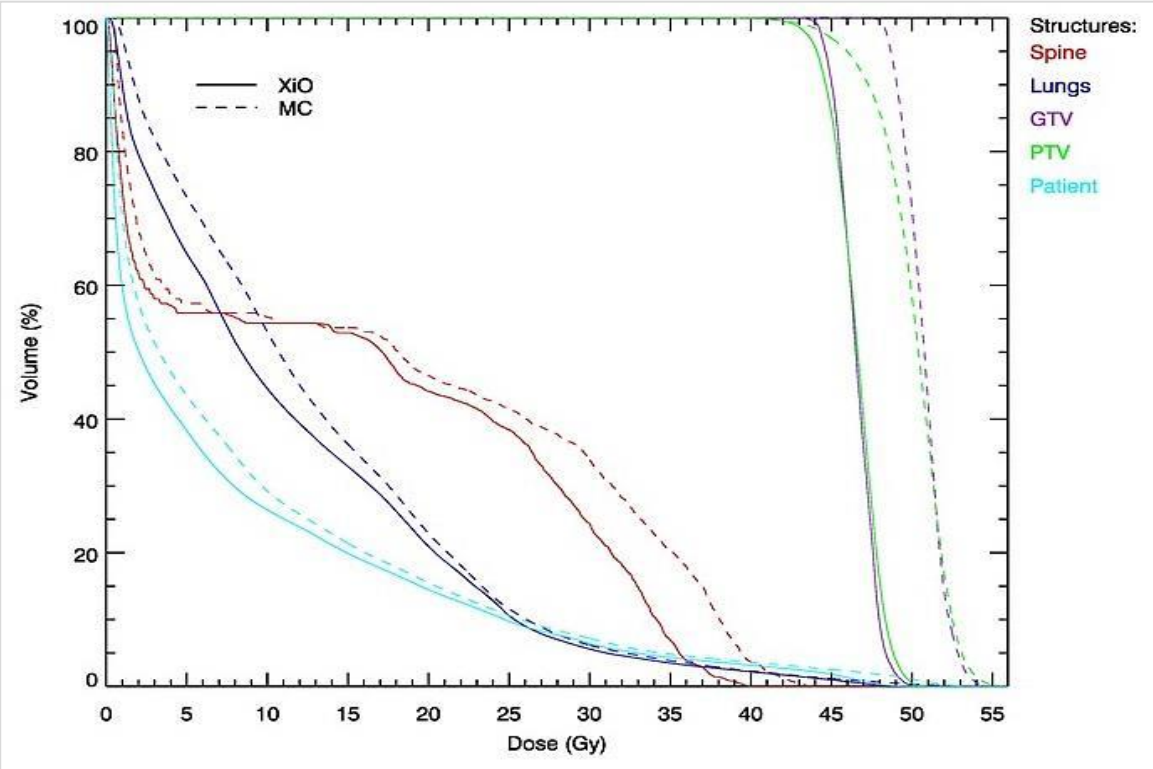


**Figure 4-42: DVH data for 10MV Esophagus IMRT plan**

The spine overdose is 11.6 % and 10.4 % for the 6 and 10 MV plans respectively, which is on the limit of acceptance according to the RTOG protocol used in this case[70]: a maximum dose above 50 Gy is unacceptable for this protocol. If the XiO plans were planned on the limit of $D_{max}$ = 45 Gy, the actual dose according to MC would exceed this 50 Gy level. Also, the PTV over-dosage greatly exceeds the stated acceptable variation of ≤ 113% of the prescribed dose.

The 10MV plan shows better agreement between XiO and MC compared to the lower energy, as is the case for the other treatment sites. Nonetheless the differences are still very big.

These overdoses are significant and can lead to severe biological effects. The QUANTEC data states an estimated risk of myelopathy of <1% and <10% at 54 Gy and 61 Gy maximum doses.[74] Although these doses are higher than what is found in the IMRT plans used in this study, the severity of biological effect with increased dose can be seen. Planning on XiO with certain clinical outcomes in mind may result in a much worse effect on the patient.

In order to investigate the cause of these deviations in more detail, a dose difference map was created from the dose distributions containing only the one beam directed at an angle of 256° of the 6MV plan. A diagonal profile was drawn along the centreline of the beam. This is shown in Figure 4-43, with the normalised dose differences still relative to the full plan prescribed dose.

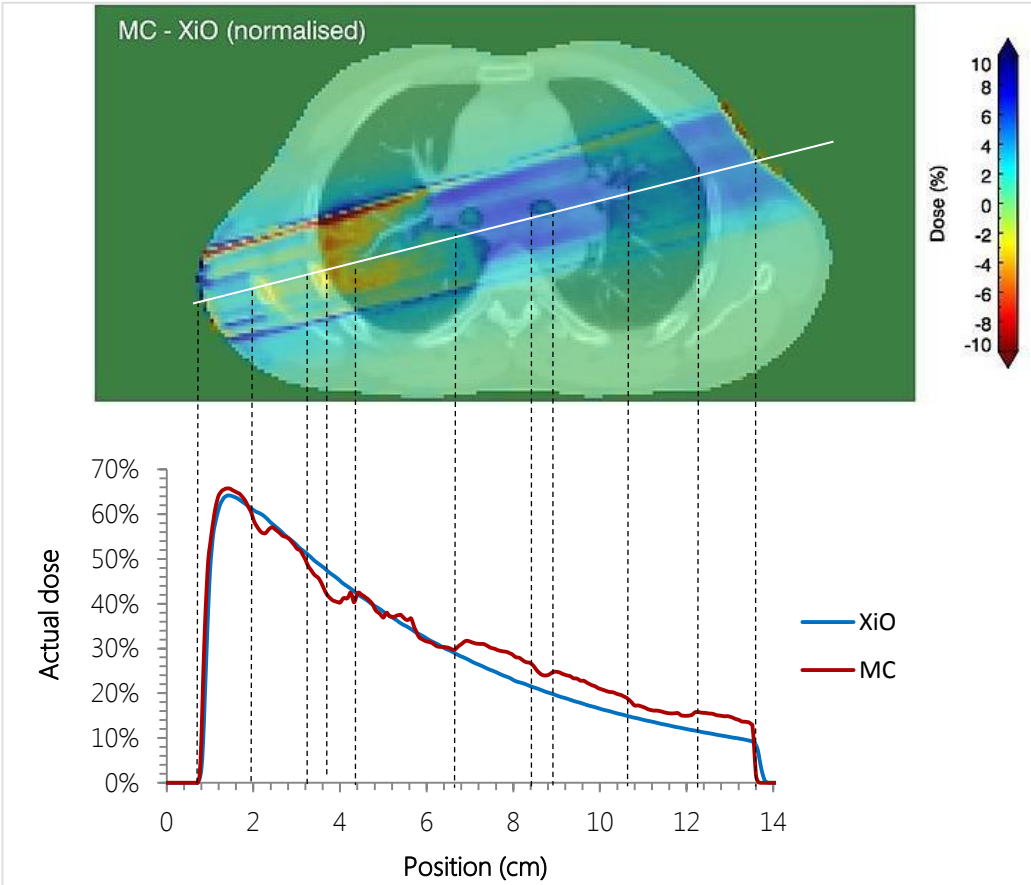


**Figure 4-43: Dose difference of single beam angle for the 6MV Esophagus IMRT plan The difference map with corresponding profiles are shown**

This single field clearly shows some of the causes of the dose discrepancy. The build-up of dose correlates well, with a slight underestimation by XiO at the maximum dose. The XiO calculated attenuation is slightly too low in bone, as was seen in the other treatment site cases. The same effect repeats at the rib interface. The big difference is then seen in the majority of the lung volume: in XiO the beam intensity simply continues to decrease almost at the same rate as in tissue, whereas the MC profile indicates much less attenuation. The MC handling of the interface beyond the lung is visibly superior to XiO, and much more of the energy of the beam is carried to this point than XiO calculates. The resulting higher dose delivered according to MC through the rest of the target area is a direct consequence of this.

The difference in profile shapes demonstrates the shortcoming in heterogeneity handling of XiO: the curve is smooth from start to finish with only a change in slope where different materials are encountered. MC is in clear contrast with definite intensity changes following the density changes in the patient. This is most probably further intensified by the addition of small beam segments used in IMRT.

# Chapter 5: CONCLUSION

This study had two main goals: to develop the building blocks towards a complete MC-based dose verification system for IMRT, and to demonstrate its accuracy on verifying the dose of a commercial TPS. The system consisted of EGSnrc MC codes as dose calculation engine to compare to the IMRT doses created on the XiO TPS using its Multigrid Superposition algorithm and various IMRT tools. The following can be concluded from this work:

### 5.1.1. Verification system

- In order to realise these goals, some preparative work was necessary: A realistic virtual linac had to be created and used to generate the necessary watertank data for commissioning on XiO. The BEAMnrc and DOSXYZnrc codes provided suitable tools to create these models. Some of these steps presented challenges, since data was not measured but generated on a computer. With some programming work and file formatting these obstacles could successfully be overcome. The accurate generation and conversion of data has had a crucial role in the work that followed it.

- The next process was accurate beam modelling to be used for IMRT planning on patient data. Modelling of beam data on XiO has a limited number of variables that can be used, which leads to compromising on some or other aspect of data fitting. The large range of FSs used in radiotherapy have varying characteristics with field shape at the extremes, which cannot be perfectly addressed through so few parameters. As suggested by the vendor, setting up a separate model for IMRT only with small fields can solve some of these problems. However, this will limit the FSs available for IMRT planning and may cause difficulty in generating a clinically acceptable plan.

- Initial setup of the reading and implementation of DICOM information for MC dose calculation had to be done with care to ensure accurate data transfer. The GUI that was created greatly simplified this task and made subsequent use of the system quick, robust and efficient. The use of a modern multiple-processor computer makes MC calculations fast, and dose calculation of even a complex IMRT plan completes within a reasonable time.

A summary of the IMRT plan MC computing times is given in Table 5-1: the simulation time is for the BEAmnrc and DOSXYZnrc calculations alone, and the total time includes computations of the XiO2MC program (preparation of files) and combining of dose files after simulation.

**Table 5-1: Summary of MC computing times for IMRT plans.**
**Simulation times are for a dual Intel Xeon™ 2.4 GHz 8-core CPU computer**

| Site | Energy | Segments | CPUs | Simulation time (h) | Total time (h) |
|---|---|---|---|---|---|
| Prostate | 6 MV | 36 | 16 | 5 | 5.5 |
| | 10 MV | 37 | 16 | 6 | 6.5 |
| Head&Neck | 6 MV | 84 | 16 | 13.5 | 14 |
| | 10 MV | 42 | 16 | 9 | 9.5 |
| Esophagus | 6 MV | 56 | 16 | 11 | 11.5 |
| | 10 MV | 51 | 16 | 10.5 | 11 |

The complete comparison of an IMRT plan can thus be done in less than a day: if simulations are run over night, the analysis can be done the next morning. This will make the verification system a viable and practical tool.

A complete verification system will not require all of the work done in this study, since an actual linac will be used in the clinical setup with measured data available. The MC model will then be benchmarked against the measured data. However, the data processing and modelling will always be a part of it and plays a vital role in setting up a proper verification system.

### 5.1.2. Dose comparison of XiO

- IMRT plans created in XiO could be compared to MC dose calculation, and the results displayed in a familiar manner: using dose maps, gamma analysis and DVHs. These methods are popular with QA software vendors all over and provide for simple evaluation.

- The Multigrid Superposition algorithm of XiO produced IMRT dose distributions that were comparable to the MC results in most cases. In tissues with densities close to water, the dose calculation of XiO is accurate, as expected. In high density materials, like bone, the dose is slightly overestimated, up to a few percent. In low density media, like lungs, the dose was also overestimated. These differences are most probably caused as result of a combination of 2 aspects of XiO's algorithm: i) the kernel scaling and lack of accurate electron scatter calculation, and ii) the spacing of calculation points of the Multigrid process, especially in low density materials.

- For IMRT specifically, these effects are exaggerated by the addition of small fields. The dose calculation accuracy is adequate for most treatment sites. The beam energy, as used in this study, does not influence the outcome of the dosimetric accuracy. Using higher energies for clinical/biological reasons or better plan quality is up to the planner to decide. However, using XiO for IMRT plans where the target lies near large volumes with low density should be approached with caution, as large dose discrepancies can be expected between the plan and reality in specific regions, targets or critical organs.

## 5.2. Similar studies

Other authors have also used the EGSnrc MC system to verify different commercial TPSs' IMRT doses/monitor unit calculations. In one study, Pinnacle was used to create Prostate and Head-and-neck plans, and dose differences at the isocenter were found of 2-3%.[75] Another study verified MU calculation to within 2%,[20] and Pisaturo *et al.* obtained clinically equivalent plans between XiO and MC in different patient sites.[21] Most studies compare MUs and not complete 2D dose distributions as in this study. However, actual linacs/source models are used which they either have available or developed by benchmarking against measurements.

## 5.3. Limitations / possible future work

The virtual linac used in this study, although based on a typical linac, differs from a real one in certain aspects. This means that dose is compared here to a simple virtual MC linac, and a full verification of IMRT on XiO will entail using a complete MC model representative of the real linac. As this study aims to develop the system and put forward the first steps toward a verification tool, this is not significant to the outcome of this study. However it must be noted that there are some simplifications/assumptions.

- The MLC model used here is very general, and different vendors have much more specialised MLCs in their machines. Typically, leafs have rounded edges or move in an arc, and have small gaps between them to allow movement. This study thus has no inter-leaf leakage of leaf-tip transmission. In an accurate model of a linac, one would use the appropriate MLC component.

- Only one plan per treatment site was created per energy. A more realistic evaluation of XiO's capabilities will be achieved by expanding the study to include more patients.

- Although the gamma test could be used satisfactorily, an incorporation of the MC statistics into this test to provide a continual type of comparison might be of greater practical use for MC studies. Also, only a single slice was evaluated by using the 2D gamma. Evaluation in 3 dimensions can possibly give a better portrayal of the dose agreement.

- The effect of the immobilisation devices and treatment couch can be investigated in more depth to truly determine how this must be handled when planning with XiO.

# REFERENCES


1. Baskar R, Lee KA, Yeo R, Yeoh K-W. Cancer and Radiation Therapy: Current Advances and Future Directions. Int J Med Sci 2012;9(3):193–9.

2. International Atomic Energy Agency (IAEA). Radiation Biology: A Handbook for teachers and students. Vienna: IAEA; 2010.

3. Connell PP, Hellman S. Advances in Radiotherapy and Implications for the Next Century: A Historical Perspective. Cancer Res 2009;69(2):383–92.

4. Bernier J, Hall EJ, Giaccia A. Radiation oncology: a century of achievements. Nat Rev Cancer 2004;4(9):737–47.

5. Bucci MK, Bevan A, Roach M. Advances in Radiation Therapy: Conventional to 3D, to IMRT, to 4D, and Beyond. CA Cancer J Clin 2005;55(2):117–34.

6. IMRT Collaborative Working Group. Intensity-modulated radiotherapy: current status and issues of interest. Int J Radiat Oncol Biol Phys 2001;51(4):880–914.

7. MacDonald SM, Ahmad S, Kachris S, Vogds BJ, DeRouen M, Gittleman AE, et al. Intensity Modulated Radiation Therapy (IMRT) Versus Three Dimensional Conformal Radiation Therapy (3DCRT) for the Treatment of High Grade Glioma: A Dosimetric Comparison. J Appl Clin Med Phys [Internet] 2007 [cited 2014 Jun 11];8(2). Available from: http://www.jacmp.org/index.php/jacmp/article/view/2423

8. Arbea L, Ramos LI, Martínez-Monge R, Moreno M, Aristu J. Intensity-modulated radiation therapy (IMRT) vs. 3D conformal radiotherapy (3DCRT) in locally advanced rectal cancer (LARC): dosimetric comparison and clinical implications. Radiat Oncol 2010;5(1):17.

9. Yu CX, Tang G. Intensity-modulated arc therapy: principles, technologies and clinical implementation. Phys Med Biol 2011;56(5):R31.

10. Mayles P, Nahum A, Rosenwald JC. Handbook of Radiotherapy Physics: Theory and Practice. CRC Press; 2007.

11. Spezi E, Lewis G. An overview of Monte Carlo treatment planning for radiotherapy. Radiat Prot Dosimetry 2008;131(1):123–9.

12. Rogers DWO. Fifty years of Monte Carlo simulations for medical physics. Phys Med Biol 2006;51(13):R287–301.

13. Monaco® - Radiobiological Planning for IMRT, VMAT and SBRT | Elekta [Internet]. Elekta AB [cited 2014 Jul 28];Available from: http://www.elekta.com/healthcare-professionals/products/elekta-software/treatment-planning-software/planning-software/monaco.html

14. Khan FM. The Physics of Radiation Therapy. Fourth. Lippincott Williams & Wilkins; 2009.

15. Palta JR, Liu C, Li JG. Quality assurance of intensity-modulated radiation therapy. Int J Radiat Oncol Biol Phys 2008;71(1 Suppl):S108–12.

16. Arsenault C, Bissonnette J-P, Dunscombe P, Johnson H, Mawko G, Seuntjens J. CAPCA Standards for Quality Control at Canadian Radiation Treatment Centres - Medical Linear Accelerators. 2005;

17. Alber M, Broggi S, De Wagter C, Eichwurzel I, Engstrom P, Fiorino C, et al. Guidelines for the verification of IMRT. 1st ed. ESTRO; 2008.

18. Lin M-H, Chao T-C, Lee C-C, Tung C-J, Yeh C-Y, Hong J-H. Measurement-based Monte Carlo dose calculation system for IMRT pretreatment and on-line transit dose verifications. Med Phys 2009;36(4):1167–75.

19. Canada G of CNRC. About NRC - National Research Council Canada [Internet]. 2012 [cited 2014 Jul 11];Available from: http://www.nrc-cnrc.gc.ca/eng/about/index.html

20. Fan J, Li J, Chen L, Stathakis S, Luo W, Plessis FD, et al. A practical Monte Carlo MU verification tool for IMRT quality assurance. Phys Med Biol 2006;51(10):2503–15.

21. Pisaturo O, Moeckli R, Mirimanoff R-O, Bochud FO. A Monte Carlo-based procedure for independent monitor unit calculation in IMRT treatment plans. Phys Med Biol 2009;54(13):4299–310.

22. Georg D, Stock M, Kroupa B, Olofsson J, Nyholm T, Ahnesjö A, et al. Patient-specific IMRT verification using independent fluence-based dose calculation software: experimental benchmarking and initial clinical experience. Phys Med Biol 2007;52(16):4981–92.

23. Yang J, Li J, Chen L, Price R, McNeeley S, Qin L, et al. Dosimetric verification of IMRT treatment planning using Monte Carlo simulations for prostate cancer. Phys Med Biol 2005;50(5):869–78.

24. Yamamoto T, Mizowaki T, Miyabe Y, Takegawa H, Narita Y, Yano S, et al. An integrated Monte Carlo dosimetric verification system for radiotherapy treatment planning. Phys Med Biol 2007;52(7):1991–2008.

25. Rogers DWO, Faddegon BA, Ding GX, Ma C-M, We J, Mackie TR. BEAM: A Monte Carlo code to simulate radiotherapy treatment units. Med Phys 1995;22(5):503–24.

26. Kawrakow I, Walters BRB. Efficient photon beam dose calculations using DOSXYZnrc with BEAMnrc. Med Phys 2006;33(8):3046–56.

27. Computerized Medical Systems (CMS). XiO v4.62. Elekta;

28. XiO® - Comprehensive RTP System - Treatment planning Software [Internet]. Elekta AB [cited 2014 Sep 10];Available from: http://www.elekta.com/healthcare-professionals/products/elekta-software/treatment-planning-software/planning-software/xio.html?utm_source=xio&utm_medium=redirect&utm_campaign=redirects

29. Brady LW, Heilmann H-P, Molls M. New Technologies in Radiation Oncology. 2006 edition. Springer; 2006.

30. Mackie TR, Scrimger JW, Battista JJ. A convolution method of calculating dose for 15-MV x rays. Med Phys 1985;12(2):188–96.

31. Scholz C, Schulze C, Oelfke U, Bortfeld T. Development and clinical application of a fast superposition algorithm in radiation therapy. Radiother Oncol 2003;69(1):79–90.

32. Computerized Medical Systems (CMS). Dose Calculation - FFT Convolution and Multigrid Superposition. 2006;

33. Mackie TR, Bielajew AF, Rogers DWO, Battista JJ. Generation of photon energy deposition kernels using the EGS Monte Carlo code. Phys Med Biol 1988;33(1):1.

34. Hoban PW, Murray DC, Round WH. Photon beam convolution using polyenergetic energy deposition kernels. Phys Med Biol 1994;39(4):669.

35. Ahnesjö A. Collapsed cone convolution of radiant energy for photon dose calculation in heterogeneous media. Med Phys 1989;16(4):577–92.

36. Woo MK, Cunningham JR. The validity of the density scaling method in primary electron transport for photon and electron beams. Med Phys 1990;17(2):187–94.

37. ICRU. Prescribing, Recording, and Reporting Photon-Beam Intensity-Modulated Radiation Therapy (IMRT), ICRU Report83. J ICRU 2010;10(1):NP – NP.

38. Bentzen SM, Constine LS, Deasy JO, Eisbruch A, Jackson A, Marks LB, et al. Quantitative Analyses of Normal Tissue Effects in the Clinic (QUANTEC): An Introduction to the Scientific Issues. Int J Radiat Oncol 2010;76(3):S3–9.

39. Brady LW, Heilmann H-P, Molls M, Nieder C. Technical Basis of Radiation Therapy: Practical Clinical Applications. 4th edition. Springer; 2006.

40. Computerized Medical Systems (CMS). Intensity Modulated Radiation Therapy (IMRT) – Technical Reference. 2007;

41. Matuszak MM, Larsen EW, Jee K-W, McShan DL, Fraass BA. Adaptive diffusion smoothing: A diffusion-based method to reduce IMRT field complexity. Med Phys 2008;35(4):1532–46.

42. Kawrakow I, Mainegra-Hing E, Rogers DWO, Tessier F, Walters BRB. The EGSnrc Code System: Monte Carlo Simulation of Electron and Photon Transport. 2011;

43. Schneider JJ, Kirkpatrick S. Stochastic Optimization [Internet]. [cited 2014 Nov 7]. Available from: http://0-www.springer.com.wagtail.ufs.ac.za/computer/ai/book/978-3-540-34559-6

44. James F. RANLUX: A Fortran implementation of the high-quality pseudorandom number generator of Lüscher. Comput Phys Commun 1994;79(1):111–4.

45. Metcalfe P, Kron T, Hoban P. The Physics of Radiotherapy X-Rays from Linear Accelerators. 1 edition. Madison, Wis.: Medical Physics Pub Corp; 1997.

46. Walters BRB, Kawrakow I. Technical note: overprediction of dose with default PRESTA-I boundary crossing in DOSXYZnrc and BEAMnrc. Med Phys 2007;34(2):647–50.

47. Bielajew AF, Rogers DWO. Presta: The parameter reduced electron-step transport algorithm for electron monte carlo transport. Nucl Instrum Methods Phys Res Sect B Beam Interact Mater At 1986;165–81.

48. Rogers DWO, Walters BRB, Kawrakow I. BEAMnrc Users Manual. 2013;

49. Walters BRB, Kawrakow I, Rogers DWO. History by history statistical estimators in the BEAM code system. Med Phys 2002;29(12):2745–52.

50. Walters BRB, Kawrakow I, Rogers DWO. DOSXYZnrc Users Manual. 2013;

51. Low DA, Dempsey JF. Evaluation of the gamma dose distribution comparison method. Med Phys 2003;30(9):2455–64.

52. Low DA, Harms WB, Mutic S, Purdy JA. A technique for the quantitative evaluation of dose distributions. Med Phys 1998;25(5):656–61.

53. Ju T, Simpson T, Deasy JO, Low DA. Geometric interpretation of the gamma dose distribution comparison technique: Interpolation-free calculation. Med Phys 2008;35(3):879–87.

54. Elekta Synergy for IMRT and IGRT | Elekta [Internet]. Elekta AB [cited 2014 Sep 10];Available from: http://www.elekta.com/healthcare-professionals/products/elekta-oncology/oncology-treatment-solutions/elekta-synergy.html

55. Precise Treatment System - providing exceptional beam characteristics for IMRT | Elekta [Internet]. Elekta AB [cited 2015 Apr 17];Available from: http://www.elekta.com/healthcare-professionals/products/elekta-oncology/oncology-treatment-solutions/precise-treatment-system.html

56. South African Standards for Quality Assurance in Radiotherapy (SASQART). Medical Linear Accelerators.

57. Computerized Medical Systems (CMS). Beam data collection list, v4.2. 2006;

58. IDL v6.3. Research Systems, Inc (RSI); 2006.

59. Li XA, Soubra M, Szanto J, Gerig LH. Lateral electron equilibrium and electron contamination in measurements of head-scatter factors using miniphantoms and brass caps. Med Phys 1995;22(7):1167–70.

60. Computerized Medical Systems (CMS). Beam Modeling Guide - XiO, v4.3.0. 2006;

61. OmniPro Accept v6.4A. Scanditronix-Wellhofer AB; 2005.

62. Simonoff JS. Smoothing Methods in Statistics. Springer Science & Business Media; 1996.

63. Microsoft Visual Basic 6.0 (SP6). Microsoft Corporation; 2000.

64. Electron Density CT Phantom RMI 467 [Internet]. [cited 2014 Sep 19];Available from: http://www.qados.co.uk/products/electron-density-ct-phantom/electron-density-ct-phantom-rmi-467

65. ICRU. Tissue Substitutes in Radiation Dosimetry and Measurement (Report 44). Intl Commission on Radiation Units and Measurements; 1989.

66. Zhan L, Jiang R, Osei EK. Beam coordinate transformations from DICOM to DOSXYZnrc. Phys Med Biol 2012;57(24):N513–23.

67. 62C IT. IEC 61217 Ed. 1.1 b:2002, Radiotherapy equipment - Coordinates, movements and scales. Multiple. Distributed through American National Standards Institute; 2007.

68. Marks LB, Yorke ED, Jackson A, Ten Haken RK, Constine LS, Eisbruch A, et al. Use of Normal Tissue Complication Probability Models in the Clinic. Int J Radiat Oncol • Biol • Phys 2010;76(3):S10–9.

69. Radiation Therapy Oncology Group (RTOG). A phase III randomized study of high dose 3D-CRT/IMRT versus standard dose 3D-CRT/IMRT in patients treated for localized prostate cancer (RTOG-0126) [Internet]. 2004;Available from: http://www.rtog.org/ClinicalTrials/ProtocolTable/StudyDetails.aspx?study=0126

70. Radiation Therapy Oncology Group (RTOG). A phase III trial evaluating the addition of trastuzumab to trimodality treatment of her2-overexpressing esophageal adenocarcinoma (RTOG-1010) [Internet]. 2013;Available from: http://www.rtog.org/ClinicalTrials/ProtocolTable/StudyDetails.aspx?study=1010

71. OmniPro I'mRT. IBA Dosimetry; 2010.

72. mcshow. Philadelphia, Pennsylvania: Fox Chase Cancer Center;

73. Elekta. iBEAM evo Couchtop [Internet]. Elekta AB [cited 2014 Nov 28];Available from: http://www.elekta.com/healthcare-professionals/products/elekta-oncology/treatment-techniques/positioning-and-immobilization/ibeam-evo-couchtop.html

74. Kirkpatrick JP, van der Kogel AJ, Schultheiss TE. Radiation Dose–Volume Effects in the Spinal Cord. Int J Radiat Oncol • Biol • Phys 2010;76(3):S42–9.

75. Francescon P, Cora S, Chiovati P. Dose verification of an IMRT treatment planning system with the BEAM EGS4-based Monte Carlo code. Med Phys 2003;30(2):144–57.

# SUMMARY

Key words: Treatment Planning System, Monte Carlo, Dose verification tool, EGSnrc, BEAMnrc, DOSXYZnrc, XiO, Intensity Modulated Radiation Therapy

Cancer treatment with external beam radiotherapy using the specialized technique of intensity modulation is a complex modality. The Treatment Planning System (TPS) is responsible for accurate calculation of dose to allow the radiotherapy team to make decisions on the patient treatment. The commercial TPS, XiO, utilizes a Multigrid Superposition algorithm as dose calculation engine, which is model based. Several approximations are inherent in this method. In-depth quality assurance (QA) of Intensity Modulated Radiation Therapy (IMRT) plans is necessary, and these tests are time-consuming and reduce the available clinical treatment time. Monte Carlo (MC) has been proven to be the most accurate method of radiation dose calculation. MC is a direct dose calculation method, and the EGSnrc codes are well suited for linear accelerator (linac) simulations.

This study aims to be a first step towards full MC-based dose verification for IMRT dose distributions produced on XiO: developing the system and demonstrating the accuracy thereof.

A generic virtual linac based on a typical Elekta linac was constructed using the EGSnrc MC software (BEAMnrc and DOSXYZnrc), for beam energies of 6 and 10 MV respectively. Simulations were either run on a watertank model or in air to produce beam data required for commissioning on XiO. Beam profiles, Percentage Depth Dose (PDD) curves and scatter factors for collimator and total scatter were extracted from the data. Software was developed to convert data to a format readable by the TPS. Modelling was done on XiO for all fields. A software graphical user interface (GUI) was developed to extract necessary information from dicom files required for MC calculations. This included CT data extracting and converting to EGSnrc format, reading all plan details, and creating scripts for automatic MC dose calculation execution. IMRT plans were created for 3 different treatment sites using the newly commissioned model on XiO. The modelling and simulation process was verified with MC dose calculations in scanned phantoms. After simulation, the IMRT plans were evaluated with isodose/profiles and 2D gamma analysis, as well as dose difference maps and Dose Volume Histogram (DVH) comparisons.

The generic linac could successfully be created on BEAMnrc, and produced clinically acceptable beams. The data for commissioning was also generated successfully, and could be extracted and read into XiO after some de-noising filters were applied. Modelling on the TPS was done to an overall agreement level of 3%/3mm and 2%/2mm for small fields. Doses in the Prostate and Head-and-Neck IMRT plans compared well between XiO and MC for both energies. Gamma pass rates were above 90% for a criterion of 3%/2mm in a region of interest (ROI) covering the target and critical organs. Only slight overestimation of dose in bony regions was observed. The Esophagus IMRT plans however indicated some discrepancies in the dose calculation of XiO, especially in the low density regions, like lung. The 2D gamma pass rates were low, and DVH comparison indicated large overestimation of dose in the target volume, as well as in the Spine, as a direct consequence of errors in dose calculation of low density media.

It is concluded that a dose verification system could successfully be developed for comparison of IMRT plans. Accurate modelling on the TPS was a vital step, and some possible issues were addressed. The system can be used routinely, and doses are calculated in a reasonable time with differences presented in a practical manner. The dose calculation of IMRT plans on XiO was compared to MC dose and found to be accurate for most treatment sites, independent of beam energy. However, caution is advised for cases where beams are directed through low density media, as clinically significant effects can possibly occur in patients.

# OPSOMMING

Sleutelwoorde: Behandelings Beplanning Stelsel, Monte Carlo, Dosis verifikasie stelsel, EGSnrc, BEAMnrc, DOSXYZnrc, XiO, Intensiteits Gemoduleerde Radioterapie.

Die behandeling van kanker met eksterne bundel bestraling d.m.v. die gespesialiseerde tegniek van intensiteit modulasie is 'n komplekse modaliteit. Die Behandelings Beplanning Stelsel (BBS) is verantwoordelik vir die akkurate berekening van dosis sodat die bestralings span besluite kan neem oor die pasiënt se behandeling. Die kommersiële BBS, XiO, maak gebruik van 'n veelvuldige-rooster Superposisie algoritme as dosis berekening enjin, wat model-gebaseerd is. Verskeie benaderings is deel van hierdie metode. Deeglike gehalteversekering (GV) is nodig in Intensiteit Gemoduleerde Radioterapie (IGR) planne, en hierdie toetse is tydrowend en verminder die beskikbare kliniese behandeling tyd. Monte Carlo (MC) is al bewys om die mees akkurate metode van stralingsdosis berekening te wees. MC is 'n direkte dosis berekening metode, en die EGSnrc kodes is geskik vir lineêre versneller simulasies.

Hierdie studie het ten doel om 'n eerste stap tot volledige MC-gebaseerde dosis verifikasie vir IGR dosis verspreidings te wees op XiO: die stelsel te ontwikkel en die akkuraatheid daarvan te demonstreer.

'n Generiese virtuele versneller gebaseer op 'n tipiese Elekta versneller is gebou met behulp van die EGSnrc MC sagteware (BEAMnrc en DOSXYZnrc) met energieë van 6 en 10 MV onderskeidelik. Simulasies was óf op 'n water tenk model of in lug gedoen om die nodige data vir ingebruikneming op XiO te produseer. Bundel profiele, Persentasie Diepte Dosis (PDD) kurwes en verstrooïngs faktore vir kollimator en totale verstrooïng is uit die data verkry. Sagteware is ontwikkel om data te omskep in 'n formaat geskik vir die BBS. Modellering is gedoen op XiO vir alle velde. 'n Sagteware grafiese gebruikerskoppelvlak (GGK) is ontwikkel om die nodige inligting van DICOM lêers vir MC berekeninge te verkry. Dit sluit in die verkryging van RT data en die omskakeling na EGSnrc formaat, inlees van alle plan besonderhede, en die skep van roetines vir outomatiese MC dosis berekening uitvoering. IGR planne vir 3 verskillende behandeling areas is geskep met behulp van díe nuwe model op XiO. Die modellering en simulasie proses is geverifieer met MC dosis berekeninge in geskandeerde fantome. Na simulasie is die IGR planne geëvalueer met isodosisse/profiele en 2D gamma analise, asook dosis-verskil kaarte en Dosis Volume Histogram (DVH) vergelykings.

Die generiese versneller kon suksesvol geskep word op BEAMnrc, en produseer klinies aanvaarbare bundels. Die data vir ingebruikneming is ook suksesvol gegenereer, en kon verkry en ingelees word in XiO nadat 'n paar vergladdings filters toegepas is. Modellering van die BBS is gedoen tot 'n algehele ooreenkoms vlak van 3%/3mm en 2%/2mm vir klein velde. Dosisse in die Prostaat en Kop-en-nek IGR planne het goed vergelyk tussen XiO en MC vir beide energieë. Die gamma slaagsyfers was bo 90 % vir 'n maatstaf van 3%/2mm in 'n gebied van belang wat die teiken en kritiese organe insluit. Slegs effense oorskatting van dosis in been is waargeneem. Die Esofagus IGR planne het egter teenstrydighede in die dosis berekening van XiO aangedui, veral in die lae digtheid gebiede soos die longe. Die 2D gamma slaagsyfers was laag, en DVH vergelyking het groot oorskatting van dosis in die teiken volume aangedui, sowel as in die spinaalkoord, as 'n direkte gevolg van foute in die dosis berekening van lae digtheid media.

Dit is die gevolgtrekking dat 'n dosis verifikasie stelsel suksesvol vir die verifikasie van IGR planne ontwikkel kon word. Akkurate modelle op die BBS was 'n belangrike stap, en 'n paar moontlike kwessies is aangespreek. Die stelsel kan gereeld gebruik word, en dosisse word bereken in 'n redelike tyd met verskille wat in 'n praktiese wyse vertoon word. Die dosis berekening van IGR planne op XiO is vergelyk met MC dosis berekeninge en gevind om akkuraat vir die meeste behandeling areas te wees, onafhanklik van bundel energie. Dit word egter aanbeveel om versigtig te wees in gevalle waar strale deur lae digtheid media beplan word, aangesien klinies beduidende effekte moontlik in pasiënte kan voorkom.

# ACKNOWLEDGEMENTS

This study is the result of years of hard work, deep thinking and most of all constant learning: not only in the science but also many aspects of life.

I give all glory to God Almighty for my talents and blessings, for by His Grace I could achieve a greater understanding of the physics of His creation to improve our caring for humankind. He also taught me countless lessons and shaped me more to His image through this endeavour.

To Johanette, who became a bigger part of my life as my studies progressed; from being girlfriend to fiancée to wife. I thank her for encouragement, unconditional love and support in the difficult times, and for tolerating my utter silliness and lame jokes the rest of the time. I am grateful for your prayers, and that you keep reminding me of humbleness and the reason for it all.

To my supervisor, dr Freek du Plessis, my gratitude for all the hard work and advice he has put into this study, as well as making available resources. The knowledge I have gained and role you have played in improving my skills are of great value.

Thank-you to my colleagues as well: Prof William Rae, Willie, Dedri, Dète, Itumeleng and Cobus, and all the others in the Medical Physics family; for listening and sharing ideas, and for giving advice and encouragement at the perfect time.

I would also like to thank my family and friends for their support and interest in my work, for their love and prayers, and making sure I maintained a bit of normality throughout.

"This research project was funded by the South African Medical Research Council (MRC) with funds from National Treasury under its Economic Competitiveness and Support Package."

"Research and any publication thereof is the result of funding provided by the Medical Research Council of South Africa in terms of the MRC's Flagship Awards Project SAMRC-RFA-UFSP-01-2013/HARD."

# Appendix A: ADDITIONAL RESULTS

## 1. Beam data for commissioning

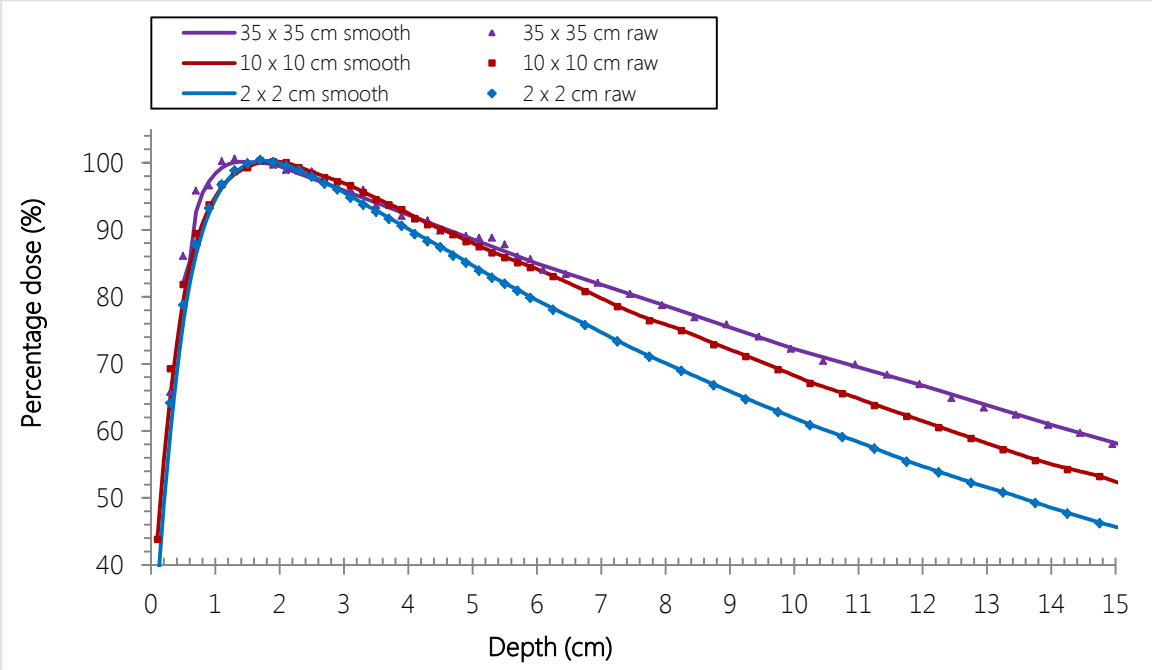


**Figure A-1: Smoothing effect on PDDs for 10MV linac**
**PDDs are normalized at $d_{max}$ (2 cm)**

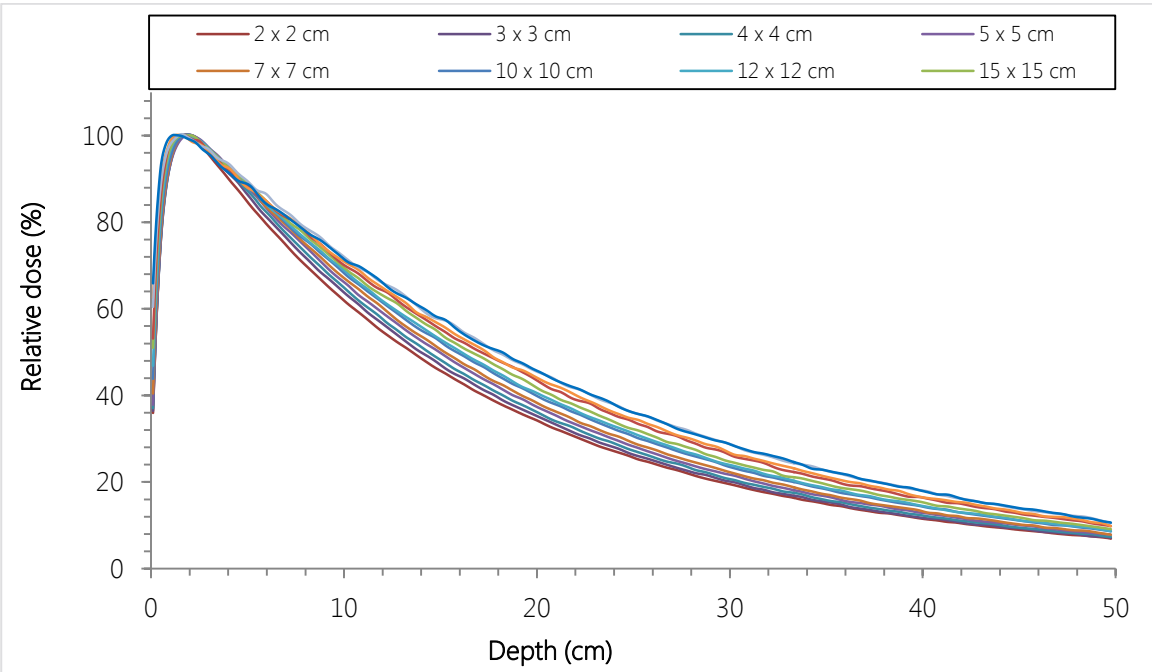


**Figure A-2: Final PDDs for the 10MV linac over all FSs**
**The curves range gradually from the $1 \times 1$ to $35 \times 35$ cm$^2$ fields**

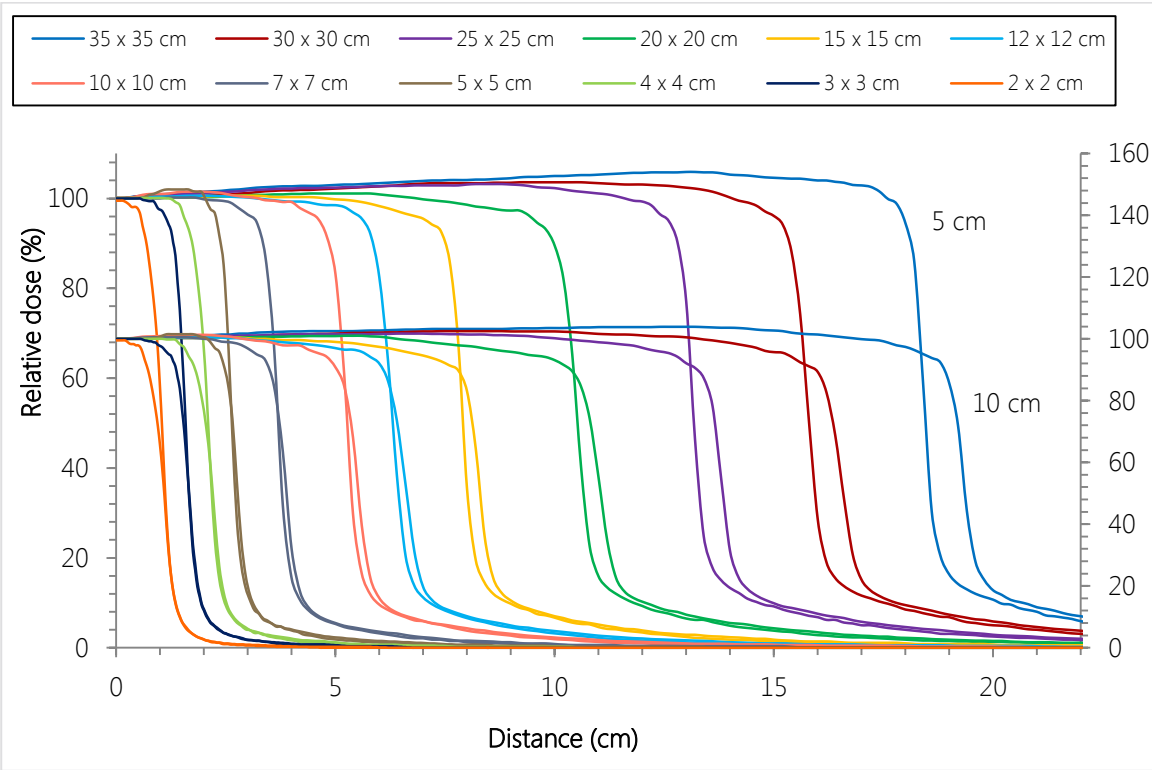


**Figure A-3: Final Crossplane profiles for 10MV linac**
**Normalised profiles are shown at 5cm depth (top curves, left axis) and 10cm depth (lower curves, right axis)**

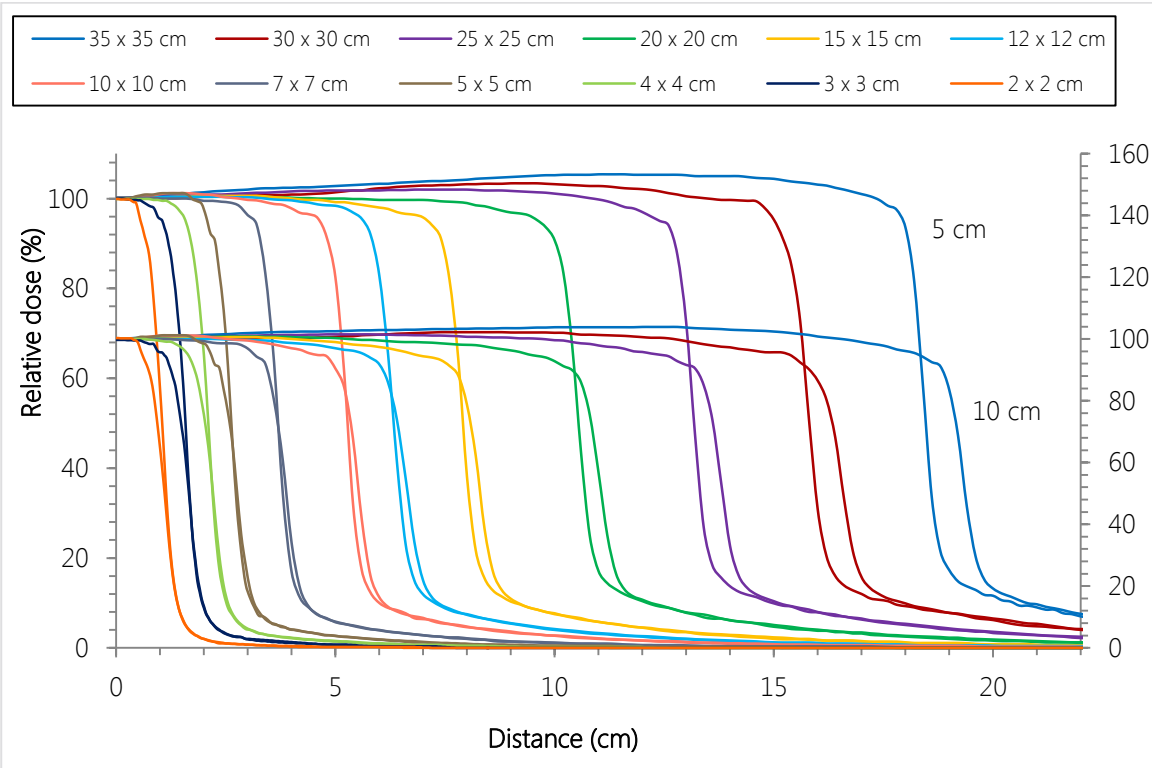


**Figure A-4: Final Inplane profiles for 10MV linac**
**Normalised profiles are shown at 5cm depth (top curves, left axis) and 10cm depth (lower curves, right axis)**

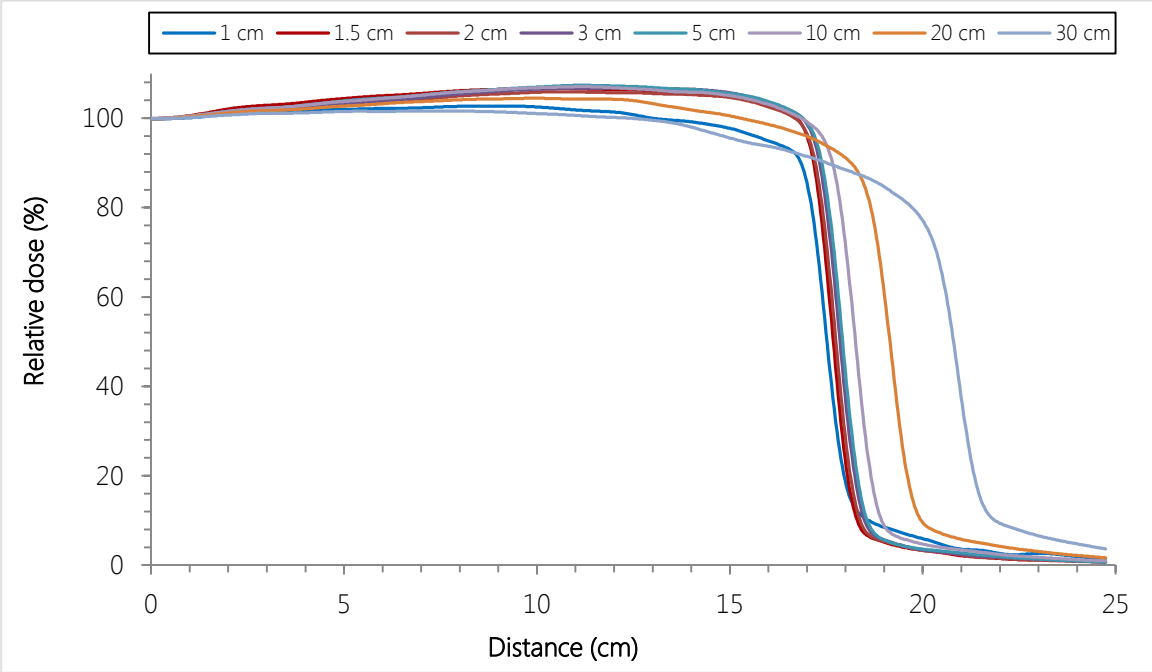


**Figure A-5: Final diagonal profiles for the 10MV linac**

## 2. XiO modelling

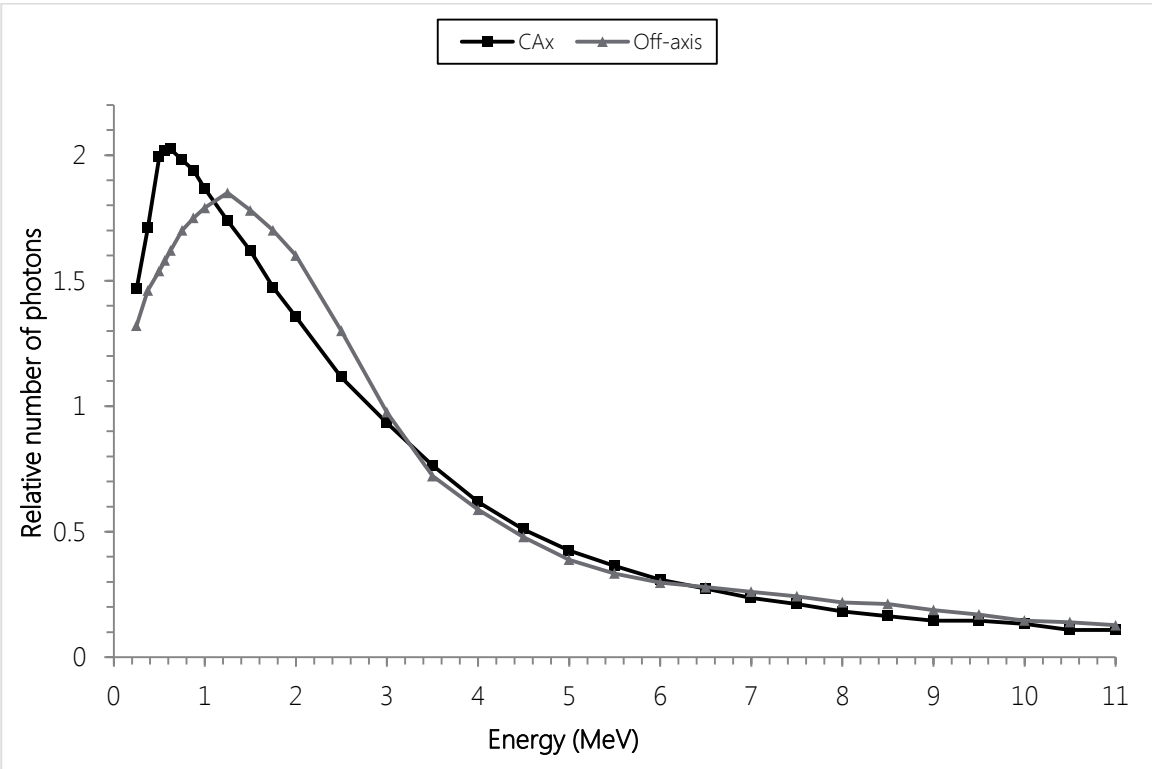


**Figure A-6: Modelled spectra**
**The CAx and off-axis spectra are shown for the 10MV model**

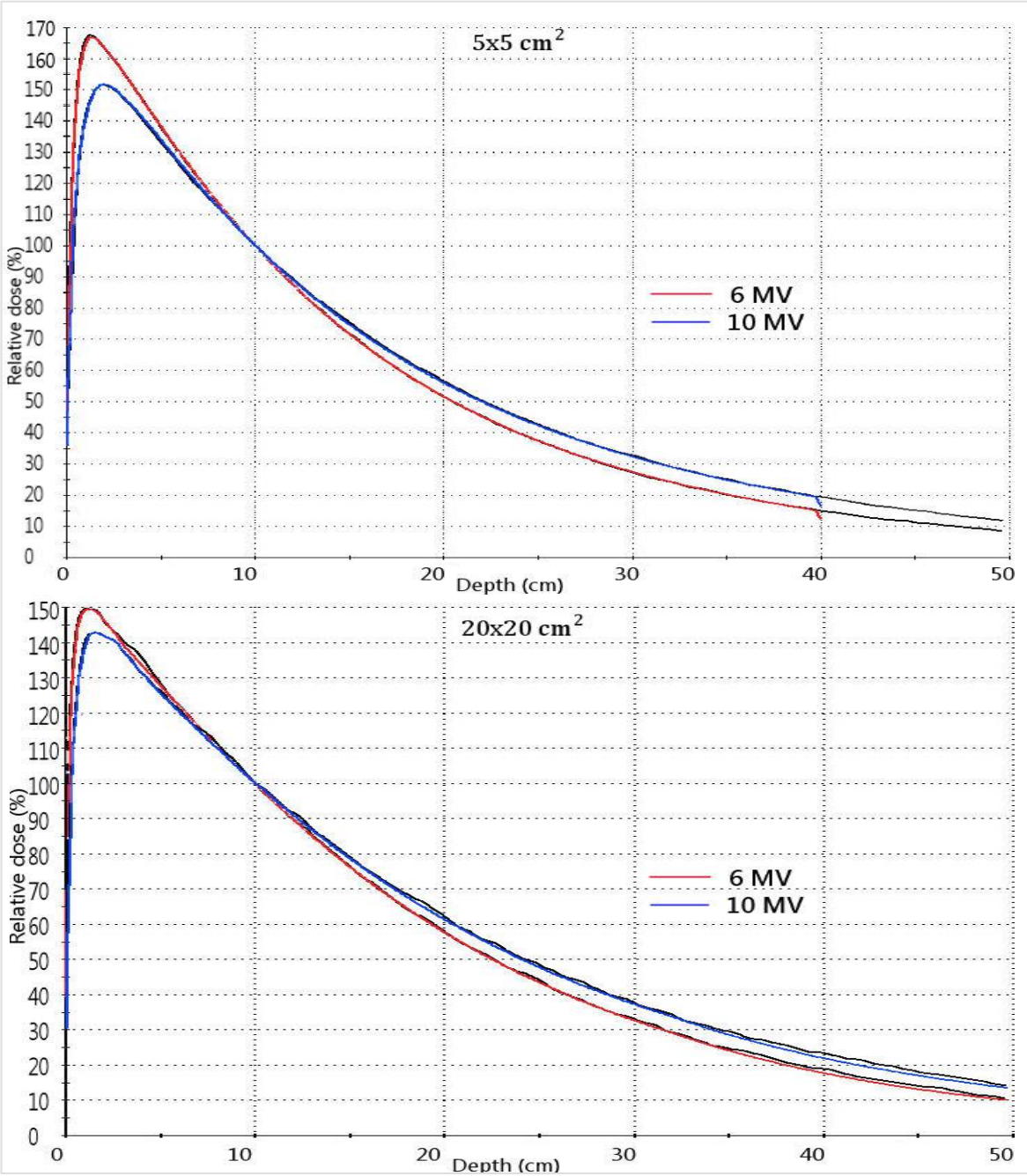


**Figure A-7: Modelled PDDs of other FSs**

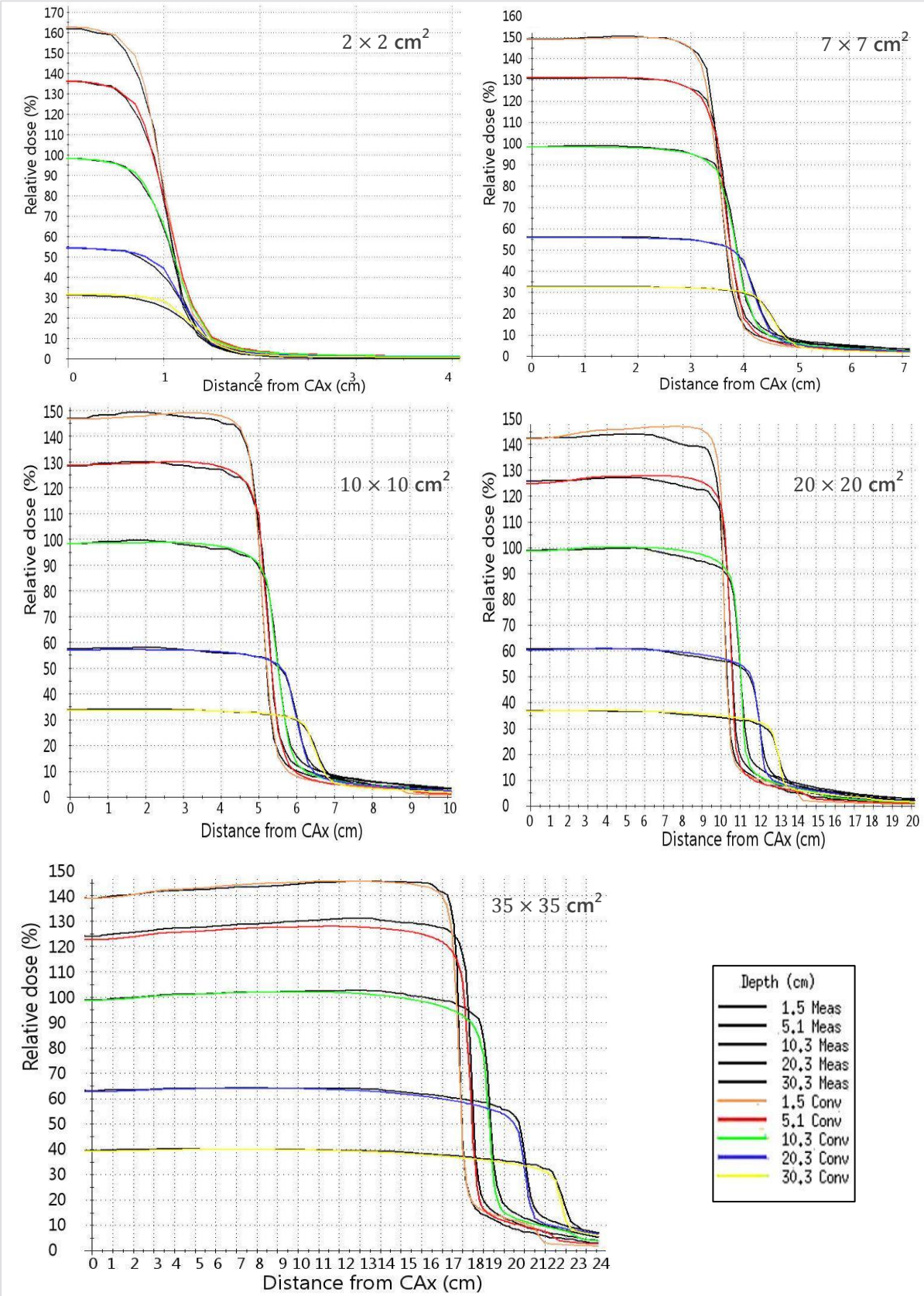


**Figure A-8: Modelled Crossplane half-profiles for 10MV**

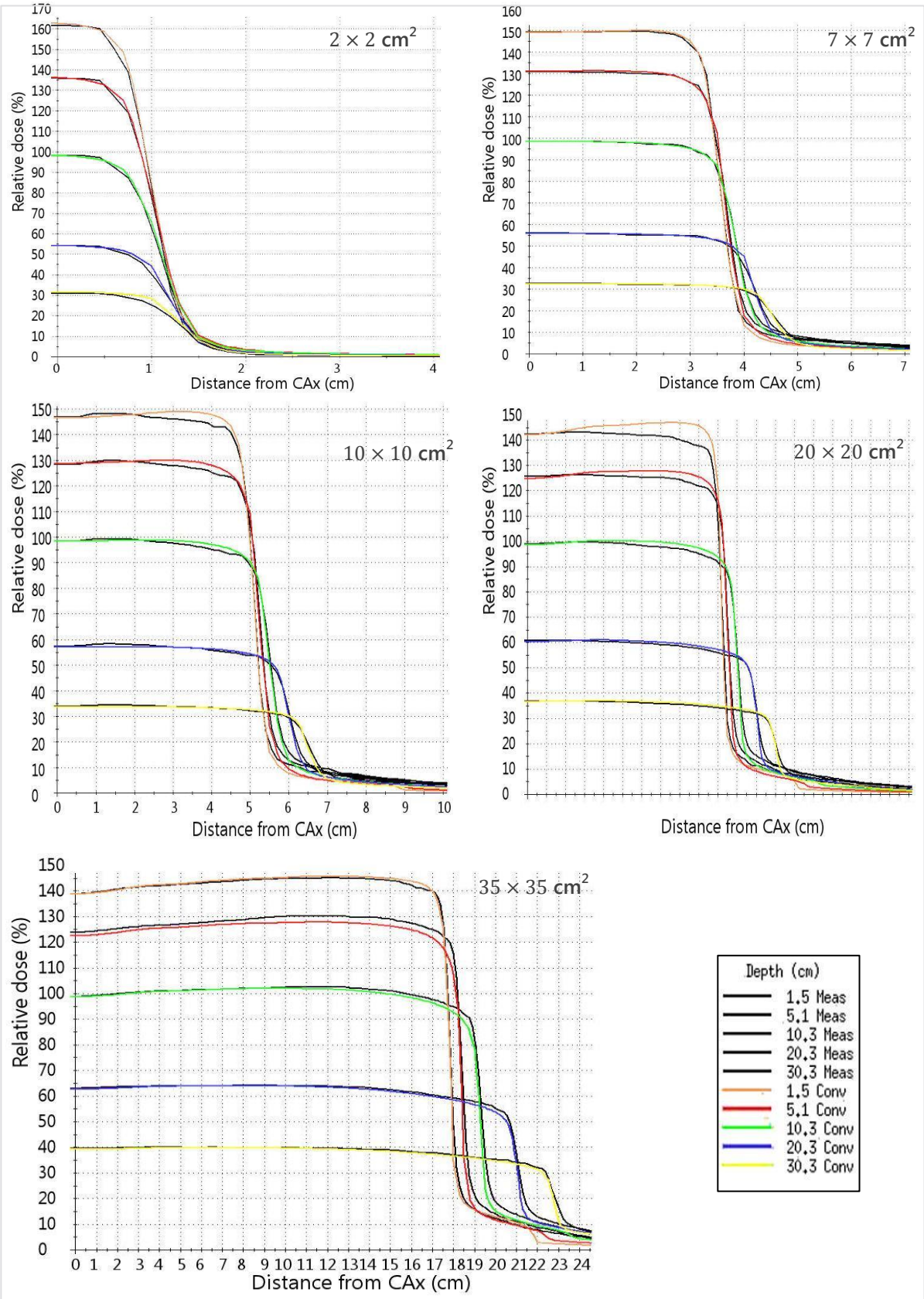


**Figure A-9: Modelled Inplane half-profiles for 10MV**

3. Model verification

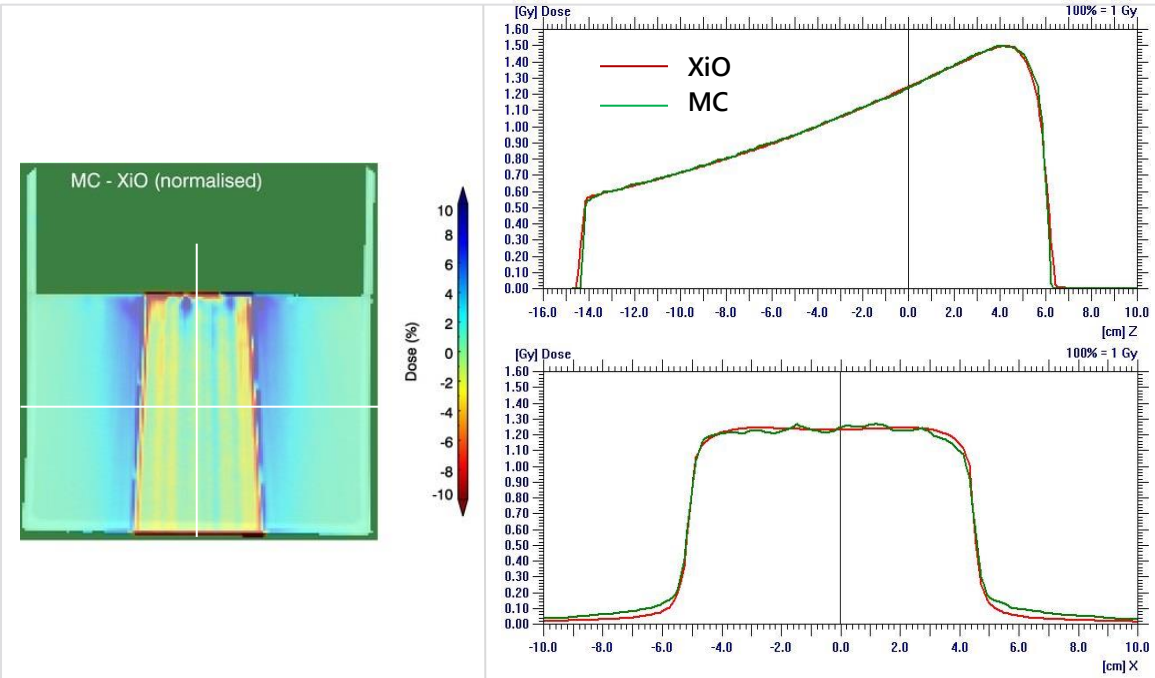


**Figure A-10: $10 \times 10$ cm$^2$ field dose comparison for the 10MV simulation**
**Dose difference maps (let) as well as CAx PDD and profile at the isocenter are shown (right)**

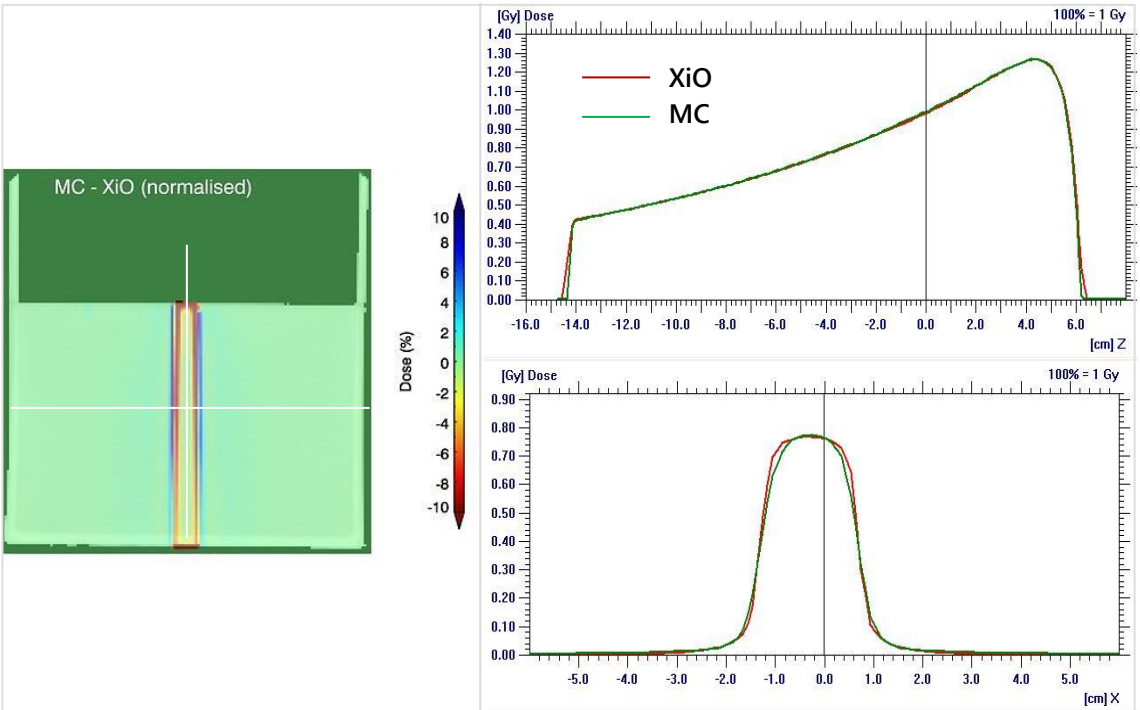


**Figure A-11: $2 \times 2$ cm$^2$ field dose comparison for the 10MV simulation**

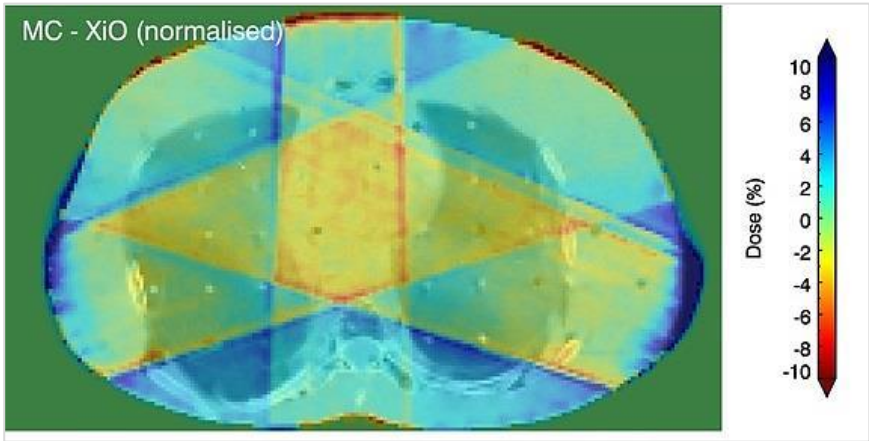


**Figure A-12: Dose difference map (MC-XiO) of 10MV 3D-CRT plan**
**Normalised differences are relative to the prescibed dose**

4. IMRT plan description

## Prostate plans

### IMRT Prescription

Patient ID: [redacted]
Name: [redacted]
Plan ID: Lou6NCsegmD
Plan Description: 6MV no couch segmented

| Structure | Type | Rank | Objective | Dose(cGy) | Volume(%) | Weight | Power | Status |
|---|---|---|---|---|---|---|---|---|
| Prostate | Target | 1 | Maximum | 8470 | 0 | 100 | 2.0 | On |
| | | | Goal | 7920 | 100 | | 1.0 | On |
| | | | Minimum | 7524 | 100 | 100 | 2.1 | On |
| Sem Ves | Target | 1 | Maximum | 8470 | 0 | 100 | 2.0 | On |
| | | | Goal | 7920 | 100 | | 1.0 | On |
| | | | Minimum | 7524 | 100 | 100 | 2.0 | On |
| PTV1 | Target | 2 | Maximum | 8470 | 0 | 100 | 2.0 | On |
| | | | Goal | 8100 | 100 | | 1.0 | On |
| | | | Minimum | 7524 | 100 | 150 | 2.2 | On |
| Iliac Nodes | Target | 3 | Maximum | 8470 | 0 | 100 | 2.0 | On |
| | | | Goal | 5040 | 100 | | 1.0 | On |
| | | | Minimum | 4788 | 100 | 100 | 2.0 | On |
| Obt nodes | Target | 3 | Maximum | 8470 | 0 | 100 | 2.0 | On |
| | | | Goal | 5040 | 100 | | 1.0 | On |
| | | | Minimum | 4788 | 100 | 100 | 2.0 | On |
| PTV2 | Target | 4 | Maximum | 8470 | 0 | 100 | 2.0 | On |
| | | | Goal | 5040 | 100 | | 1.0 | On |
| | | | Minimum | 4788 | 100 | 100 | 2.0 | On |
| Rectum | OAR | 5 | Maximum | 8470 | 0 | 100 | 2.0 | On |
| | | | Dose Volume | 7500 | 15 | 100 | 2.0 | On |
| | | | Dose Volume | 7000 | 25 | 100 | 2.0 | On |
| | | | Dose Volume | 6500 | 35 | 100 | 2.0 | On |
| | | | Dose Volume | 6000 | 50 | 100 | 2.0 | On |
| Bladder | OAR | 5 | Maximum | 8470 | 0 | 100 | 2.0 | On |
| | | | Dose Volume | 8000 | 15 | 100 | 2.0 | On |
| | | | Dose Volume | 7500 | 25 | 100 | 2.0 | On |
| | | | Dose Volume | 7000 | 35 | 100 | 2.0 | On |
| | | | Dose Volume | 6500 | 50 | 100 | 2.0 | On |
| Small bowel | OAR | 5 | Maximum | 8000 | 0 | 100 | 2.0 | On |
| | | | Dose Volume | 4500 | 33 | 100 | 2.0 | On |
| Patient | OAR | 6 | Maximum | 8000 | 0 | 100 | 2.0 | On |
| | | | Dose Volume | 2800 | 15 | 100 | 2.0 | On |
| | | | Dose Volume | 2300 | 20 | 100 | 2.0 | On |
| Outline | OAR | 6 | Dose Volume | 0 | 100 | 100 | 2.0 | Off |

# IMRT Optimization Summary

Patient ID: [redacted]
Name: [redacted]
Plan ID: Lou6NCsegmD
Plan Description: 6MV no couch segmented
Calculation Volume Width/Height/Depth Spacing(cm): 0.2000/0.2000/0.2000
Modulator: MLC
Minimum Transmission Multiplier: 1.0
Step Increment(cm): 1.0
Initial Optimization
    Convergence Criterion(%): 0.0050
    Maximum Iterations: 50
    Scatter Extent(cm): 1.0
    Optimization Margin(cm): 0.5
Smoothing Parameters: GeneralHighSmoothing
Beam Weight Optimization
    Convergence Criterion(%): 1.0000
    Maximum Iterations: 10

# IMRT Delivery Summary

Patient ID: [redacted]
Name: [redacted]
Plan ID: Lou6NCsegmD
Plan Description: 6MV no couch segmented
Modulator: MLC
Delivery Method: Step and Shoot
    Segmentation Method: Smart Sequencing(TM)
Minimum MU/Segment: 3.0
Minimum Segment Area(cm^2): 2.0
Segment Suppression Factor: 3.0
Segment Weight Optimization
    Convergence Criterion(%): 1.0000
    Minimum Segment MU: 3.0
    Use Fast Superposition: yes
    SWO Grid Spacing(cm): 0.2000
    Maximum Iterations: 15
    Revise Iterations: 5

**Table A-1: Segment summary for Prostate IMRT plans**

| | | | 6 MV | | 10MV | |
|---|---|---|---|---|---|---|
| Beam # | Description | Calculation | MLC Segments | MU | MLC Segments | MU |
| 1 | G207 | Superposition | 4 | 49.59 | 4 | 46.79 |
| 2 | G258 | Superposition | 7 | 66.849 | 8 | 62.717 |
| 3 | G309 | Superposition | 4 | 37.56 | 3 | 30.05 |
| 4 | G0 | Superposition | 7 | 71.796 | 8 | 71.561 |
| 5 | G51 | Superposition | 3 | 26.891 | 3 | 25.69 |
| 6 | G102 | Superposition | 6 | 49.807 | 7 | 52.144 |
| 7 | G153 | Superposition | 5 | 51.818 | 4 | 39.63 |
| Total | | | 36 | 354.31 | 37 | 328.58 |

Prostate plan with couch

**Table A-2: Segment summary for Prostate IMRT plan with couch**

| | | | 6 MV | |
|---|---|---|---|---|
| Beam # | Description | Calculation | MLC Segments | MU |
| 1 | G207 | Superposition | 4 | 52.79 |
| 2 | G258 | Superposition | 7 | 66.93 |
| 3 | G309 | Superposition | 4 | 37.54 |
| 4 | G0 | Superposition | 7 | 72.13 |
| 5 | G51 | Superposition | 3 | 26.94 |
| 6 | G102 | Superposition | 6 | 49.83 |
| 7 | G153 | Superposition | 5 | 55.34 |
| Total | | | 36 | 361.5 |

Head-and-Neck plans

# IMRT Prescription

Patient ID: [redacted]
Name: [redacted]
Plan ID: Lou6NCsegm
Plan Description: 6MV no couch segmentedSS

| Structure | Type | Rank | Objective | Dose(cGy) | Volume(%) | Weight | Power | Status |
|---|---|---|---|---|---|---|---|---|
| GTV | Target | 1 | Maximum | 8132 | 0 | 100 | 2.0 | On |
| | | | Goal | 7600 | 100 | | 1.0 | On |
| | | | Minimum | 7220 | 100 | 100 | 2.0 | On |
| patientImmEXT | OAR | 11 | | | | | | |
| PTV | Target | 2 | Maximum | 8132 | 0 | 100 | 2.3 | On |
| | | | Goal | 7250 | 100 | | 1.0 | On |
| | | | Minimum | 6888 | 100 | 100 | 2.0 | On |
| Parotid R | OAR | 3 | Maximum | 8132 | 0 | 100 | 2.0 | On |
| | | | Dose Volume | 2000 | 50 | 100 | 2.0 | On |
| spinalcord | OAR | 3 | Maximum | 5000 | 0 | 100 | 2.0 | On |
| Spinalcord+mar | OAR | 3 | Maximum | 5200 | 0 | 100 | 2.0 | On |
| Patient+Imm | OAR | 4 | Maximum | 8132 | 0 | 100 | 2.0 | On |
| | | | Dose Volume | 2500 | 10 | 100 | 2.0 | On |
| | | | Dose Volume | 1500 | 20 | 100 | 2.0 | On |
| patient2 | OAR | 5 | | | | | | |
| Head rest | OAR | 6 | | | | | | |
| Outline | OAR | 7 | | | | | | |
| patient | OAR | 10 | | | | | | |

# IMRT Optimization Summary

Patient ID: [redacted]
Name: [redacted]
Plan ID: Lou6NCsegm
Plan Description: 6MV no couch segmentedSS
Calculation Volume Width/Height/Depth Spacing(cm): 0.2001/0.2011/0.2000
Modulator: MLC
Minimum Transmission Multiplier: 1.0
Step Increment(cm): 1.0
Initial Optimization
    Convergence Criterion(%): 0.0100
    Maximum Iterations: 100
    Scatter Extent(cm): 1.0
    Optimization Margin(cm): 0.5
Smoothing Parameters: GeneralHighSmoothing
Beam Weight Optimization
    Convergence Criterion(%): 1.0000
    Maximum Iterations: 10

# IMRT Delivery Summary

Patient ID: [redacted]
Name: [redacted]
Plan ID: Lou6NCsegm
Plan Description: 6MV no couch segmentedSS
Modulator: MLC
Delivery Method: Step and Shoot
    Segmentation Method: Smart Sequencing(TM)
Minimum MU/Segment: 2.0
Minimum Segment Area(cm^2): 2.0
Segment Suppression Factor: 1.0
Segment Weight Optimization
Convergence Criterion(%): 0.5000
Minimum Segment MU: 2.0
Use Fast Superposition: yes
SWO Grid Spacing(cm): 0.2000
Maximum Iterations: 100
Revise Iterations: 5

**Table A-3: Segment summary for Head-and-Neck IMRT plans**

| | | | 6 MV | | 10MV | |
|---|---|---|---|---|---|---|
| Beam # | Description | Calculation | MLC Segments | MU | MLC Segments | MU |
| 1 | | Superposition | 9 | 31.25 | 3 | 31.35 |
| 2 | | Superposition | 13 | 49.21 | 7 | 49.72 |
| 3 | | Superposition | 16 | 53.2 | 7 | 44.95 |
| 4 | | Superposition | 12 | 52.55 | 6 | 46.08 |
| 5 | | Superposition | 12 | 50.74 | 5 | 43.68 |
| 6 | | Superposition | 10 | 52.79 | 4 | 38.31 |
| 7 | | Superposition | 7 | 56.02 | 6 | 52.3 |
| 8 | | Superposition | 5 | 41.61 | 4 | 38.72 |
| Total | | | 84 | 387.37 | 42 | 345.11 |

# IMRT Prescription

Patient ID: [redacted]
Name: [redacted]
Plan ID: 6segm
Plan Description: LL4 imrt segmented

| Structure | Type | Rank | Objective | Dose(cGy) | Volume(%) | Weight | Power | Status |
|---|---|---|---|---|---|---|---|---|
| GTV hn | Target | 1 | Maximum | 4750 | 0 | 100 | 2.0 | On |
| | | | Goal | 4600 | 100 | | 1.0 | On |
| | | | Minimum | 4500 | 100 | 100 | 2.1 | On |
| PTV | Target | 2 | Maximum | 4750 | 0 | 100 | 2.0 | On |
| | | | Goal | 4600 | 100 | | 1.0 | On |
| | | | Minimum | 4500 | 100 | 100 | 2.3 | On |
| Spine | OAR | 3 | Maximum | 4500 | 0 | 100 | 2.0 | On |
| Longe | OAR | 3 | Maximum | 4800 | 0 | 100 | 2.0 | On |
| | | | Dose Volume | 3000 | 20 | 100 | 2.0 | On |
| | | | Dose Volume | 2000 | 25 | 100 | 2.0 | On |
| | | | Dose Volume | 1000 | 40 | 100 | 2.1 | On |
| | | | Dose Volume | 500 | 50 | 100 | 2.2 | On |

# IMRT Optimization Summary

Patient ID: [redacted]
Name: [redacted]
Plan ID: 6segm
Plan Description: LL4 imrt segmented
Calculation Volume Width/Height/Depth Spacing(cm): 0.2009/0.2001/0.2000
Modulator: MLC
Minimum Transmission Multiplier: 1.0
Step Increment(cm): 1.0
Initial Optimization
- Convergence Criterion(%): 0.0100
- Maximum Iterations: 100
- Scatter Extent(cm): 1.0
- Optimization Margin(cm): 0.5

Smoothing Parameters: GeneralHighSmoothing
Beam Weight Optimization
- Convergence Criterion(%): 1.0000
- Maximum Iterations: 10

# IMRT Delivery Summary

Patient ID: [redacted]
Name: [redacted]
Plan ID: 6segm
Plan Description: LL4 imrt segmented
Modulator: MLC
Delivery Method: Step and Shoot
- Segmentation Method: Smart Sequencing(TM)

Minimum MU/Segment: 3.0
Minimum Segment Area(cm^2): 2.0
Segment Suppression Factor: 3.0
Segment Weight Optimization
- Convergence Criterion(%): 0.0100
- Minimum Segment MU: 3.0
- Use Fast Superposition: yes
- SWO Grid Spacing(cm): 0.2000
- Maximum Iterations: 50
- Revise Iterations: 5

**Table A-4: Segment summary for Esophagus IMRT plans**

| | | | 6 MV | | 10MV | |
|---|---|---|---|---|---|---|
| Beam # | Description | Calculation | MLC Segments | MU | MLC Segments | MU |
| 1 | | Superposition | 9 | 88.81 | 9 | 83.12 |
| 2 | | Superposition | 13 | 129.66 | 15 | 148.38 |
| 3 | | Superposition | 13 | 121.78 | 9 | 103.53 |
| 4 | | Superposition | 13 | 93.06 | 12 | 111.51 |
| 5 | | Superposition | 8 | 57.98 | 6 | 38.89 |
| Total | | | 56 | 491.29 | 51 | 485.43 |

5. MC input files

```
BEAMnrc input file for [redacted] Segment001
AIR700ICRU
0, 0, 0, 0, 0, 2, 0, IWATCH ETC.
140927216, 97, 33, 100, 0, 0, 0, 0, NCASE ETC.
0, 21, 1, 10, 0, 0, 0, 0, 0, 0, IQIN, ISOURCE + OPTIONS
/home/beamnrc/egsnrc_mp/BEAM_s1/LouLinac4_6MV.egsphsp1
0, 0, 0.7, 0.01, 0, 2, 0.7,  0 , ECUT,PCUT,IREJCT,ESAVE
0, 0, 0, 0, 0,  PHOTON FORCING
1, 2,  SCORING INPUT
0, 0
0,  DOSE COMPONENTS
0.1, Z TO FRONT FACE
*********** start of CM MLC with identifier MLC  ***********
20, RMAX
MLCs
1, IDMLFC
3.85, ZMIN
7.5, ZTHICK
40, 11.94, # LEAVES, TOTAL WIDTH
-26, ZFOCUS(1)
-26, ZFOCUS(2)
  -0.3881,   -0.2090, 1
  -0.3881,   -0.2090, 1
  -0.3881,   -0.2090, 1
  -0.3881,   -0.2090, 1
  -0.3881,   -0.2090, 1
  -0.3881,   -0.2090, 1
  -0.3881,   -0.2090, 1
  -0.3881,   -0.2090, 1
  -0.3881,   -0.2090, 1
  -0.3881,   -0.2090, 1
  -0.3881,   -0.2090, 1
  -0.3881,   -0.2090, 1
  -0.3881,   -0.2090, 1
  -0.5970,    0.0000, 1
  -0.5970,    0.0000, 1
  -0.8955,    0.2985, 1
  -0.8955,    0.8955, 1
  -0.8955,    0.8955, 1
  -0.8955,    0.8955, 1
```

```
  -0.8955,    0.8955, 1
  -0.8955,    0.8955, 1
  -0.8955,    0.8955, 1
  -0.8955,    0.8955, 1
  -0.8955,    0.8955, 1
  -0.8955,    0.8955, 1
  -0.8955,    0.8955, 1
  -0.8955,    0.8955, 1
  -0.8955,    0.8955, 1
  -0.0896,    0.0896, 1
  -0.0896,    0.0896, 1
  -0.0896,    0.0896, 1
  -0.0896,    0.0896, 1
  -0.0896,    0.0896, 1
  -0.0896,    0.0896, 1
  -0.0896,    0.0896, 1
  -0.0896,    0.0896, 1
  -0.0896,    0.0896, 1
  -0.0896,    0.0896, 1
  -0.0896,    0.0896, 1
  -0.0896,    0.0896, 1
  -0.0896,    0.0896, 1
0.7, 0.01, 0, 1,
AIR700ICRU
1.5, 0.01, 0, 1,
WNICU700
*********** start of CM JAWS with identifier Jaws  ***********
20, RMAX
Jaws (x&y)
2, # PAIRED BARS OR JAWS
X
13.6, 16.6,  1.188,  1.278, -1.188, -1.278
Y
17.1, 24.9,  3.017,  3.563, -2.586, -3.054
0.7, 0.01, 0, 1,
1.5, 0.01, 0, 1,
WNICU700
1.5, 0.01, 0, 1,
WNICU700
*********************end of all CMs*****************************
 #########################
 :Start MC Transport Parameter:

 Global ECUT= 0.7
 Global PCUT= 0.01
 Global SMAX= 5
 ESTEPE= 0.25
 XIMAX= 0.5
 Boundary crossing algorithm= EXACT
 Skin depth for BCA= 0
 Electron-step algorithm= PRESTA-II
 Spin effects= On
 Brems angular sampling= Simple
 Brems cross sections= BH
 Bound Compton scattering= Off
```

```
Compton cross sections= default
Pair angular sampling= Simple
Pair cross sections= BH
Photoelectron angular sampling= Off
Rayleigh scattering= Off
Atomic relaxations= Off
Electron impact ionization= Off
Photon cross sections= si
Photon cross-sections output= Off

:Stop MC Transport Parameter:
##########################
```

```
DOSXYZnrc input file for [redacted] Segment001          #!GUI1.0
0
/home/beamnrc/egsnrc_mp/dosxyznrc/CT[redacted].egsphant
0.7, 0.01, 0
0, 1, 0,
2, 2,   0.3, -0.2, -2.8,  90.0,  166.0, 49.1,  270.0, 0, 0, 0, 0, 0
2, 0, 0, 0, 0, 0, 0, 0
/home/beamnrc/egsnrc_mp/BEAM_j1/[redacted]_S001.egsphsp1
233669088, 0, 40, 33, 97, 100.0, 0, 0, 2, 0, , 10, 0, 0, 1, 0
 ##########################
 :Start MC Transport Parameter:

Global ECUT= 0.7
Global PCUT= 0.01
Global SMAX= 1e10
ESTEPE= 0.25
XIMAX= 0.5
Boundary crossing algorithm= PRESTA-I
Skin depth for BCA= 0
Electron-step algorithm= PRESTA-II
Spin effects= On
Brems angular sampling= Simple
Brems cross sections= BH
Bound Compton scattering= Off
Compton cross sections= default
Pair angular sampling= Simple
Pair cross sections= BH
Photoelectron angular sampling= Off
Rayleigh scattering= Off
Atomic relaxations= Off
Electron impact ionization= Off
Photon cross sections= si
Photon cross-sections output= Off

:Stop MC Transport Parameter:
 ##########################
```

# Appendix B: SOFTWARE CODES

The following list of software codes was developed for this study:

Short codes

| **Fortran** | **IDL** |
|---|---|
| dcombine.f | export_ascii_INP_CROSSPLANE_6MV.pro |
| dcombine_commissioning.f | export_ascii_INP_CROSSPLANE_10MV.pro |
| getdiag3.f | export_ascii_DIAG_6MV.pro |
| getdiag3_10.f | export_ascii_DIAG_10MV.pro |
| getpdd_5.f | export_ascii_PDD_6MV.pro |
| getpro_avg.f | export_ascii_PDD_10MV.pro |
| ReadCF.f | makeionchamber.pro |
| | makeionchamber10MV.pro |
| IMRTcombine.f90 | |
| IMRTcombine_1beam.f90 | mcdose_to_ascii.pro |
| split_inputDOSxyz.f95 | read_dicom_dose.pro |
| | read_dicom_struct.pro |
| | get_dvh_withdisp.pro |
| | plot_dvh.pro |

Main program (XiO2MC)

| **Visual Basic** | **IDL** |
|---|---|
| xio_to_mc_VB.vbp | patient_outline.pro |
| | remove_outside.pro |
| | xio_to_mc.pro |